

# Introducing bioactivity into electrospun scaffolds for in situ cardiovascular tissue engineering

**Citation for published version (APA):**

Thakkar, S. H. (2018). *Introducing bioactivity into electrospun scaffolds for in situ cardiovascular tissue engineering*. [Phd Thesis 1 (Research TU/e / Graduation TU/e), Biomedical Engineering]. Technische Universiteit Eindhoven.

**Document status and date:**

Published: 14/05/2018

**Document Version:**

Publisher's PDF, also known as Version of Record (includes final page, issue and volume numbers)

**Please check the document version of this publication:**

- A submitted manuscript is the version of the article upon submission and before peer-review. There can be important differences between the submitted version and the official published version of record. People interested in the research are advised to contact the author for the final version of the publication, or visit the DOI to the publisher's website.
- The final author version and the galley proof are versions of the publication after peer review.
- The final published version features the final layout of the paper including the volume, issue and page numbers.

[Link to publication](#)

**General rights**

Copyright and moral rights for the publications made accessible in the public portal are retained by the authors and/or other copyright owners and it is a condition of accessing publications that users recognise and abide by the legal requirements associated with these rights.

- Users may download and print one copy of any publication from the public portal for the purpose of private study or research.
- You may not further distribute the material or use it for any profit-making activity or commercial gain
- You may freely distribute the URL identifying the publication in the public portal.

If the publication is distributed under the terms of Article 25fa of the Dutch Copyright Act, indicated by the "Taverne" license above, please follow below link for the End User Agreement:

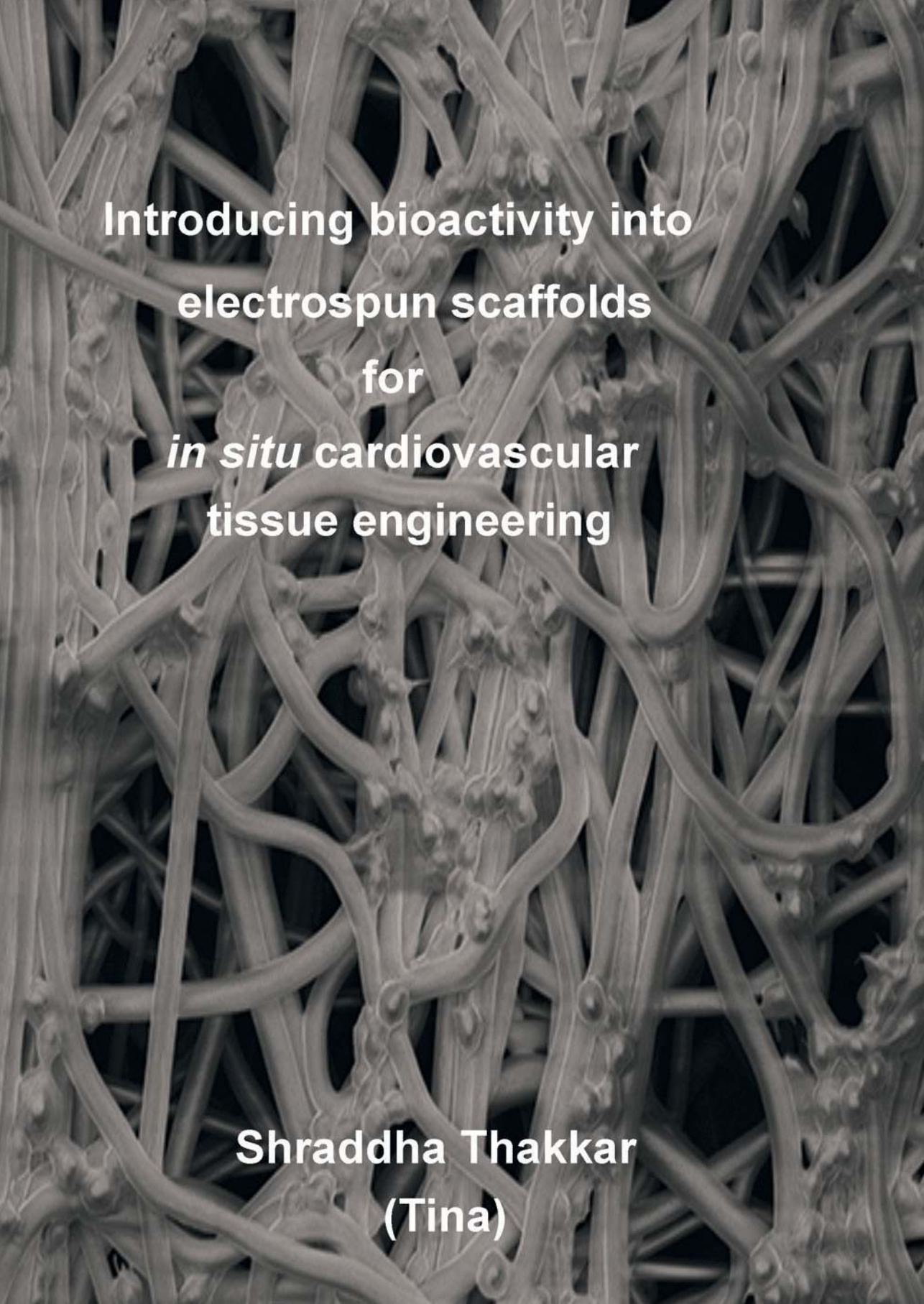
[www.tue.nl/taverne](http://www.tue.nl/taverne)

**Take down policy**

If you believe that this document breaches copyright please contact us at:

[openaccess@tue.nl](mailto:openaccess@tue.nl)

providing details and we will investigate your claim.

The background of the slide is a scanning electron micrograph (SEM) of an electrospun scaffold. It shows a dense, interconnected network of thin, fibrous structures. The fibers are randomly oriented and cross each other at various points, creating a porous, mesh-like structure. The fibers appear to have a slightly irregular, textured surface. The overall appearance is that of a complex, three-dimensional network of fibers.

**Introducing bioactivity into  
electrospun scaffolds  
for  
*in situ* cardiovascular  
tissue engineering**

**Shraddha Thakkar  
(Tina)**



**Introducing bioactivity into  
electrospun scaffolds for  
*in situ* cardiovascular tissue engineering**

Shraddha Harshad Thakkar  
(Tina)

Financial support by the Dutch Heart Foundation for the publication of this thesis is gratefully acknowledged

A catalogue record is available from the Eindhoven University of Technology Library

ISBN: 978-90-386-4501-8

Printed by Ipskamp Drukkers BV, Enschede, The Netherlands.

This research was supported by a grant from the Dutch government to the Netherlands Institute for Regenerative Medicine (NIRM).

# Introducing bioactivity into electrospun scaffolds for *in situ* cardiovascular tissue engineering

PROEFSCHRIFT

ter verkrijging van de graad van doctor aan de  
Technische Universiteit Eindhoven, op gezag van de  
rector magnificus prof.dr.ir. F.P.T. Baaijens,  
voor een commissie aangewezen door het College  
voor Promoties, in het  
openbaar te verdedigen op  
maandag 14 mei 2018 om 16:00 uur

door

Shraddha Harshad Thakkar

geboren te Bombay, India

Dit proefschrift is goedgekeurd door de promotoren en de samenstelling van de promotiecommissie is als volgt:

voorzitter:	prof.dr. P.A.J. Hilbers
1 <sup>e</sup> promotor:	prof.dr. C.V.C. Bouten
2 <sup>e</sup> promotor:	prof.dr.dr. P.Y.W. Dankers
leden:	prof.dr.ir. Lorenzo Moroni (Maastricht University) prof.dr. C.M. Sahlgren prof.dr.ir. G.W.M. Peters
adviseur:	dr.ir. A.I.P.M. Smits

*Dedicated to Mayur, Tamz and my parents*

*“Research is what I’m doing when I don’t know what I’m doing.”*

*-Wernher von Braun*





# Table of Contents

<b>Summary</b> .....	1
----------------------	---

## **Chapter 1: Introduction**

1.1 Cardiovascular tissue engineering .....	2
1.2 Scaffolds for in situ CVTE.....	2
1.2.1 Scaffold materials .....	2
1.2.2 Scaffold processing .....	4
1.3 Host response to scaffold materials .....	6
1.3.1 Role of macrophages in host response to biomaterials .....	7
1.3.2 Modulating the immune response .....	7
1.4 Rational and outline of the thesis .....	9
Chapter 1 References .....	12

## **Chapter 2: Porous Scaffolds using Dual Electrospinning for *in situ* Cardiovascular Tissue Engineering**

2.1 Introduction .....	17
2.2 Electrospinning .....	19
2.2.1 Single nozzle electrospinning .....	20
2.2.2 Dual nozzle electrospinning.....	23
2.2.3 Coaxial nozzle electrospinning .....	25
2.3 Cell infiltration into electrospun scaffolds .....	27
2.4 Scaffold (An) Isotropy .....	27
2.5 Controlling scaffold porosity .....	29
2.5.1 Increasing Fiber Diameter .....	29
2.5.2 Tailoring collectors.....	30
2.5.3 Low temperature electrospinning .....	31

2.5.4	Multimodal fiber electrospinning .....	31
2.5.5	Selective removal of polymer .....	32
2.5.6	Comparison of techniques .....	33
2.6	Mechanical properties and degradation rate .....	34
2.7	Conclusion and Future Outlook .....	36
	Chapter 2 References .....	37

### **Chapter 3: Decellularized human mesenchymal stem cell derived matrix skews macrophages towards a regenerative phenotype**

3.1	Introduction .....	51
3.2	Materials & Methods .....	52
3.2.1	Human mesenchymal stem cell isolation and ECM synthesis .....	52
3.2.2	Decellularized ECM processing and characterization .....	53
3.2.3	Biochemical assays .....	54
3.2.4	Elastin Assay .....	54
3.2.5	Collagen staining .....	54
3.2.6	Preparation and characterization of 3D electrospun scaffolds .....	55
3.2.7	Scanning electron microscopy .....	56
3.2.8	Human peripheral mononuclear cell isolation .....	56
3.2.9	Monocyte migration assay .....	57
3.2.10	Macrophage polarization experiments .....	57
3.2.11	Immunohistochemistry .....	58
3.2.12	qPCR .....	59
3.2.13	Statistical analysis .....	60
3.3	Results .....	62
3.3.1	Characterization of ECM .....	62
3.3.2	dECM and LECM experiments in 2D .....	64
	• Bioactivity of ECM assessed by migration assay .....	64
	• Macrophage phenotype assessment via immunostaining .....	65
	• Macrophage polarization assessment using gene expression analysis .....	67

3.3.3	LECM experiments in 3D.....	68
	• Bioactivity of ECM assessed by migration assay.....	69
	• Cell morphology assessment and immunostaining.....	70
3.4	Discussion .....	73
3.5	Conclusion .....	76
	Chapter 3 References .....	77

**Chapter 4: Mesoporous silica nanoparticles enhances loading efficiency of MCP1 on electrospun scaffolds**

4.1	Introduction.....	83
4.2	Experimental.....	85
4.2.1	Particle synthesis.....	85
4.2.2	Scanning electron microscopy (SEM) .....	85
4.2.3	Transmission electron microscopy (TEM).....	85
4.2.4	Preparation of electrospun scaffolds.....	86
4.2.5	Adsorption of MSNs on electrospun scaffolds.....	86
4.2.6	Drug loading .....	86
4.2.7	Release of MCP1 .....	87
4.2.8	Human peripheral blood mononuclear cells (hPBMCs) isolation ..	88
4.2.9	Migration assay .....	88
4.2.10	Immunohistochemistry.....	89
4.2.11	Cell viability (WST-8) assay.....	89
4.2.12	Statistical analysis .....	90
4.3	Results and Discussion .....	91
4.3.1	MSNs synthesis, characterization and adsorption to PCLBU electrospun scaffolds.....	91
4.3.2	Loading MSNs with MCP1.....	91
4.3.3	Loading and release of MCP1 from scaffolds with MSNs .....	96
4.3.4	Cytocompatibility of [MSN + MCP1] scaffolds .....	98
4.3.5	The effect of released MCP1 on migration of cells towards the scaffold .....	101

4.4	Conclusion .....	103
	Chapter 4 References .....	104

## **Chapter 5: Dual electrospun supramolecular polymer systems for selective cell migration**

5.1.	Introduction .....	109
5.2.	Experimental section .....	111
5.2.1	Supramolecular polymers and SDF1 $\alpha$ peptide .....	111
5.2.2	Preparation of electrospun scaffolds .....	113
5.2.3	Scanning electron microscopy.....	114
5.2.4	Mechanical characterisation of electrospun meshes .....	114
5.2.5	Scaffold incubation / erosion of UPyPEG .....	114
5.2.6	UV irradiation and fluorescent microscopy.....	115
5.2.7	hPBMCs isolation .....	115
5.2.8	Migration Assay .....	115
5.2.9	Cell attachment by electrospun SDF1 $\alpha$ peptide scaffolds.....	116
5.2.10	DNA assay.....	116
5.2.11	Cell morphology.....	116
5.2.12	Immunohistochemistry.....	117
5.2.13	Statistical analysis .....	117
5.3.	Results and Discussion .....	118
5.3.1	Production and characterization of dual spun supramolecular polymer meshes .....	118
5.3.2	Mechanical properties of dual spun meshes .....	122
5.3.3	Bioactivity of SDF1 $\alpha$ peptide .....	124
5.3.4	Cell recruitment on electrospun scaffolds with SDF1 $\alpha$ peptide...	128
5.3.5	Immunohistochemistry.....	128
5.4.	Conclusion .....	129
	Chapter 5 References .....	130

## **Chapter 6: General Discussion**

6.1. Introduction .....	134
6.2. Key Findings .....	134
6.2.1 Decellularized extracellular matrix incorporated in both 2D and 3D influences macrophage polarization .....	135
6.2.2 Extended release of bioactive factors through incorporation of mesoporous silica nanoparticles .....	137
6.2.3 Release of bioactives factors via selective removal of a supramolecular hydrogelator .....	139
6.2.4 Techniques for developing functionalized scaffolds .....	140
6.3. Towards the design of an immunomodulatory scaffold .....	141
6.4. Study limitations .....	145
6.5. Future perspectives .....	147
6.6. Conclusion .....	148
Chapter 6 References .....	149

<b>Supporting data</b> .....	153
------------------------------	-----

Chapter 3 .....	154
-----------------	-----

Chapter 4 .....	156
-----------------	-----

Chapter 5 .....	160
-----------------	-----

<b>Acknowledgements</b> .....	163
-------------------------------	-----

<b>Curriculum Vitae</b> .....	167
-------------------------------	-----

<b>List of Publications</b> .....	169
-----------------------------------	-----



# Summary

## **Introducing bioactivity into electrospun scaffolds for *in situ* cardiovascular tissue engineering**

*In situ* cardiovascular tissue engineering is a promising approach that utilizes the regenerative potential of the body to remodel and repopulate synthetic scaffolds with endogenous cells. This approach focuses on mimicking the native microenvironment of the cell by using synthetic scaffolds. Such scaffolds should be designed to promote cell adhesion and proliferation, evoke minimal inflammatory response and eventually facilitate tissue regeneration. Modulating the immune response can positively influence tissue formation. The aim of this thesis is to fabricate functionalized constructs that can modulate the early immune response towards tissue regeneration by exploring the combination of biomimetic electrospun scaffolds with bioactive molecules.

Since synthetic scaffolds lack a biological component, bioactive molecules can be introduced to create an *in vivo* like environment. Furthermore, the geometrical design and structural architecture of the scaffolds are crucial factors in order for them to function immediately after implantation. Scaffold implantation is generally accompanied by injury, which induces an inflammatory response. The damage caused during an injury initiates an acute response, followed by chronic inflammatory response and ends with a foreign body response that can result in either fibrosis or tissue regeneration. In the entire cascade of processes, macrophages are key mediators in wound healing. These cells have the ability to switch their phenotype from a pro-inflammatory polarized state M1 to a reparative profile M2 in response to the changing environmental stimuli. Thus the plasticity of macrophages, i.e. the balance between M1 and M2, plays a decisive role in tissue repair and regeneration. This immune response can be modulated by



modifying the design and properties of the scaffold, and by introducing specific bioactive molecules.

The electrospinning technique was applied to fabricate a mesh that resembles the fibrous morphology of native extracellular matrix (ECM). The fabricated electrospun scaffolds were functionalized with cell derived ECM as a biological element due to its role in influencing immune cell behaviour. We investigated the immunomodulatory properties of ECM, derived from human mesenchymal stem cells (hMSCs), with respect to human monocyte recruitment and macrophage polarization, both in 2D and 3D; the latter in the form of a hybrid electrospun scaffold. hMSC-derived decellularized ECM (2D) had a positive influence on human monocyte recruitment and favoured macrophage polarization towards a pro-regenerative M2 phenotype. The 3D scaffolds created by electrospinning lyophilized ECM with poly ( $\epsilon$ -caprolactone) preserved the immunomodulatory effects of the ECM after electrospinning. These findings demonstrate that hMSC-derived ECM maintains its beneficial intrinsic immunomodulatory functions after decellularization, lyophilisation, and electrospinning.

Monocyte Chemoattractant Protein (MCP1) is one of the key chemokines mediating an immune response that enhances monocyte migration and regulates macrophage polarization. Vascular grafts incorporated with MCP1 have demonstrated rapid influx of monocytes, leading to improved neo artery formation *in vivo*. The amount of MCP1 incorporated into the scaffold can influence the release of MCP1 and accordingly the local MCP1 concentration. We introduced MCP1 in electrospun scaffolds by employing aminofunctionalized mesoporous silica nanoparticles (MSN). These MSNs act as depots of MCP1 to enhance the amount of the latter on the scaffold. The electrospun polycaprolactone bisurea (PCLBU) scaffolds with MSNs demonstrated a higher loading efficiency of MCP1 compared to scaffolds without MSNs. The developed [MSN+MCP1] scaffolds exhibit a fast release of MCP1 within the first few hours and reached a plateau after 24 h. MSNs maintain the biological effect of MCP1 by inducing selective migration of monocytes towards the scaffolds. This study suggests that the MCP1

loading efficiency and release from electrospun scaffolds can be improved by incorporating MSN as delivery agents.

Stromal cell derived factor 1 alpha (SDF1 $\alpha$ ) is another chemokine that regulates the inflammatory and regenerative microenvironment of the cells. SDF1 $\alpha$  peptide grafts have been shown to increase attachment of lymphocytes, reduce inflammatory signals and increase cellularity after one week of implantation. We have introduced SDF1 $\alpha$  peptides in supramolecular hydrogel polymers. Two synthetic supramolecular polymers with different material properties were electrospun simultaneously to create a multi-fibrous mesh. The dual spun scaffolds were modularly tuned by mixing supramolecular hydrogelators with different polymer lengths, to control swelling of the hydrogel fiber, while maintaining the mechanical properties of the scaffold. The swelling and erosion of hydrogel fiber resulted in increase of void spaces and release of incorporated SDF1 $\alpha$  peptide. This released SDF1 $\alpha$  peptide facilitates selective lymphocyte recruitment towards the scaffold.

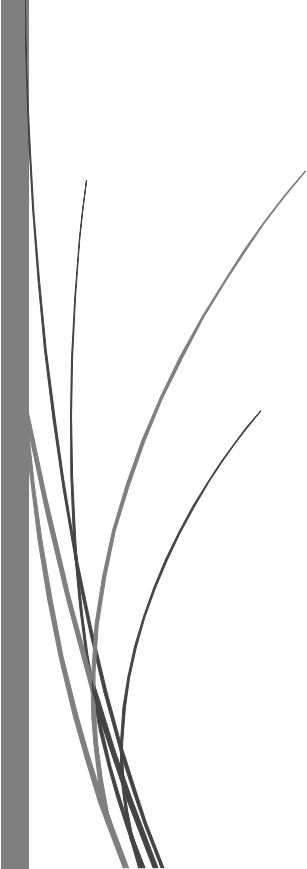
In conclusion, this thesis highlights the introduction of bioactivity in electrospun scaffolds using different techniques, starting with hybrid scaffolds and moving to purely synthetic scaffolds. These developed functionalized electrospun constructs provide knowledge on scaffold-induced immunomodulation. Introducing bioactivity in an electrospun scaffold is demonstrated as a powerful tool to design and fabricate immunomodulatory scaffolds for *in situ* tissue engineering applications.





Chapter 1

General Introduction



## 1.1 Cardiovascular tissue engineering

As the name suggests, cardiovascular tissue engineering (CVTE) focuses on engineering living tissues that aim to replace native malfunctioning cardiovascular components, such as heart valves, blood vessels or cardiac muscle, either completely or partially [1]. Engineered tissues are traditionally developed *in vitro* by isolating and expanding cells from patients, seeding the cells on an appropriate scaffold and conditioning the cell-scaffold construct in a bioreactor to form a functional tissue [2]. The developed tissue is then implanted into the patient to replace the function of a diseased or damaged component. However, tissues fabricated with this conventional approach face increased cost and procedural obstacles prior to *in vivo* implantation. Thus, in this thesis we adopted the concept of *in situ* tissue engineering that focuses on direct implantation of the scaffold and uses the body as a bioreactor to create living tissues at the site of implantation *in vivo*, thereby eliminating the *in vitro* tissue culture phase [3-4]. The scaffold is a crucial component in this *in situ* approach, since it should function immediately upon implantation and throughout the process of neotissue formation. The scaffold is anticipated to create an ideal microenvironment to attract cells, promote adhesion, proliferation, and support target tissue regeneration. Additionally, the scaffold should degrade in pace with development of the tissue. Since the scaffold forms the framework for tissue formation, the selection of biomaterial, the fabrication technique and the resulting scaffold properties (such as structure, porosity, bioactivity or biodegradability) play an essential role in the success of *in situ* CVTE [5].

## 1.2 Scaffolds for *in situ* CVTE

### 1.2.1 Scaffold materials

Currently available biomaterials are either natural or synthetic in origin. Naturally occurring materials include collagen [6], alginate [7], and chitosan [8]. Recently, extracellular matrix (ECM) based materials are gaining a lot of interest as potential scaffold materials for different biomedical applications [9-

10]. These ECM based materials are derived from decellularized tissues or organs of a donor, sometimes also from animals [11-12]. A decellularization technique is employed, which removes the cellular components, while maintaining the structure and composition of ECM as intact as possible. The resulting decellularized ECM-based material (dECM) provides a microenvironment comparable to the native tissue, while simultaneously promoting cell signalling and cellular interaction with ECM proteins [10]. In addition, the structural and matricellular proteins residing in dECM can regulate cell behaviour [13-14]. However, a major drawback of this method is risk of zoonoses transfer (in case of ECM from animal origin) or limited availability of tissue or organ source [15]. This limitation can be circumvented by obtaining cell derived matrix *in vitro*. In this method, cells are cultured *in vitro* to deposit ECM which is decellularized using suitable (decellularization) techniques [16]. Cell derived matrix offers the flexibility of being able to use different cell types and to obtain ECM in various forms (as required) such as cell culture substrates. In general naturally derived biomaterials demonstrate excellent biocompatibility and degradability. However, such materials lack the tunability and processability of synthetic materials and may exhibit differences in composition due to batch to batch variation [17]. To overcome this shortcoming, natural materials can be combined with synthetic materials to improve the processability of these materials.

Synthetic materials have been employed as scaffolds due to the ease and flexibility in optimizing material properties such as structure, mechanical properties and degradation rates [18]. Some commonly used synthetic polymers include polycaprolactone (PCL), polylactic acid (PLA), poly(lactide-co-glycolide) (PLGA), polyethylene glycol (PEG) and polyethylene glycol (PEO) [19]. Depending on the specified application, synthetic materials can be tailored into different forms of scaffolds with customised porosity, architecture and other desired properties. PCL has been extensively used as a scaffold material due to its biocompatibility and compliance [20]. Additionally, devices fabricated from PCL have been approved by the FDA to be used for applications in the human body. Due to its wide range of

applications, ease to use and regulatory approval we combined dECM with a PCL backbone to fabricate scaffolds.

Besides the commercially available synthetic polymers, a lot of progress has been made on development of supramolecular materials [21]. Supramolecular polymers are based on monomeric units that are fasten together by bidirectional and irreversible interactions [22]. The benefit of these materials depends on the nature of supramolecular interactions that offer the flexibility to tune properties in a reversible, dynamic and modular fashion [23]. However, the preparation of supramolecular materials from small molecules often requires complex procedures, resulting in low yield and high costs [24]. These limitations must be overcome prior to using supramolecular polymers as scaffolding material in regular clinical practise.

### 1.2.2 Scaffold processing

Besides selection of the material, the architecture of the scaffold (porosity, mass transport properties) is important to facilitate cell attachment and eventually guide tissue regeneration. Various fabrication techniques have been developed to design scaffolds in different structures and forms [25-27]. The appropriate fabrication technique depends on the design criteria specific to the site of implantation. Scaffolds for *in situ* CVTE typically consist of fibrous constructs with porous architecture that promote cell recruitment, differentiation, and support tissue formation and remodelling [28-29]. Amongst the currently available techniques for fabrication of fibrous scaffolds, electrospinning is the most widely studied approach [30-35]. The unique advantage of this technique is the fabrication of micrometer to nanometer range fibers, which resemble the native fibrous ECM structure [36-38].

The basic principle of electrospinning involves the use of an electrostatic field to stretch a polymer drop into a fiber, which forms a fibrous mesh upon collection on a target. Briefly, the set up consists of four major components: a syringe pump, a grounded target, a single spinneret (nozzle), and a high voltage power supply. The polymeric solution is fed into the spinneret at a fixed flow rate and held as a droplet at the tip of the nozzle due to its surface

tension. High voltage is applied at the spinneret while the target is grounded. The applied electric field develops a charge on the droplet and this droplet forms a Taylor cone as the intensity of the electric field increases [39-40]. When the electric field surpasses the surface tension of the fluid, a polymeric jet is ejected from the cone. While the ejected jet travels, the solvent is evaporated and the polymeric fiber is deposited on the grounded target [41]. In general, the versatile setup allows to electrospin different materials and tune fiber morphology by varying the electrospinning parameters. The fibrous architecture of the scaffold encompasses a large surface to volume ratio that promotes cell attachment and growth, making it an attractive technique for biomedical application. Figure 1.1 visually demonstrates the effect of flow rate and rotation of the target, during electrospinning poly-4-hydroxybutyrate (P4HB), where a random mesh is formed at higher flow rate and lower rotation speed. This shows that lower flow rate and higher speed generates completely aligned fibers. Besides the above mentioned single spinneret standard electrospinning setup, many variations to the standard set up are possible. For instance two spinnerets can be employed simultaneously to deposit fibers on a common target.



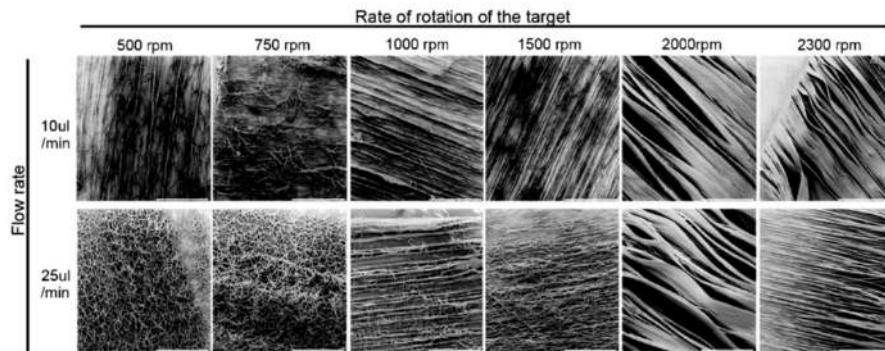


**Figure 1.1: Electrospinning of P4HB at two different flow rates (10ul/min and 25ul/min).** The rotation speed of the target was varied from 500 rpm, 750 rpm, 1000rpm, 1500 rpm, 2000rpm and 2300 rpm. The SEM images show highly aligned fibers at high rotational speed of the target. Scale bar 1 mm.

### 1.3 Host response to scaffold materials

Implantation of any biomaterial in a living tissue generates a host response [43]. In case of cardiovascular implants, the biomaterial first comes in contact with blood and initiates an inflammatory response. The proteins in the blood are adsorbed on the surface of the scaffold, and activate the coagulation cascade, complement system and interaction with immune cells [43]. Polymorphonuclear leukocytes (predominant inflammatory cells) from the blood migrate towards the site of injury and secrete chemokines and activation factors such as monocyte chemoattractant protein 1 (MCP-1) to promote monocyte migration [44-45]. The monocytes mobilize in response to the local chemoattractant and chemokines. The infiltrated monocytes subsequently undergo phenotypic differentiation into macrophages. The signalling factors present in the microenvironment modulate the actions of immune cells and regulate the healing process.

### **1.3.1 Role of macrophages in host response to biomaterials**

Scaffold implantation is always accompanied by injury (tissue damage), which induces an immune response. Immune response to a biomaterial starts with an acute response to injury and recognition of foreign material. This is followed by chronic inflammatory response and ends with a foreign body response that can result in fibrosis or tissue regeneration. Macrophages have been identified as key players in modulating the immune response. It is known that macrophages demonstrate high plasticity and have an ability to switch their phenotype in response to changing environmental stimuli [42].

Macrophages have been initially classified in two sets, namely M1 and M2, according to their function [43-44]. The classically activated or M1 type macrophages have an ability to induce pro-inflammatory responses by releasing cytokines, like IL-6, IL-12, TNF $\alpha$  and MCP1. The alternatively activated or M2 type macrophages are associated with reducing the inflammation signal and promoting repair and remodelling. They are characterized by high expression of anti-inflammatory cytokines like IL-10, CD206 and CD163 [45]. M1 and M2 are distinct in their cytokine expression profile. However, the transition between M1 and M2 results in an intermediate state, with overlap of functions and characteristics of both phenotypes [46]. The plasticity of macrophages i.e. the balance between M1 and M2 plays a decisive role in tissue repair and regeneration [47-48]. The exact mechanism, specific environmental factors and stimuli that control the switching of macrophage into different phenotypes is largely unknown. Yet biomaterials and their properties can be tuned to modulate the immune response towards a regenerative tissue formation.

### **1.3.2 Modulating the immune response**

Since there is an interplay between biomaterials and the immune response cascade, modifying the properties of the scaffolds can help to harness the immune response. The next paragraphs review some strategies to alter or adjust the properties of scaffolds ranging from optimising the biomaterial

surface roughness, scaffold microstructure and incorporation of bioactive factors (or components).

Biomaterial surface chemistry is an important parameter as it influences protein adsorption, which in turn mediates the interaction and activation of immune cells. Thus, the degree of wettability and the nature as well as distribution of charged groups mediate protein adsorption on the surface [49]. Besides the material chemistry, the surface topography can also influence cell behaviour. Surface roughness of electrospun vascular scaffolds has been shown to influence blood activation [50]. Topography-induced changes were demonstrated to affect cell adhesion, morphology and cytokine secretion [51], and promoted activation of macrophages [52].

Scaffold architecture or microstructure can influence cell infiltration, cell behaviour, and evoke an immune response [42-44]. Scaffold microstructure in terms of fiber diameter and porosity can regulate macrophage polarization [45]. Saino et al. demonstrated minimized inflammatory response on nanofibrous electrospun scaffolds compared to microfibrillar electrospun scaffolds and 2D surface [46]. In contrast, macrophages on electrospun meshes with thin fiber diameter (less than 1 $\mu$ m) polarize towards a pro-inflammatory phenotype while those cultured on thick fiber diameter (more than 5 $\mu$ m) polarize towards M2 phenotype [53]. Although the precise fiber diameter that directly correlates to positive M2 polarization is ambiguous, it is clear that the microstructure of the electrospun scaffold is a cue that alters the macrophage phenotypic profile.

As previously mentioned the signalling factors present in the native microenvironment modulate the activation of immune cells and regulate the healing process. Thus, incorporating bioactive factors into a synthetic scaffold is another possible strategy of mimicking the native ambience [54]. Specifically, the bioactive factors released locally have the potential to selectively recruit cells or enhance the interaction of the immune cells to promote the healing process. Chemokines induce migration and recruitment of immune cells at the site of injury. MCP-1 has been established as a key mediator to initiate migration and recruitment of monocytes by binding to C-C

chemokine receptor 2 (CCR2) [55]. Studies have demonstrated that a burst release of MCP1 creates a gradient and guides the monocytes towards the site of injury [56-57]. Furthermore, rapid infiltration of monocytes into the MCP1 scaffold creates a positive inflammatory response and triggers tissue repair and remodelling [58]. Stromal derived factor-1 alpha (SDF-1 $\alpha$ ) is another bioactive factor whose long term release enhances recruitment of cells and modifies the inflammatory cellular response [59]. In recent years, synthetic derived peptides are gaining a lot of interest as 'smart scaffolds' that mediate the host response. Our group has developed supramolecular biomaterials based on the four-fold hydrogen bonding ureido-pyrimidinone (UPy) moiety that were functionalized with SDF1 $\alpha$  derived peptides via these supramolecular UPy-interactions [60]. We showed that UPy-SDF1 $\alpha$  grafts increased attachment of lymphocytes and reduced the inflammatory signal compared to the controls *in vitro*. Furthermore, one week implantation of UPy-SDF1  $\alpha$  graft in a rat aorta interposition graft model showed increased cellularity demonstrating the effect of incorporated SDF1  $\alpha$  peptide. Besides incorporating specific bioactive factors in the scaffold, combining decellularized ECM with scaffold develops a hybrid scaffold capturing the advantages of both materials i.e. the bioactivity of ECM and mechanical properties of a synthetic scaffold material [61-62].

## 1.4 Rational and outline of the thesis

The aim of this thesis is to explore different techniques for combining electrospun scaffolds with bioactive molecules to engineer a biological microenvironment that helps to modulate cell recruitment and macrophage polarization for *in situ* CVTE. Figure 1.2 demonstrates the different techniques used in this thesis to develop a functionalized scaffold.

Fibrous scaffolds used for *in situ* CVTE were generated using electrospinning. [Chapter 2](#) reviews the different electrospinning techniques for fabricating electrospun scaffolds. Methods to modify the porosity of the electrospun scaffold and the impact of porosity on mechanical properties and degradation rate were discussed.

Extracellular matrix (ECM) is known to play an important role in influencing immune cell behaviour. [Chapter 3](#) describes the effect of decellularized human mesenchymal stem cell derived ECM on monocyte recruitment and macrophage polarization in both 2D and 3D.

Next, an *in vitro* animofunctionalized mesoporous silica nanoparticle (MSN) delivery system was developed to enhance the loading efficiency of recombinant Monocyte Chemoattractant Protein-1 (MCP1) on electrospun scaffolds. The effect of MCP1 released from MSN on early cell recruitment was studied in [Chapter 4](#).

[Chapter 5](#) describes fabrication of dual electrospun scaffold using a supramolecular hydrogel polymer and SDF1 $\alpha$  peptide. The effect of selective removal of hydrogel, increase of porosity and mechanical properties of the developed scaffold were investigated. Furthermore, the effect of incorporated SDF1 $\alpha$  peptide on cell recruitment was studied.

The main outcomes of the thesis are summarized and discussed in [Chapter 6](#). It also includes the limitations, future perspectives and challenges that need to be overcome to develop a functionalized immunomodulatory scaffold.

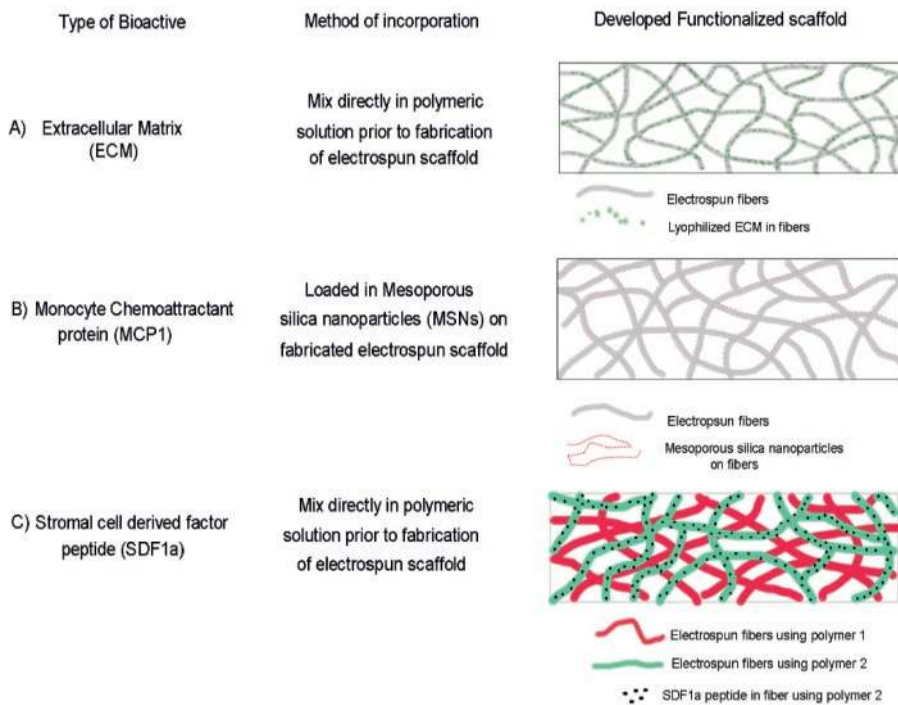


**Figure 1.2: Techniques used for introducing bioactive factors in electrospin scaffold.** A) Direct electrospinning of lyophilized ECM with polymer, B) MSN used as carriers for loading MCP1, released MCP1 was measured up to 1 day, C) Incorporation of supramolecular SDF1 $\alpha$  peptide in polymer 2 (hydrogelator) fibers, swelling followed by erosion of hydrogelator releases the peptide.

---

## References

1. Mol, A., et al., *Tissue engineering of heart valves: advances and current challenges*. Expert Review of Medical Devices, 2009. **6**(3): p. 259-275.
2. Godbey, W.T. and A. Atala, *In Vitro Systems for Tissue Engineering*. Annals of the New York Academy of Sciences, 2002. **961**(1): p. 10-26.
3. Smits, A.I.P.M., V. Bonito, and M. Stoddart, *In Situ Tissue Engineering: Seducing the Body to Regenerate*. Tissue Engineering Part A, 2016. **22**(17-18): p. 1061-1062.
4. Bouten, C.V.C., A. Driessen-Mol, and F.P.T. Baaijens, *In situ heart valve tissue engineering: simple devices, smart materials, complex knowledge*. Expert Review of Medical Devices, 2012. **9**(5): p. 453-455.
5. O'Brien, F.J., *Biomaterials & scaffolds for tissue engineering*. Materials Today, 2011. **14**(3): p. 88-95.
6. Parenteau-Bareil, R., R. Gauvin, and F. Berthod, *Collagen-Based Biomaterials for Tissue Engineering Applications*. Materials, 2010. **3**(3): p. 1863-1887.
7. Rinaudo, M., *Biomaterials based on a natural polysaccharide: alginate*. TIP, 2014. **17**(1): p. 92-96.
8. Croisier, F. and C. Jérôme, *Chitosan-based biomaterials for tissue engineering*. European Polymer Journal, 2013. **49**(4): p. 780-792.
9. Badylak, S.F., *The extracellular matrix as a biologic scaffold material*. Biomaterials, 2007. **28**(25): p. 3587-3593.
10. Badylak, S.F., D.O. Freytes, and T.W. Gilbert, *Extracellular matrix as a biological scaffold material: Structure and function*. Acta Biomaterialia, 2009. **5**(1): p. 1-13.
11. Mihardja, S.S., J. Yu, and R.J. Lee, *Extracellular matrix-derived peptides and myocardial repair*. Cell Adh Migr, 2011. **5**(2): p. 111-3.
12. Badylak, S., et al., *Extracellular matrix for myocardial repair*. Heart Surgery Forum, 2003. **6**(2): p. E20-6.
13. Bornstein, P. and E.H. Sage, *Matricellular proteins: extracellular modulators of cell function*. Current Opinion in Cell Biology, 2002. **14**(5): p. 608-616.
14. Streuli, C., *Extracellular matrix remodelling and cellular differentiation*. Current Opinion in Cell Biology, 1999. **11**(5): p. 634-640.
15. Bouten, C.V.C., et al., *Substrates for cardiovascular tissue engineering*. Advanced Drug Delivery Reviews, 2011. **63**(4): p. 221-241.
16. Fitzpatrick, L.E. and T.C. McDevitt, *Cell-derived matrices for tissue engineering and regenerative medicine applications*. Biomaterials Science, 2015. **3**(1): p. 12-24.
17. Lee, C.H., A. Singla, and Y. Lee, *Biomedical applications of collagen*. International Journal of Pharmaceutics, 2001. **221**(1): p. 1-22.
18. Dhandayuthapani, B., et al., *Polymeric Scaffolds in Tissue Engineering Application: A Review*. International Journal of Polymer Science, 2011.
19. Ma, P.X., *Scaffolds for tissue fabrication*. Materials Today, 2004. **7**(5): p. 30-40.
20. Mondal, D., M. Griffith, and S.S. Venkatraman, *Polycaprolactone-based biomaterials for tissue engineering and drug delivery: Current scenario and challenges*. International Journal of Polymeric Materials and Polymeric Biomaterials, 2016. **65**(5): p. 255-265.
21. Webber, M.J., et al., *Supramolecular biomaterials*. Nature Materials, 2015. **15**: p. 13.
22. Brunsveld, L., et al., *Supramolecular polymers*. Chemical Reviews, 2001. **101**(12): p. 4071-4097.
23. Webber, M.J., et al., *Supramolecular biomaterials*. Nature Materials, 2016. **15**(1): p. 13-26.
24. Webber, M.J., *Engineering responsive supramolecular biomaterials: Toward smart therapeutics*. Bioengineering & Translational Medicine, 2016. **1**(3): p. 252-266.
25. Lu, T., Y. Li, and T. Chen, *Techniques for fabrication and construction of three-dimensional scaffolds for tissue engineering*. International Journal of Nanomedicine, 2013. **8**: p. 337-350.
26. Kunjachan, V., et al., *Comparison of different fabrication techniques used for processing 3-dimensional, porous, biodegradable scaffolds from modified starch for bone tissue engineering*. Biomedical Sciences Instrumentation, Vol 40, 2004. **449**: p. 129-135.

27. Landers, R., et al., *Fabrication of soft tissue engineering scaffolds by means of rapid prototyping techniques*. Journal of Materials Science, 2002. **37**(15): p. 3107-3116.
28. Wissing, T.B., et al., *Biomaterial-driven in situ cardiovascular tissue engineering—a multi-disciplinary perspective*. npj Regenerative Medicine, 2017. **2**(1): p. 18.
29. Hasan, A., et al., *Electrospun scaffolds for tissue engineering of vascular grafts*. Acta Biomaterialia, 2014. **10**(1): p. 11-25.
30. Thorvaldsson, A., et al., *Electrospinning of highly porous scaffolds for cartilage tissue engineering*. Tissue Engineering Part A, 2008. **14**(5): p. 845-846.
31. Teo, W.E. and S. Ramakrishna, *A review on electrospinning design and nanofibre assemblies*. Nanotechnology, 2006. **17**(14): p. R89-R106.
32. Teo, W.E., R. Inai, and S. Ramakrishna, *Technological advances in electrospinning of nanofibers*. Science and Technology of Advanced Materials, 2011. **12**(1).
33. Lu, W.J., J.S. Sun, and X.Y. Jiang, *Recent advances in electrospinning technology and biomedical applications of electrospun fibers*. Journal of Materials Chemistry B, 2014. **2**(17): p. 2369-2380.
34. Liu, H.F., et al., *Electrospinning of Nanofibers for Tissue Engineering Applications*. Journal of Nanomaterials, 2013.
35. Lannutti, J., et al., *Electrospinning for tissue engineering scaffolds*. Materials Science & Engineering C-Biomimetic and Supramolecular Systems, 2007. **27**(3): p. 504-509.
36. Fridrikh, S.V., et al., *Controlling the fiber diameter during electrospinning*. Physical Review Letters, 2003. **90**(14).
37. Doshi, J. and D.H. Reneker, *Electrospinning Process and Applications of Electrospun Fibers*. Journal of Electrostatics, 1995. **35**(2-3): p. 151-160.
38. Agarwal, S., J.H. Wendorff, and A. Greiner, *Use of electrospinning technique for biomedical applications*. Polymer, 2008. **49**(26): p. 5603-5621.
39. *Disintegration of pairs of water drops in an electric field*. Proceedings of the Royal Society of London. Series A. Mathematical and Physical Sciences, 1966. **295**(1440): p. 84-97.
40. Taylor, G., *Electrically Driven Jets*. Proceedings of the Royal Society of London Series a-Mathematical and Physical Sciences, 1969. **313**(1515): p. 453-&.
41. Yarin, A.L., S. Koombhongse, and D.H. Reneker, *Bending instability in electrospinning of nanofibers*. Journal of Applied Physics, 2001. **89**(5): p. 3018-3026.
42. Garg, K., et al., *Macrophage functional polarization (M1/M2) in response to varying fiber and pore dimensions of electrospun scaffolds*. Biomaterials, 2013. **34**(18): p. 4439-4451.
43. Mantovani, A., A. Sica, and M. Locati, *Macrophage polarization comes of age*. Immunity, 2005. **23**(4): p. 344-6.
44. Martinez, F.O. and S. Gordon, *The M1 and M2 paradigm of macrophage activation: time for reassessment*. F1000Prime Rep, 2014. **6**: p. 13.
45. Duque, G.A. and A. Descoteaux, *Macrophage cytokines: involvement in immunity and infectious diseases*. Frontiers in Immunology, 2014. **5**: p. 1-12.
46. Mosser, D.M. and J.P. Edwards, *Exploring the full spectrum of macrophage activation*. Nature Reviews Immunology, 2008. **8**(12): p. 958-969.
47. Martinez, F.O., et al., *Macrophage activation and polarization*. Frontiers in Bioscience, 2008. **13**: p. 453-61.
48. Brown, B.N., et al., *Macrophage polarization: an opportunity for improved outcomes in biomaterials and regenerative medicine*. Biomaterials, 2012. **33**(15): p. 3792-802.
49. Ekdahl, K.N., et al., *Innate immunity activation on biomaterial surfaces: A mechanistic model and coping strategies*. Advanced Drug Delivery Reviews, 2011. **63**(12): p. 1042-1050.
50. Milleret, V., et al., *Influence of the fiber diameter and surface roughness of electrospun vascular grafts on blood activation*. Acta Biomaterialia, 2012. **8**(12): p. 4349-4356.
51. Chen, S.L., et al., *Characterization of topographical effects on macrophage behavior in a foreign body response model*. Biomaterials, 2010. **31**(13): p. 3479-3491.
52. Paul, N.E., et al., *Topographical control of human macrophages by a regularly microstructured polyvinylidene fluoride surface*. Biomaterials, 2008. **29**(30): p. 4056-64.
53. Wang, Z., et al., *The effect of thick fibers and large pores of electrospun poly(epsilon-caprolactone) vascular grafts on macrophage polarization and arterial regeneration*. Biomaterials, 2014. **35**(22): p. 5700-10.

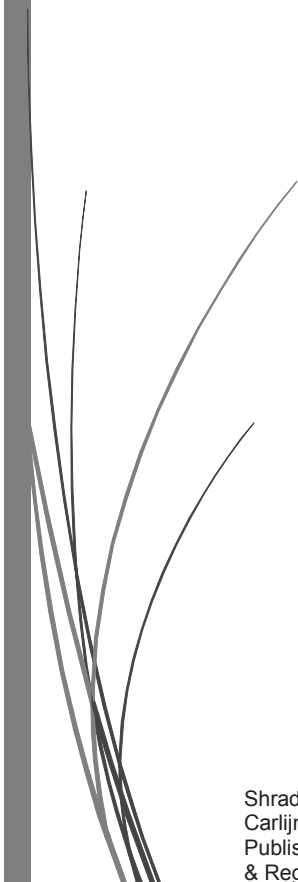


54. Ji, W., et al., *Bioactive Electrospun Scaffolds Delivering Growth Factors and Genes for Tissue Engineering Applications*. *Pharmaceutical Research*, 2011. **28**(6): p. 1259-1272.
55. Deshmane, S.L., et al., *Monocyte chemoattractant protein-1 (MCP-1): an overview*. *J Interferon Cytokine Res*, 2009. **29**(6): p. 313-26.
56. Talacua, H., et al., *In Situ Tissue Engineering of Functional Small-Diameter Blood Vessels by Host Circulating Cells Only*. *Tissue Engineering Part A*, 2015. **21**(19-20): p. 2583-2594.
57. Smits, A.I.P.M., et al., *Shear flow affects selective monocyte recruitment into MCP-1-loaded scaffolds*. *Journal of Cellular and Molecular Medicine*, 2014. **18**(11): p. 2176-2188.
58. Roh, J.D., et al., *Tissue-engineered vascular grafts transform into mature blood vessels via an inflammation-mediated process of vascular remodeling*. *Proceedings of the National Academy of Sciences of the United States of America*, 2010. **107**(10): p. 4669-4674.
59. Thevenot, P., et al., *The Effect of Incorporation of SDF-1 $\alpha$  into PLGA Scaffolds on Stem Cell Recruitment and the Inflammatory Response*. *Biomaterials*, 2010. **31**(14): p. 3997-4008.
60. Muylaert, D.E.P., et al., *Early in-situ cellularization of a supramolecular vascular graft is modified by synthetic stromal cell-derived factor-1 alpha derived peptides*. *Biomaterials*, 2016. **76**: p. 187-195.
61. Baiguera, S., et al., *Electrospun gelatin scaffolds incorporating rat decellularized brain extracellular matrix for neural tissue engineering*. *Biomaterials*, 2014. **35**(4): p. 1205-1214.
62. Francis, M.P., et al., *Electrospinning adipose tissue-derived extracellular matrix for adipose stem cell culture*. *Journal of Biomedical Materials Research Part A*, 2012. **100A**(7): p. 1716-1724.



Chapter 2

Porous Scaffolds using  
Dual electrospinning for  
in situ Cardiovascular  
Tissue Engineering



Shraddha Thakkar, Anita Driessen-Mol, Frank P.T.Baaijens and  
Carlijn V.C.Bouten.  
Published in Handbook of Intelligent Scaffolds for Tissue Engineering  
& Regenerative Medicine, Second Edition in May 2017

## Abstract

*In situ* cardiovascular tissue engineering is emerging as a promising approach for replacing diseased or damaged tissues by the use of biodegradable synthetic grafts. Functional porous scaffolds are implanted to create *in vivo* complex tissues that are functionally similar to their native counterparts. A biodegradable starter matrix permits cell infiltration and tissue formation at the site of implantation, while maintaining tissue mechanical and biological function. This chapter elaborates on the fabrication of porous scaffolds via the electrospinning technique, including advantages, as well as limitations of various approaches like single nozzle, dual nozzle, and coaxial electrospinning. The benefit of using dual electrospinning is distribution of function of each polymer. One polymer degrades slowly providing the necessary mechanical support and fast degrading polymer increases porosity and improves cell infiltration. In addition, optimization techniques for modifying the porosity of electrospun scaffolds are described, along with their influence on graft's mechanical properties and biodegradation rate.

## 2.1 Introduction

Cardiovascular Tissue Engineering (CVTE) aims at engineering living tissues that replace various components of the cardiovascular system, like blood vessels, heart valves or cardiac muscles. These engineered tissues replace completely or partially the diseased component, thereby helping to restore, regenerate and improve the functionality of the organ [1]. In the conventional approach, CVTE aims at harvesting autologous cells from the patient, *in vitro* proliferation, and subsequently seeding on a specially designed degradable scaffold [2]. This cell-scaffold construct then needs to be conditioned in a bioreactor, which transforms it into the desired tissue that can eventually be implanted in the patient [3]. This conventional approach is not only costly and time consuming, but the *in vitro* processing also increases the number of variables in an already complex procedure. Recent advances in CVTE have led to an *in situ* tissue engineering approach that utilizes the regenerative potential of the body itself to remodel and revive a synthetic implant [4-5], and eliminates the above-mentioned *in vitro* steps. This innovative approach offers the possibility of using synthetic 'off the shelf' starter matrices that can gradually transform into living tissues directly inside the body. Such a starter matrix, recruits endogenous cells upon implantation from the surrounding tissue (e.g. blood) to create a neo tissue at the host site [6-7]. This technique eliminates the need of cell harvest and tissue culture in the lab, thereby reducing the logistics and regulatory complexity and offering cost effective future therapies. A major challenge for *in situ* CVTE is to allow for guided tissue regeneration, by providing an appropriate structural and biological microenvironment by the implanted scaffold to facilitate cell migration and tissue formation [8-9]. Since this scaffold forms the framework in which the tissue develops under load bearing conditions, its design should also provide an optimal balance between mechanical stability and biodegradability. A key design feature of the scaffold is its porous architecture, which allows the cells to invade the scaffold, proliferate, and support extracellular matrix formation [10-13]. These requirements are understandably limited by the availability of

suitable biomaterials and fabrication techniques to process the materials into a micro- and nano-architecture [14-15]. A wide range of biomaterials has been identified for tissue engineering [16-18]. Choosing an appropriate material from such a list depends not only on the application, but also the versatility of the employed processing technique [19]. Dhandayuthapani et al. have listed the different types of scaffolds, including microsphere scaffolds, hydrogel scaffolds, and fibrous scaffolds along with their processing techniques [20]. Synthetic scaffolds for CVTE typically consist of fibrous scaffolds (shown in Figure 2.1) that promote selective cell recruitment, cell differentiation, and support tissue formation and remodeling. Amongst the mentioned techniques for fibrous scaffold development, electrospinning is the most widely studied approach and also exhibits the most promising results [21-25]. For example, electrospun tubular scaffolds which mimic the structure of blood vessels were successfully implanted in small animals with short follow up time [26-41]. This chapter elaborates on the different electrospinning techniques and the crucial parameters in respective approaches that have an influence on scaffold design. Specific attention is provided to dual electrospinning, which offers substantial benefits for manipulating porosity as opposed to conventional electrospinning.

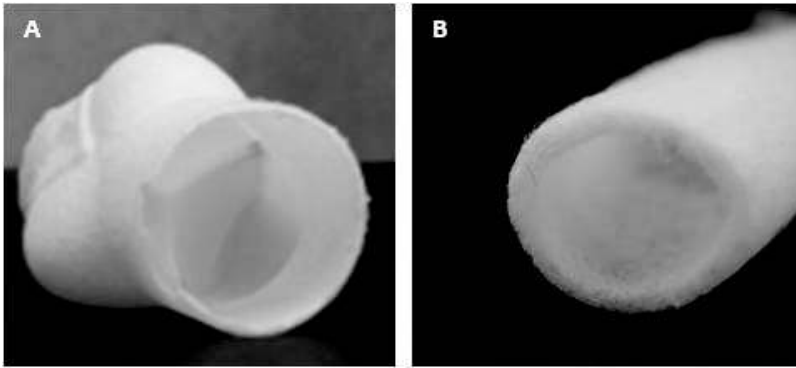


**Figure 2.1: Photographs of scaffolds fabricated by electrospinning Poly Caprolactone (PCL).** A) Electrospun scaffold demonstrating three dimensional structure of heart valve. B) Electrospun PCL mimicking the architecture of a blood vessel. (scale bar =100  $\mu\text{m}$ , Adapted from van Loon et al.

## 2.2 Electrospinning

The primary motivation behind the electrospinning technique is to generate a fibrous mesh that mimics the microenvironment of the native extracellular matrix (ECM) [42]. Collagen is the most abundantly found fibrous protein in the ECM, which is vital for the load bearing properties of cardiovascular tissues. Although other techniques, like molecular self-assembly or phase separation techniques can generate nanofibrous scaffolds [14, 43], unlike electrospinning, these conventional techniques neither mimic the native ECM structure, nor are able to control matrix porosity [44]. Electrospinning is capable of generating up to micrometer range fibers that are morphologically similar to native load bearing collagen bundles [45-50]. Further, the electrospun fibrous architecture encompasses a large surface to volume ratio that promotes cell ingrowth [51-52]. This approach has been widely used to electrospin a variety of materials including biodegradable, non degradable, natural, and synthetic polymers [53-54], making it very attractive for many biomedical applications [55-61].

### 2.2.1 Single nozzle electrospinning

A standard electrospinning apparatus consists of four major components: a syringe pump, a grounded target, a single spinneret (nozzle), and a high voltage power supply (Figure 2.2). During the electrospinning process, a high voltage is applied to the spinneret while the target (fiber collector) is grounded. This high voltage generates an electric field at the tip of the spinneret. A desired polymeric solution is held at the tip of the spinneret as a droplet, due to its inherent surface tension. Due to the subjected electric field, a charge is developed on the droplet and the electrostatic repulsion causes a force directly opposite to the surface tension. As the intensity of the electric field is increased, the droplet at the tip of the spinneret elongates to form a conical shape known as the Taylor cone [62]. Once the electrical field overcomes the surface tension of the polymer solution, a polymeric jet is ejected from the Taylor cone tip [63]. During the ejected jet travel, the solvent gradually evaporates and the electrostatic forces cause the charged polymer drop to stretch into a thin fiber, which is deposited onto the grounded target [63-64]. The properties of the deposited fibers can be optimized by controlling parameters like temperature and/or humidity of the spinning chamber, the horizontal motion of the spinneret and rotation of the target. In addition, customized scaffolds can be fabricated by depositing fibers on targets of different shapes like plates, discs and cylinders [65]. For instance, a cylindrical target would yield a synthetic tubular scaffold as shown in Figure 2.1B, which could mimic the structure of a blood vessel. Furthermore, the alignment of fibers can be altered by the rotation of the (cylindrical) target, to achieve the targeted structural morphology [66-69]. The morphology can be additionally adjusted by choice of an appropriate polymeric material. Table 2.1 provides an overview of the effects of conventional (single) electrospinning parameters on the electrospun fiber morphology [adapted from [70]].

Recently research is focused on blending different polymers with attractive properties; to create new enhanced hybrid scaffold materials. However, the lack of a common solvent for different polymers and variation in the electrospinning parameters such as concentration, viscosity, and applied

voltage for different polymers, makes it unfeasible to electrospin blends of polymeric solutions using a single nozzle set up. These limitations can be circumvented by transforming the single set up into dual or coaxial nozzle upon modification of nozzle /spinneret configuration. These two techniques, as outlined in the following sections, offer the additional possibility of varying the spinning parameters of individual polymers independently, thereby forming the desired hybrid composite. This further highlights the versatility and sustainability of the electrospinning technique, since the same setup can be employed to produce different scaffold configurations pertaining to the specific application or case.



Table 2.1: The effect of various parameters on morphology of electrospun fiber.

Processing parameters	Effect on fiber morphology
Flow rate	Low flow rate yields fibers with <b>smaller diameter</b> and fibers without beads [71] and high flow rate forms <b>fibers</b> that are <b>not dry</b> when they reach the collector as the solvent may not completely evaporate [72-73].
Voltage	High voltage is mentioned to favour smooth fibers formation with a <b>low/small fiber diameter</b> [71, 74-75], while ambiguous correlation between voltage and fiber diameter is also stated [76].
Distance between needle and target	A certain minimum distance is required to obtain drying of the fibers before reaching the collector. If the distance is too small, <b>wet fibers</b> will be collected at the target [77-78]. If the distance is too large, <b>beads will be formed</b> [79], depends on the material.
Collectors	Shape and size of collectors affect the fiber <b>morphology and orientation</b> [80-81]. Speed of rotation of collectors helps to induce <b>fiber alignment</b> [82].
Solution parameters	Effect on fiber morphology
Molecular weight of polymer	The fiber <b>diameter increases</b> with increasing molecular weight [83-84].
Viscosity	Low viscosity results in <b>spraying of the solution</b> and the <b>formation</b> of a large number of <b>beads</b> during spinning [85-86].
Concentration of polymer	An increasing concentration changes the <b>fiber morphology</b> from beaded fibers to uniform fibers [87-89].
Surface tension	While keeping the concentration constant, reducing surface tension results in the <b>formation of smooth fibers</b> rather than beaded fibers [90-91].
Conductivity / Surface charge density	Increasing the solution conductivity results in a higher surface charge that favours the formation of <b>fibers with a smaller diameter</b> [92-93].
Ambient Parameters	Effect on fiber morphology
Temperature	Increasing temperature (until a certain maximum) results in <b>smaller fiber diameter</b> [94-95].
Humidity	Increasing humidity results in <b>large fiber diameter</b> (due to reduction in stretching forces) [95-96].

---

### 2.2.2 Dual nozzle electrospinning

Dual nozzle electrospinning employs two nozzles (connected with individual power supplies) which function simultaneously, as shown in Figure 2.3. This technique offers the possibility of combining a variety of polymers to make a composite scaffold based on customized requirements. At each nozzle, polymeric solutions prepared in independent solvents can be electrospun at the same time to fabricate a hybrid scaffold. This offers the extra degree of freedom of being able to adjust the electrospinning parameters for individual polymers at each nozzle. Furthermore, the ratio of the polymers as well as the distribution of the electrospun fibers in the scaffolds can be controlled by varying individual polymer concentration during dual electrospinning [97-99]. Zhan et al. fabricated bead-on-string and microfiber morphology to prepare super hydrophobic polystyrene (PS) meshes [100]. The mechanical property of the PS meshes was controlled by altering the mass ratio of the bead-on-string and the microfibers. In another study, the mass ratio of Polyacrylonitrile (PAN) nanofibers to Polyamide 66 (PA-66) microfibers was tuned to improved tensile strength compared to PAN nanofibers [101].

Besides optimizing the ratio of polymers, the distance between nozzles, and applied voltage also have an effect on the resulting fiber diameter, morphology, and distribution [102-103]. Fiber properties can also be affected by the configuration of the nozzle. Studies focused on different nozzle/spinneret configurations, such as opposite [104-105], or angled configurations [106-108], have been conducted. It is possible to use more nozzles simultaneously; however this is not common practice. Three nozzle configurations have been employed twice till now. In one of the study, three nozzles were placed at an angular configuration of 90, 100, and 180 degrees. This study demonstrated that the fiber diameter of the electrospun fibers can be controlled by selecting the nozzle configuration, while maintaining all other parameters [109]. Another study three nozzle configuration was used to control and vary the ratio of polymers deposited on the target [110]. Mechanical properties of the scaffold were retained after selective removal of a polymer.

Dual nozzle electrospinning provides an opportunity to incorporate multiple biological cues in hybrid scaffolds. The degradation of the individual polymers subsequently results in release of these incorporated biological cues. For example, Wang et al. fabricated novel bicomponent scaffolds for bone tissue engineering consisting of recombinant human bone morphogenetic protein (rhBMP-2) and calcium phosphate (Ca-P) particles to modulate osteoinductivity and osteoconductivity [111]. Poly (D, L-lactic acid) (PDLLA) containing rhBMP-2 was electrospun at one nozzle and poly (lactico-glycolic acid) (PLGA) with Ca-P particle at the other. The ratio of the two scaffold components was varied to modulate the release of rhBMP-2 and control scaffold degradation. This technique prevents the interaction between the loaded drugs compared to single nozzle electrospinning. Therefore, dual nozzle electrospinning is a suitable method to prepare multi drug-loaded scaffolds [112].

Another motivation to select dual nozzle electrospinning over single nozzle is to increase the porosity of the hybrid scaffold by selective removal of a polymer, as discussed in detail in section 1.5.6. Furthermore, the dual nozzle technique has shown to increase the production compared to the single nozzle, important for future commercialization [113].

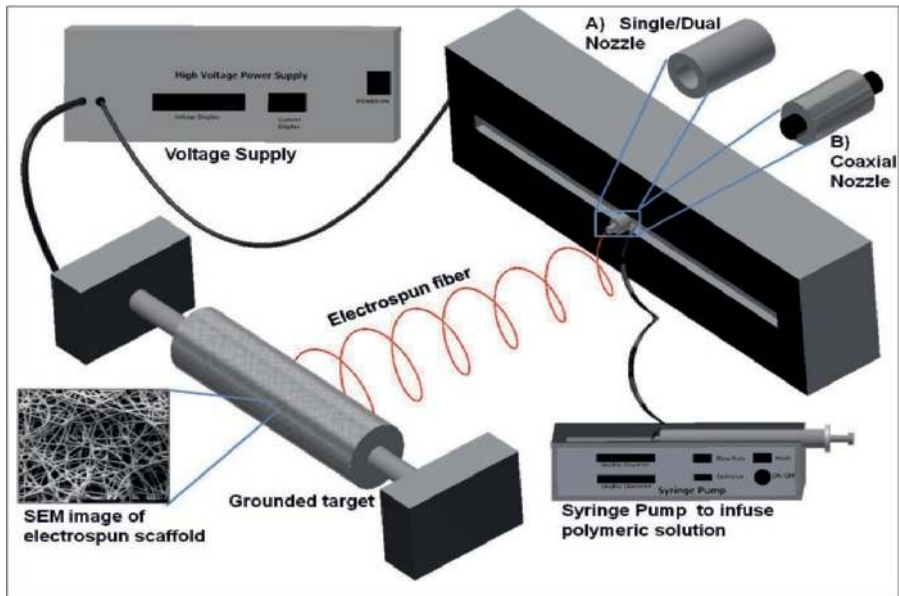


**Figure 2.2:** Electrospinning set up with high voltage power supply, syringe pump, target and spinneret for electrospinning A) single/dual and B) coaxial. The scanning electron microscope image of electrospun scaffold shows the structure and orientation of the fiber. Scale bar = 200 $\mu$ m

### 2.2.3 Coaxial nozzle electrospinning

The standard electrospinning set up can be modified by replacing a single nozzle with a coaxial nozzle, consisting of two concentrically aligned needles [Figure 2.2B displaying coaxial needle]. The unique property of this technique is to fabricate a single polymeric fiber composed of two different simultaneously spun polymers [114-116]. The fabricated fiber structure consists of a core-shell assembly. Of the two polymers, one of the polymer forms the core structure and other forms the shell around the core polymer [117]. The property of this core-shell assembly can be altered by changing the electrospinning parameters. Zhang et al. fabricated PCL and gelatin nano

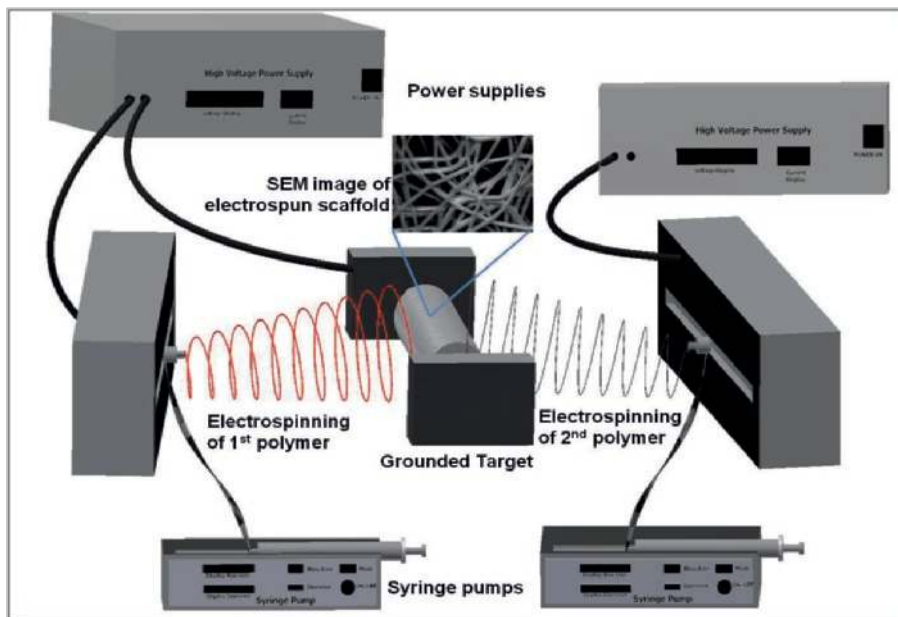


**Figure 2.3: Dual nozzle electrospinning set up:** It consists of a common grounded target in the center and on either sides of the target different polymers are electrospun using high voltage power supply, syringe pump, and spinneret. SEM images demonstrates the morphology of electrospun fibers. Scale bar = 200μm

fibrous scaffolds using coaxial electrospinning [118]. By varying the concentration of the gelatin in the inner core, an increase in core diameter, as well as overall diameter, was observed. Besides using different polymers to fabricate a single fiber, it is possible to use identical/ similar polymers. However, using identical polymers makes it difficult to distinguish between the core-shell structures. Different concentrations of bromophenole were co-spun to form nano fibers [119]. Variation in the concentration helped to gain optical contrast to view the core shell assembly clearly. Furthermore, this technique can be applied to fabricate hollow fibers, by treating the core-shell assembly to carefully remove the core fiber. Li et al. demonstrated formation of core/sheath and hollow fibers by coaxial electrospinning of two immiscible liquids [120]. The formation of continuous and uniform fibers relies on the immiscibility of the liquids. By incorporating drugs to the core-shell assembly, drug delivery systems can also be developed [121-124]. Coaxial

electrospinning depends on same parameters as single nozzle electrospinning. However the difference in viscosity, conductivity and solidification of polymers, may influence the electrospinning process [125]. Thus the selection of the material is critical to obtain the required fibers.

## **2.3 Cell infiltration into electrospun scaffolds**

The success of a 3D tissue engineering scaffold relies on its integration into the host tissue. This integration can be facilitated by mimicking the native matrix microenvironment and enhancing cell infiltration into the scaffold. Fibrous electrospun scaffolds are attractive as the fibers are morphologically similar to the collagen bundles found in native ECM [126]. The 3D microenvironment created by the electrospun fibers promotes cell attachment and proliferation. However, limited cell infiltration throughout the electrospun scaffold was reported in several studies [127-130]. In-depth research indicates that structural organization plays a vital role in cell migration [131-133]. Reports suggest that orientation of the fibers and the fiber diameter influences cell behavior [134-136]. It has been demonstrated that electrospun scaffolds with a large fiber diameter form larger pores due to the loose packing of the fibers, therewith providing sufficient void space for cells to penetrate [137]. In contrast, poor cell penetration was observed with nanometer fiber diameter [127, 138]. To foster cell infiltration, methods have been developed to increase porosity of the scaffolds; details explained in paragraph 1.5. To improve *in vitro* cell infiltration, dynamic seeding methods [139-140] in combination with a flow perfusion bioreactor system were suggested [141-143]. In addition, the influence of the orientation of electrospun fibers on cell response is discussed in the next paragraph.

## **2.4 Scaffold (An) Isotropy**

The spatial organization of electrospun fibers is a significant parameter for scaffold integrity, porosity, stability, as well as cell behaviour [144]. Numerous methods have been developed to fabricate a variety of biomimetic fibrous

scaffolds with tuned orientation [145-147]. Modifications of the traditional electrospinning technique rendered possibilities to produce scaffolds with controlled fiber orientation [70, 148-149]. For instance, fiber alignment can be manipulated by employing a rotating mandrel (modification of the target) [148, 150], controlling the motion of the mandrel [151-152], and by controlling the electric field [153]. The resulting fiber orientation enables to modulate the cell interaction with the scaffold through contact guidance (i.e. cellular response to alignment of fibers in its surrounding). The effect of fiber orientation (i.e. random or aligned fibers) on meniscal fibrochondrocytes (MFCs) or mesenchymal stem cells (MSC) was studied [154]. Results demonstrated significantly better mechanical properties for aligned scaffolds compared to random scaffolds although cellularity and ECM production were similar for both scaffolds. Furthermore, the aligned electrospun fibers induce alignment and cause elongation of the cells [155-156]. Rockwood et al studied the impact of alignment of fibers on cardiac cell phenotype [144]. Primary cardiac ventricular cells were grown on polyurethane (ES-PU) electrospun scaffolds with either aligned or unaligned microfibers. Atrial natriuretic peptide (ANP) a critical marker for the molecular phenotype was significantly reduced in cultures grown on aligned scaffold compared to unaligned scaffolds. The structural alignment of electrospun fibers affected cell phenotype and cell organization. In addition, studies have demonstrated the influence of anisotropically oriented fibers on cell orientation, referred to as directional growth [157-161]. Kai et al. have compared aligned and random electrospun polycaprolactone/gelatin scaffolds as cardiac grafts [162]. Rabbit cardiomyocytes grown on these scaffolds preferred an anisotropic architecture that provides contact guidance cues for their growth and alignment. In another study, primary cardiomyocytes were cultured on electrospun scaffolds fabricated from poly (L-lactic acid) (PLLA) and PLGA [163]. It was shown that porous scaffolds with aligned fibers provided guidance for cell growth. It is noteworthy to realize that orientation and morphology of the fibers are relevant for the mechanical properties of the scaffold. Thomas et al. showed a decrease in stiffness and young's modulus

of fibers with an increase in alignment of fibers, whereas uni-axial tensile properties of scaffolds increased with increasing collector rotation speed [164]. In addition, the uniaxial bulk tensile strength (along fiber alignment) increased with an increase in alignment. Besides the fiber orientation, cell behavior may be influenced by the microstructural stiffness of the scaffold [165-166]. It is important to note that the fiber anisotropy is expected to impact the pore dimensions and macroscopic properties of the scaffold, which are discussed later in this chapter.

## **2.5 Controlling scaffold porosity**

The small dimensions of pores in electrospun scaffolds are a known limitation of electrospun scaffolds, hindering penetration of the cells [167-172]. In particular parallel (aligned) orientation of fibers in one direction as discussed in the previous paragraph, minimizes the space between fibers, thereby reducing the pore size [164]. A direct correlation between cell infiltration and fiber diameter was demonstrated, indicating that pore size should be tailored in accordance to cell type [173-174]. *In vitro* and *in vivo* cell studies support increased cell infiltration with increase in porosity [175-177]. Therefore, increasing the porosity of the electrospun scaffolds will improve cell infiltration [173, 178-179]. Several methods are reported to improve the porosity of the electrospun scaffolds [60, 180-181], including tuning of the electrospinning parameters mentioned in Table 2.1, tailoring collectors, low temperature or cryogenic electrospinning, multimodal fiber electrospinning, salt leaching, and selective removal of sacrificial polymers after dual electrospinning. These methods are outlined in the following paragraphs.

### **2.5.1 Increasing Fiber Diameter**

Tuning porosity is an intricate interplay between material properties and spinning parameters. The simplest and most common used technique to increase porosity of scaffold is by increasing the fiber diameter [182-185]. A direct relation between pore size and fiber diameter was predicted by statistical modeling [186]. Balguid et al. demonstrated an increase in cell



infiltration in scaffolds with larger fiber diameter [173]. Alterations in individual electrospinning parameters affect the fiber diameter, as summarized in Table 2.1, which in turn causes changes in the porosity of the scaffold. For example, increasing the flow rate during electrospinning is an indirect way of controlling porosity. Synthetic human elastin electrospun at high (3 ml/h) flow rate resulted in an increased fiber diameter, pore size, and porosity compared to lower (1 ml/h) flow rate [187].

### **2.5.2 Tailoring collectors**

Recent studies showed that tailoring the geometry or pattern of the collectors is an effective way to increase porosity of the scaffold [188]. It is believed that the pore size distribution depends on the void gap in the collector [189-190]. Introduction of a non-conductive gap in the collector changes the external shape of the electrostatic field. The perturbation of the electrostatic field results in specific orientation of fibers. Li et al studied the effect of the area and geometric shape of the void gap on deposition of fibers [191]. Collectors were designed with varying void gap geometries like round, square, triangle and rectangle, to obtain certain degree of orientation of the fibers. Electrospun fibers accurately followed the pattern of the collector, therewith increasing the porosity of the scaffold [189, 192]. The patterned collectors attracted more fibres to the conductive zones of the collector, resulting in significant differences in the number of fibres deposited in certain regions. Furthermore, Zhu et al. developed a collector consisting of a rotating frame cylinder with metal struts to extend the pore size and increase the porosity of scaffolds [177]. Due to the electrostatic forces, higher density fibers were deposited on the struts and lesser density fibers were deposit between the struts, thereby, increasing the porosity of the mesh. An increase in dermal fibroblasts viability, collagen deposition, cell migration, and infiltration was observed when seeded into these porous electrospun scaffolds.

### 2.5.3 Low temperature or cryogenic electrospinning

Low temperature, or cryogenic spinning, is a technique in which ice crystals are used as spacers to increase the degree of porosity of the scaffold. Simonet et al. increased humidity during spinning to facilitate the precipitation of ice crystals (from humid air) onto the collector surface and co-depositing the polymer mesh [193]. The scaffold deposited on the chilled collector is subsequently dried, resulting in a scaffold with macropores between the fibers. A series of humidities was assessed to measure the deposition of ice crystals and its influence on the mesh density and porosity of the scaffold. Higher difference in scaffold porosity was observed at higher humidity; however humidity higher than 30% did not significantly affect the mesh density. *In vitro* cell studies showed improved cell infiltration on natural silk scaffolds fabricated using cryogenic spinning [194]. In another study, Leong et al. fabricated porous poly(D, L-lactic) (PLA) scaffolds using cryogenic spinning and demonstrated increased cell infiltration into porous scaffolds compared to non-porous conventional scaffolds *in vitro*, as well as *in vivo* [172]. Though cryogenic spinning represents a promising technique to increase porosity of a scaffold, it remains difficult to control the pore size and homogeneity of pore formation throughout the scaffold [195].

### 2.5.4 Multimodal fiber electrospinning

Multimodal fiber electrospinning features the fabrication of scaffolds by combining two or more fiber populations. The scaffold consists of sequential layers of micrometer and nanometer fibers, inheriting the advantages of a wide range of fiber populations [196]. A proof of concept was demonstrated for a bimodal scaffold consisting of two fiber populations, with a distribution of 600 nm and 3.3  $\mu\text{m}$ . In the bimodal scaffold, the nanofibers bridged the neighbouring microfibers which improved cell infiltration and mechanical properties over conventional scaffold [197]. Subsequent *in vitro* cell studies demonstrated improved cell viability [198] and altered cell morphology on multimodal fibrous scaffolds [199]. The thickness of the layers can be tuned by varying the electrospinning time. Increasing the thickness of nanofibrous

layers enhanced cell spreading but did not improve cell attachment and reduced cell infiltration under static and perfusion flow conditions. Ju et al. tuned the mechanical properties of the scaffold by varying fiber diameter, therewith regulating cellular interactions [200]. Bi-layered poly ( $\epsilon$ -caprolactone) (PCL) and collagen scaffolds (0.27 to 4.45 $\mu$ m) were fabricated consisting of small pores at the lumen and larger pores on the outer side. The larger pores enhanced smooth muscle cells infiltration and the smaller pores improved endothelial cell attachment on the lumen. It is necessary to optimize a balance between the layers microstructure helps enhance cell infiltration and nanofibrous structure helps to gain stability [138].

The salt leaching technique is based on the simple principle of including salt particles in the polymeric solution while electrospinning. The particles are subsequently leached out to form porous scaffolds. The pore size, as well as porosity, can be controlled by size and concentration of the salt particles in the solution [201]. Nam et al. fabricated scaffolds by incorporation of salt particles in a PCL solution at specific depositional intervals during electrospinning to increase porosity [179]. In another study, a scaffold with nanosized pores was fabricated by dispersing nanosized calcium carbonate particles in the PCL solution, followed by salt leaching [202]. The size and dispersion of salt had a significant effect on the pore size and pore distribution. Particles, such as sucrose [203-204] or gelatin [205-206], are alternatives to salt and can be used to induce similar effects.

### **2.5.5 Selective removal of polymer**

Hybrid scaffolds, based on two polymers, can be produced with the intent to retain one of the spun polymers and dissolve the other. The polymer to be removed, referred to as the sacrificial polymer, will create void space within the scaffold after removal, resulting in larger pores and improved porosity [207-208]. Dual nozzle electrospinning can be used for fabrication of hybrid scaffolds as discussed earlier. Skotak et al. dual spun gelatin with poly ethylene glycol (PEG) [209]. After fabrication, the gelatin was crosslinked with glutaraldehyde and the PEG was dissolved in tert-butanol. The resulting

gelatin/PEG scaffolds consisted of 10 to 100 $\mu$ m pores. An increase in porosity was observed when compared to the reference pure gelatin scaffolds with 1 $\mu$ m pores. A subsequent *in vitro* cell study demonstrated cell infiltration up to 250 $\mu$ m in the gelatin/PEG scaffolds compared to 90 $\mu$ m in pure gelatin scaffolds. In another study, the pore size was altered by increasing the ratio of sacrificial polymer. Baker et al. dual spun poly caprolactone (PCL) with poly ethylene oxide (PEO) to produce composite fibrous aligned scaffolds and controlled the pore size of the scaffold with increasing PEO content [210]. When seeded with mesenchymal stem cells (MSC), the pure PCL scaffold showed only cells lining the periphery, while PCL scaffolds with an equal ratio of PEO showed cell penetration throughout the scaffold. Another alternative is spinning of both polymers to form a multilayered scaffold [208] and then remove the sacrificial polymer. Reports suggest that varying the concentration of the sacrificial polymer helps to adjust the pore size [211-212] and the resulting mechanical properties [213-214]. Horst et al. dual spun PLGA/PEG scaffolds and investigated cell infiltration after PEG removal both *in vitro* and *in vivo* [176]. The porosity of scaffolds increased after extraction of PEG compared to scaffolds spun without PEG. The *in vitro* cell study demonstrated significantly higher cell penetration into PLGA/PEG and the *in vivo* study showed increased micro vessel density in the PLGA/PEG scaffolds. Aligned nanofibrous PCL/PEO scaffolds with increasing fractions of sacrificial polymer were developed and human meniscus fibro-chondrocytes were cultured for 12 weeks onto these scaffolds [110]. Though the mechanical functionality of such scaffolds is hampered by the increased porosity, it was observed that ECM deposited by the cells helped to increase the tensile strength of the scaffold almost equivalent to native tissue. In addition, by taking advantage of the removal of sacrificial polymer, researchers have applied this technique for the release of drug or proteins [215-216].

### **2.5.6 Comparison of techniques**

In order to find the most effective approach to increase pore size, several researchers have compared different techniques. In a study by Phipps et al.,

three techniques were analyzed, including protease digestion, reducing fiber density, and sacrificial removal of a polymer, to enlarge the pores of PCL, collagen I, and nanoparticulate hydroxyapatite [217]. Sacrificial removal of polymer showed the best results for pore size, as well as cell infiltration. If variation of fiber diameter was compared with removal of sacrificial polymer, contradictory results were obtained. Infiltration of neuron like PC12 cells was increased in scaffolds with a range of PCL fiber diameters and reduced in PCL scaffolds after removal of PEO [218]. The most appropriate approach depends on the type of the technique compared, the cell line used, and on the specific application.

## **2.6 Mechanical properties and degradation rate**

The scaffold should be able to withstand the load at the site of implantation and its degradation rate should coincide with the rate of new tissue formation. It is critical to reach a balance depending on the repair, remodeling of the neo tissue, and degradation rate of the material. Increasing porosity of the scaffold favors cell infiltration. However, porosity has an impact on the mechanical properties as well as the degradation of the scaffold [219-222].

A crucial parameter for scaffolds mechanical properties is the choice of material. The selection of the polymer is based on the intended biomedical application. Hasan et al. gives an overview of mechanical properties of scaffolds electrospun using different polymers for TE vascular grafts [223]. Tubular scaffolds can be characterized by uniaxial tensile tests, suture retention tests, burst strength assessment, and compliance testing [52, 223-226]. There are several other parameters including pore size, physiological environment, molecular weight, and composition of the polymer [227] that influence the tensile properties of the scaffold. A computational model to predict the effects of porosity is provided by Zhang et al. [228]. In addition to porosity, changing the microstructural parameters, such as fiber diameter [229], orientation or spatial distribution of fibers, helps to control the mechanical properties [223, 230-231]. In another study, the mechanical

properties were controlled by fiber alignment and rotational speed of the collecting target (mandrel) [164, 232].

*In vitro* biodegradation [233] and hydration of scaffolds in PBS [234], as well as encapsulation of drugs or proteins [205, 235], also affect the mechanical properties of the scaffold. Mechanical loading in turn influences degradation rate of scaffolds as accelerated degradation was observed of scaffolds subjected to mechanical loading [236-238]. Properties of electrospun PLGA scaffolds were examined under different tensile loads and compared to that under no load. The molecular weight, thermal properties, and lactic acid release demonstrated faster degradation under loading conditions [236].

Degradation of the scaffold affects the host response during tissue formation [239]. In an ideal *in vivo* scenario, scaffold degradation and tissue formation should be complementary [240]. Tubular electrospun implants in mice induced a foreign body response, in favor of tissue growth [241]. However, the acidic environment due to the degradation products affected cell invasion [240]. Scaffolds fabricated with PLGA degrade by hydrolysis and generate acidic products that limit cell mobilization and reduced angiogenesis when compared to PCL scaffolds [240]. To circumvent this limitation, nano-apatitic particles (nAp) were incorporated into PLGA scaffolds. Scaffolds with nAp showed a delay in polymer degradation and an amount dependent effect on pH. A 4 week *in vivo* implantation confirmed an improved host response [242]. Dong et al. focused on understanding the degradation mechanism of electrospun polyester nanofibers [243]. In order to control degradation different pathways including surface and bulk degradation were studied [244-245]. Other possible options to control degradation include blending polymer ratios and stimulating physiological conditions [244, 246-249]. A variation in degradation rate may be advantageous for release of bioactives incorporated in microspheres within the scaffold [250-251]. In summary, the mechanical properties and degradation of the biomaterial are critical determinants for the success of the implant [252-253].

## 2.7 Conclusion and Future Outlook

This chapter provides insight into various electrospinning techniques for fabrication of scaffolds. The selection of the technique depends on the polymer and the application. For *in situ* CVTE one needs to harness and modulate the inflammatory response of the scaffold to support tissue regeneration. The scaffold design, in terms of material selection, stiffness, porosity and anisotropic architecture, may assist in obtaining the appropriate host response. The dual electrospinning technique is of interest for CVTE to generate a fibrous network mimicking the native microenvironment, while providing sufficient strength for the demanding hemodynamic environment and space for invading cells. With this technique hybrid scaffolds can be fabricated using two polymers. Each polymer executes separate function. One of the polymers can be loaded with bioactives to control cell recruitment and proliferation, while the other supplies mechanical strength. The properties of the electrospun fibrous network depend on the polymer selected. The porosity of the scaffold can be enhanced by selectively removing one of the polymers, thereby enhancing cell infiltration. Controlling fiber orientation may further help to manipulate tissue structure via contact guidance and, therewith, improve functionality of the eventually developing tissue.

To ensure selective recruitment of cells, bioactive moieties, such as growth factors and cytokines, can be incorporated into the polymer to create a bio hybrid scaffold. Upon fast degradation of the polymer, the incorporated moieties will be release from the scaffold, which will promote target cell recruitment, repopulate the scaffold and support tissue formation. The effect of porosity and an anisotropic structure on the mechanical properties and degradation rate depends on the polymer. Thus, microscopic and macroscopic properties of bio hybrid scaffold along with its interaction with cells and the subsequent effect on the host response will together determine the success of the scaffold.

---

## References

1. Langer, R. and J.P. Vacanti, Tissue Engineering. Science, 1993. 260(5110): p. 920-926.
2. Rabkin, E. and F.J. Schoen, Cardiovascular tissue engineering. Cardiovascular Pathology, 2002. 11(6): p. 305-17.
3. Stock, U.A. and J.P. Vacanti, Tissue engineering: Current state and prospects. Annual Review of Medicine, 2001. 52: p. 443-451.
4. Li, S., D. Sengupta, and S. Chien, Vascular tissue engineering: from *in vitro* to *in situ*. Wiley Interdisciplinary Reviews-Systems Biology and Medicine, 2014. 6(1): p. 61-76.
5. Ko, I.K., et al., *In situ* tissue regeneration through host stem cell recruitment. Experimental and Molecular Medicine, 2013. 45.
6. Loon, S.L.M.v., et al., The Immune Response in *In Situ* Tissue Engineering of Aortic Heart Valves. 2013.
7. Bouten, C.V., A. Driessen-Mol, and F.P. Baaijens, *In situ* heart valve tissue engineering: simple devices, smart materials, complex knowledge. Expert Review of Medical Devices, 2012. 9(5): p. 453-455.
8. Dijkman, P.E., et al., Decellularized homologous tissue-engineered heart valves as off-the-shelf alternatives to xeno- and homografts. Biomaterials, 2012. 33(18): p. 4545-4554.
9. Bouten, C.V.C., et al., Substrates for cardiovascular tissue engineering. Advanced Drug Delivery Reviews, 2011. 63(4-5): p. 221-241.
10. Hollister, S.J., Porous scaffold design for tissue engineering. Nature Materials, 2005. 4(7): p. 518-524.
11. Shalumon, K.T., et al., Fabrication of three-dimensional nano, micro and micro/nano scaffolds of porous poly(lactic acid) by electrospinning and comparison of cell infiltration by Z-stacking/three-dimensional projection technique. Iet Nanobiotechnology, 2012. 6(1): p. 16-25.
12. Hu, J.A., et al., Porous nanofibrous PLLA scaffolds for vascular tissue engineering. Biomaterials, 2010. 31(31): p. 7971-7977.
13. Cipitria, A., et al., Porous scaffold architecture guides tissue formation. Journal of Bone and Mineral Research, 2012. 27(6): p. 1275-1288.
14. Lu, T.L., Y.H. Li, and T. Chen, Techniques for fabrication and construction of three-dimensional scaffolds for tissue engineering. International Journal of Nanomedicine, 2013. 8: p. 337-350.
15. Naderi, H., M.M. Matin, and A.R. Bahrami, Review paper: Critical Issues in Tissue Engineering: Biomaterials, Cell Sources, Angiogenesis, and Drug Delivery Systems. Journal of Biomaterials Applications, 2011. 26(4): p. 383-417.
16. Lam, M.T. and Joseph C. Wu, Biomaterial applications in cardiovascular tissue repair and regeneration. Expert Review of Cardiovascular Therapy, 2012. 10(8): p. 1039-1049.
17. Jaganathan, S.K., et al., Biomaterials in Cardiovascular Research: Applications and Clinical Implications. Biomed Research International, 2014. 2014: p. 11.
18. O'Brien, F.J., Biomaterials & scaffolds for tissue engineering. Materials Today, 2011. 14(3): p. 88-95.
19. Chan, B.P. and K.W. Leong, Scaffolding in tissue engineering: general approaches and tissue-specific considerations. European Spine Journal, 2008. 17(4): p. 467-479.
20. Dhandayuthapani, B., et al., Polymeric Scaffolds in Tissue Engineering Application: A Review. International Journal of Polymer Science, 2011.
21. Kumbar, S.G., et al., Electrospun nanofiber scaffolds: engineering soft tissues. Biomedical Materials, 2008. 3(3).
22. Shamnugasundaram, S., et al., Applications of electrospinning: Tissue engineering scaffolds and drug delivery system. Proceedings of the IEEE 30th Annual Northeast Bioengineering Conference, 2004: p. 140-141.
23. Nair, L.S., S. Bhattacharyya, and C.T. Laurencin, Development of novel tissue engineering scaffolds via electrospinning. Expert Opinion on Biological Therapy, 2004. 4(5): p. 659-668.



24. Khil, M.S., et al., Novel fabricated matrix via electrospinning for tissue engineering. *Journal of Biomedical Materials Research Part B-Applied Biomaterials*, 2005. 72B(1): p. 117-124.
25. Lannutti, J., et al., Electrospinning for tissue engineering scaffolds. *Materials Science & Engineering C-Biomimetic and Supramolecular Systems*, 2007. 27(3): p. 504-509.
26. Nottelet, B., et al., Factorial design optimization and *in vivo* feasibility of poly(epsilon-caprolactone)-micro- and nanofiber-based small diameter vascular grafts. *Journal of Biomedical Materials Research Part A*, 2009. 89A(4): p. 865-875.
27. de Valence, S., et al., Long term performance of polycaprolactone vascular grafts in a rat abdominal aorta replacement model. *Biomaterials*, 2012. 33(1): p. 38-47.
28. Mrowczynski, W., et al., Porcine carotid artery replacement with biodegradable electrospun poly-epsilon-caprolactone vascular prosthesis. *Journal of Vascular Surgery*, 2014. 59(1): p. 210-219.
29. Pektok, E., et al., Degradation and Healing Characteristics of Small-Diameter Poly(epsilon-Caprolactone) Vascular Grafts in the Rat Systemic Arterial Circulation. *Circulation*, 2008. 118(24): p. 2563-2570.
30. Innocente, F., et al., Paclitaxel-Eluting Biodegradable Synthetic Vascular Prostheses A Step Towards Reduction of Neointima Formation? *Circulation*, 2009. 120(11): p. S37-S45.
31. Wise, S.G., et al., A multilayered synthetic human elastin/polycaprolactone hybrid vascular graft with tailored mechanical properties. *Acta Biomaterialia*, 2011. 7(1): p. 295-303.
32. He, W., et al., Tubular nanofiber scaffolds for tissue engineered small-diameter vascular grafts. *Journal of Biomedical Materials Research Part A*, 2009. 90A(1): p. 205-216.
33. Cattaneo, I., et al., *In vivo* regeneration of elastic lamina on fibroin biodegradable vascular scaffold. *International Journal of Artificial Organs*, 2013. 36(3): p. 166-174.
34. Soletti, L., et al., *In vivo* performance of a phospholipid-coated bioerodable elastomeric graft for small-diameter vascular applications. *Journal of Biomedical Materials Research Part A*, 2011. 96A(2): p. 436-448.
35. Hong, Y., et al., A small diameter, fibrous vascular conduit generated from a poly(ester urethane)urea and phospholipid polymer blend. *Biomaterials*, 2009. 30(13): p. 2457-2467.
36. Zheng, W.T., et al., Endothelialization and patency of RGD-functionalized vascular grafts in a rabbit carotid artery model. *Biomaterials*, 2012. 33(10): p. 2880-2891.
37. Kuwabara, F., et al., Novel Small-Caliber Vascular Grafts With Trimeric Peptide for Acceleration of Endothelialization. *Annals of Thoracic Surgery*, 2012. 93(1): p. 156-163.
38. Hashi, C.K., et al., Antithrombogenic Modification of Small-Diameter Microfibrous Vascular Grafts. *Arteriosclerosis Thrombosis and Vascular Biology*, 2010. 30(8): p. 1621-1627.
39. Yu, J., et al., The effect of stromal cell-derived factor-1 alpha/heparin coating of biodegradable vascular grafts on the recruitment of both endothelial and smooth muscle progenitor cells for accelerated regeneration. *Biomaterials*, 2012. 33(32): p. 8062-8074.
40. Walpoth, B.H., et al., Biodegradable small calibre polydioxanone-based vascular prostheses: Potential as coronary bypass grafts. *Circulation*, 2007. 116(16): p. 444-444.
41. de Valence, S., et al., Advantages of bilayered vascular grafts for surgical applicability and tissue regeneration. *Acta Biomaterialia*, 2012. 8(11): p. 3914-3920.
42. Wang, X.F., B. Ding, and B.Y. Li, Biomimetic electrospun nanofibrous structures for tissue engineering. *Materials Today*, 2013. 16(6): p. 229-241.
43. H. Chen, R.T., C. van Blitterswijk and L. Moroni, Fabrication of nanofibrous scaffolds for tissue engineering applications *Nanomaterials in tissue engineering*, 2013. 56: p. 158-182.
44. Murugan, R. and S. Ramakrishna, Nano-featured scaffolds for tissue engineering: A review of spinning methodologies. *Tissue Engineering*, 2006. 12(3): p. 435-447.
45. Ramachandran, K. and P.I. Gouma, Electrospinning for Bone Tissue Engineering. *Recent Patents on Nanotechnology*, 2008. 2(1): p. 1-7.

46. Thorvaldsson, A., et al., Electrospinning of highly porous scaffolds for cartilage tissue engineering. *Tissue Engineering Part A*, 2008. 14(5): p. 845-846.
47. Martins, A., R.L. Reis, and N.M. Neves, Electrospinning: processing technique for tissue engineering scaffolding. *International Materials Reviews*, 2008. 53(5): p. 257-274.
48. Liu, H.F., et al., Electrospinning of Nanofibers for Tissue Engineering Applications. *Journal of Nanomaterials*, 2013.
49. Chen, R., et al., Fabrication Tissue Engineering Heart Valve Leaflet Scaffold Using Complex Electrospinning Method. 2010 International Forum on Biomedical Textile Materials, Proceedings, 2010: p. 261-266.
50. Greiner, A. and J.H. Wendorff, Electrospinning: A fascinating method for the preparation of ultrathin fibres. *Angewandte Chemie-International Edition*, 2007. 46(30): p. 5670-5703.
51. Agarwal, S., J.H. Wendorff, and A. Greiner, Use of electrospinning technique for biomedical applications. *Polymer*, 2008. 49(26): p. 5603-5621.
52. Li, W.J., et al., Electrospun nanofibrous structure: A novel scaffold for tissue engineering. *Journal of Biomedical Materials Research*, 2002. 60(4): p. 613-621.
53. Lorenz, H.P. and J.-C. Wu, Electrospinning of Biomaterials and their applications in Tissue Engineering. *Nano LIFE*, 2012. 02(04): p. 1230010.
54. Agarwal, P. and P. Srivastava, Electrospun Biomaterial for biomedical application 2011. Vol. 2. 2011.
55. Shalumon, K.T., et al., Electrospinning of carboxymethyl chitin/poly(vinyl alcohol) nanofibrous scaffolds for tissue engineering applications. *Carbohydrate Polymers*, 2009. 77(4): p. 863-869.
56. Pham, Q.P., U. Sharma, and A.G. Mikos, Electrospinning of polymeric nanofibers for tissue engineering applications: A review. *Tissue Engineering*, 2006. 12(5): p. 1197-1211.
57. Bae, M.S., et al., Nanofiber scaffold for tissue regeneration using electrospinning method. *Tissue Engineering and Regenerative Medicine*, 2008. 5(2): p. 196-203.
58. Lu, W.J., J.S. Sun, and X.Y. Jiang, Recent advances in electrospinning technology and biomedical applications of electrospun fibers. *Journal of Materials Chemistry B*, 2014. 2(17): p. 2369-2380.
59. Boland, E.D., et al., Electrospinning polydioxanone for biomedical applications. *Acta Biomaterialia*, 2005. 1(1): p. 115-123.
60. Agarwal, S., J.H. Wendorff, and A. Greiner, Progress in the Field of Electrospinning for Tissue Engineering Applications. *Advanced Materials*, 2009. 21(32-33): p. 3343-3351.
61. Lao, L.H., et al., Poly(lactide-co-glycolide)/hydroxyapatite nanofibrous scaffolds fabricated by electrospinning for bone tissue engineering. *Journal of Materials Science-Materials in Medicine*, 2011. 22(8): p. 1873-1884.
62. Taylor, G., Electrically Driven Jets. *Proceedings of the Royal Society of London Series a-Mathematical and Physical Sciences*, 1969. 313(1515): p. 453-&.
63. Doshi, J. and D.H. Reneker, Electrospinning Process and Applications of Electrospun Fibers. *Journal of Electrostatics*, 1995. 35(2-3): p. 151-160.
64. Chew, S.Y., et al., The role of electrospinning in the emerging field of nanomedicine. *Current Pharmaceutical Design*, 2006. 12(36): p. 4751-4770.
65. Teo, W.E. and S. Ramakrishna, A review on electrospinning design and nanofibre assemblies. *Nanotechnology*, 2006. 17(14): p. R89-R106.
66. Rogina, A., Electrospinning process: Versatile preparation method for biodegradable and natural polymers and biocomposite systems applied in tissue engineering and drug delivery. *Applied Surface Science*, 2014. 296: p. 221-230.
67. Beachley, V. and X.J. Wen, Effect of electrospinning parameters on the nanofiber diameter and length. *Materials Science & Engineering C-Biomimetic and Supramolecular Systems*, 2009. 29(3): p. 663-668.
68. Evcin, A. and D.A. Kaya, Effect of production parameters on the structure and morphology of aluminum titanate nanofibers produced using electrospinning technique. *Scientific Research and Essays*, 2010. 5(23): p. 3682-3686.
69. Bosworth, L.A. and S. Downes, Acetone, a Sustainable Solvent for Electrospinning Poly(epsilon-Caprolactone) Fibres: Effect of Varying Parameters and Solution Concentrations on Fibre Diameter. *Journal of Polymers and the Environment*, 2012. 20(3): p. 879-886.

70. Murugan, R. and S. Ramakrishna, Design strategies of tissue engineering scaffolds with controlled fiber orientation. *Tissue Engineering*, 2007. 13(8): p. 1845-1866.
71. Yuan, X.Y., et al., Morphology of ultrafine polysulfone fibers prepared by electrospinning. *Polymer International*, 2004. 53(11): p. 1704-1710.
72. Zargham, S., et al., The Effect of Flow Rate on Morphology and Deposition Area of Electrospun Nylon 6 Nanofiber. *Journal of Engineered Fibers and Fabrics*, 2012. 7(4): p. 42-49.
73. Chowdhury, M. and G.K. Stylios, Analysis of the effect of experimental parameters on the morphology of electrospun polyethylene oxide nanofibres and on their thermal properties. *Journal of the Textile Institute*, 2012. 103(2): p. 124-138.
74. Zuo, W.W., et al., Experimental study on relationship between jet instability and formation of beaded fibers during electrospinning. *Polymer Engineering and Science*, 2005. 45(5): p. 704-709.
75. Jarusuwannapoom, T., et al., Effect of solvents on electro-spinnability of polystyrene solutions and morphological appearance of resulting electrospun polystyrene fibers. *European Polymer Journal*, 2005. 41(3): p. 409-421.
76. Wannatong, L., A. Sirivat, and P. Supaphol, Effects of solvents on electrospun polymeric fibers: preliminary study on polystyrene. *Polymer International*, 2004. 53(11): p. 1851-1859.
77. Baumgart.Pk, Electrostatic Spinning of Acrylic Microfibers. *Journal of Colloid and Interface Science*, 1971. 36(1): p. 71-&.
78. Reneker, D.H. and I. Chun, Nanometre diameter fibres of polymer, produced by electrospinning. *Nanotechnology*, 1996. 7(3): p. 216-223.
79. Megelski, S., et al., Micro- and nanostructured surface morphology on electrospun polymer fibers. *Macromolecules*, 2002. 35(22): p. 8456-8466.
80. Liu, H.Q. and Y.L. Hsieh, Ultrafine fibrous cellulose membranes from electrospinning of cellulose acetate. *Journal of Polymer Science Part B-Polymer Physics*, 2002. 40(18): p. 2119-2129.
81. Katta, P., et al., Continuous electrospinning of aligned polymer nanofibers onto a wire drum collector. *Nano Letters*, 2004. 4(11): p. 2215-2218.
82. Afifi, A.M., et al., Fabrication of Aligned Poly(L-lactide) Fibers by Electrospinning and Drawing. *Macromolecular Materials and Engineering*, 2009. 294(10): p. 658-665.
83. Koski, A., K. Yim, and S. Shivkumar, Effect of molecular weight on fibrous PVA produced by electrospinning. *Materials Letters*, 2004. 58(3-4): p. 493-497.
84. Supaphol, P., C. Mit-Uppatham, and M. Nithitanakul, Ultrafine electrospun polyamide-6 fibers: Effect of emitting electrode polarity on morphology and average fiber diameter. *Journal of Polymer Science Part B-Polymer Physics*, 2005. 43(24): p. 3699-3712.
85. Fong, H., I. Chun, and D.H. Reneker, Beaded nanofibers formed during electrospinning. *Polymer*, 1999. 40(16): p. 4585-4592.
86. Ki, C.S., et al., Characterization of gelatin nanofiber prepared from gelatin-formic acid solution. *Polymer*, 2005. 46(14): p. 5094-5102.
87. Koombhongse, S., W.X. Liu, and D.H. Reneker, Flat polymer ribbons and other shapes by electrospinning. *Journal of Polymer Science Part B-Polymer Physics*, 2001. 39(21): p. 2598-2606.
88. Zhang, C.X., et al., Study on morphology of electrospun poly(vinyl alcohol) mats. *European Polymer Journal*, 2005. 41(3): p. 423-432.
89. Ryu, Y.J., et al., Transport properties of electrospun nylon 6 nonwoven mats. *European Polymer Journal*, 2003. 39(9): p. 1883-1889.
90. Yang, Q.B., et al., Influence of solvents on the formation of ultrathin uniform poly(vinyl pyrrolidone) nanofibers with electrospinning. *Journal of Polymer Science Part B-Polymer Physics*, 2004. 42(20): p. 3721-3726.
91. Fridrikh, S.V., et al., Controlling the fiber diameter during electrospinning. *Physical Review Letters*, 2003. 90(14).
92. Huang, C.B., et al., Electrospun polymer nanofibres with small diameters. *Nanotechnology*, 2006. 17(6): p. 1558-1563.
93. Angammana, C.J. and S.H. Jayaram, Analysis of the Effects of Solution Conductivity on Electro-spinning Process and Fiber Morphology. 2008 IEEE Industry Applications Society Annual Meeting, Vols 1-5, 2008: p. 1890-1893.

94. Mit-uppatham, C., M. Nithitanakul, and P. Supaphol, Ultrafine Electrospun Polyamide-6 Fibers: Effect of Solution Conditions on Morphology and Average Fiber Diameter. *Macromolecular Chemistry and Physics*, 2004. 205(17): p. 2327-2338.
95. De Vrieze, S., et al., The effect of temperature and humidity on electrospinning. *Journal of Materials Science*, 2009. 44(5): p. 1357-1362.
96. Casper, C.L., et al., Controlling surface morphology of electrospun polystyrene fibers: Effect of humidity and molecular weight in the electrospinning process. *Macromolecules*, 2004. 37(2): p. 573-578.
97. Duan, B., et al., Hybrid nanofibrous membranes of PLGA/chitosan fabricated via an electrospinning array. *Journal of Biomedical Materials Research Part A*, 2007. 83A(3): p. 868-878.
98. Kang, J.C., M. Wang, and X.Y. Yuan, An investigation into dual-source and dual-power electrospinning of nanofibrous membranes for medical applications. *Multi-Functional Materials and Structures, Pts 1 and 2*, 2008. 47-50: p. 1454-1457.
99. Min, B.M., et al., Formation of nanostructured poly(lactic-co-glycolic acid)/chitin matrix and its cellular response to normal human keratinocytes and fibroblasts. *Carbohydrate Polymers*, 2004. 57(3): p. 285-292.
100. Zhan, N.Q., et al., A novel multinozzle electrospinning process for preparing superhydrophobic PS films with controllable bead-on-string/microfiber morphology. *Journal of Colloid and Interface Science*, 2010. 345(2): p. 491-495.
101. Zhang, C.Q., et al., A novel two-nozzle electrospinning process for preparing microfiber reinforced pH-sensitive nano-membrane with enhanced mechanical property. *European Polymer Journal*, 2011. 47(12): p. 2228-2233.
102. Ryu, G.S., J.T. Oh, and H. Kim, Observation of Spline Behavior of Dual Nozzle Electrospinning and Its Fiberweb Morphology. *Fibers and Polymers*, 2010. 11(1): p. 36-41.
103. Gu, M.B., et al., Preparation and Characterization of PVA/PU Blend Nanofiber Mats by Dual-jet Electrospinning. *Fibers and Polymers*, 2011. 12(1): p. 65-72.
104. Xu, F., L.M. Li, and X.J. Cui, Fabrication of Aligned Side-by-Side TiO<sub>2</sub>/SnO<sub>2</sub> Nanofibers via Dual-Opposite-Spinneret Electrospinning. *Journal of Nanomaterials*, 2012.
105. Pan, H., et al., Continuous aligned polymer fibers produced by a modified electrospinning method. *Polymer*, 2006. 47(14): p. 4901-4904.
106. Tijjing, L.D., et al., One-step fabrication of antibacterial (silver nanoparticles/poly(ethylene oxide)) - Polyurethane bicomponent hybrid nanofibrous mat by dual-spinneret electrospinning. *Materials Chemistry and Physics*, 2012. 134(2-3): p. 557-561.
107. Park, C.H., et al., An angled robotic dual-nozzle electrospinning set-up for preparing PU/PA6 composite fibers. *Textile Research Journal*, 2013. 83(3): p. 311-320.
108. Tijjing, L.D., et al., Two-nozzle electrospinning of (MWNT/PU)/PU nanofibrous composite mat with improved mechanical and thermal properties. *Current Applied Physics*, 2013. 13(7): p. 1247-1255.
109. Park, C.H., H.R. Pant, and C.S. Kim, Novel robot-assisted angled multi nozzle electrospinning set up: computer simulation with experimental observation on electric field and fiber morphology. *Textile Research Journal*, 2014.
110. Baker, B.M., et al., Sacrificial nanofibrous composites provide instruction without impediment and enable functional tissue formation. *Proceedings of the National Academy of Sciences of the United States of America*, 2012. 109(35): p. 14176-14181.
111. Wang, C. and M. Wang, Dual-source dual-power electrospinning and characteristics of multifunctional scaffolds for bone tissue engineering. *Journal of Materials Science-Materials in Medicine*, 2012. 23(10): p. 2381-2397.
112. Toncheva, A., et al., Dual vs. single spinneret electrospinning for the preparation of dual drug containing non-woven fibrous materials. *Colloids and Surfaces a-Physicochemical and Engineering Aspects*, 2013. 439: p. 176-183.
113. Li, M., et al., Dual electrode mode electrospinning of biodegradable polymers. *Applied Physics Letters*, 2008. 92(21).
114. Loscertales, I.G., et al., Electrically forced coaxial nanojets for one-step hollow nanofiber design. *Journal of the American Chemical Society*, 2004. 126(17): p. 5376-5377.
115. Wang, M., et al., Production of submicron diameter silk fibers under benign processing conditions by two-fluid electrospinning. *Macromolecules*, 2006. 39(3): p. 1102-1107.

116. Wang, M., et al., Electrospinning of silica nanochannels for single molecule detection. *Applied Physics Letters*, 2006. 88(3).
117. Zhang, H., et al., Electrospinning of ultrafine core/shell fibers for biomedical applications. *Science China-Chemistry*, 2010. 53(6): p. 1246-1254.
118. Zhang, Y.Z., et al., Preparation of core-shell structured PCL-r-gelatin Bi-component nanofibers by coaxial electrospinning. *Chemistry of Materials*, 2004. 16(18): p. 3406-3409.
119. Sun, Z.C., et al., Compound core-shell polymer nanofibers by co-electrospinning. *Advanced Materials*, 2003. 15(22): p. 1929-+.
120. Li, D. and Y.N. Xia, Direct fabrication of composite and ceramic hollow nanofibers by electrospinning. *Nano Letters*, 2004. 4(5): p. 933-938.
121. Jiang, Y.N., H.Y. Mo, and D.G. Yu, Electrospun drug-loaded core-sheath PVP/zein nanofibers for biphasic drug release. *International Journal of Pharmaceutics*, 2012. 438(1-2): p. 232-239.
122. Zhuang, X.P., et al., Coaxial Solution Blown Core-Shell Structure Nanofibers for Drug Delivery. *Macromolecular Research*, 2013. 21(4): p. 346-348.
123. He, C.L., et al., Coaxial electrospun poly(L-lactic acid) ultrafine fibers for sustained drug delivery. *Journal of Macromolecular Science Part B-Physics*, 2006. 45(4): p. 515-524.
124. Qian, W., et al., Dual Drug Release Electrospun Core-Shell Nanofibers with Tunable Dose in the Second Phase. *International Journal of Molecular Sciences*, 2014. 15(1): p. 774-786.
125. Qu, H.L., S.Y. Wei, and Z.H. Guo, Coaxial electrospun nanostructures and their applications. *Journal of Materials Chemistry A*, 2013. 1(38): p. 11513-11528.
126. Thakkar, S., et al., Mesenchymal stromal cell-derived extracellular matrix influences gene expression of chondrocytes. *Biofabrication*, 2013. 5(2).
127. Blakeney, B.A., et al., Cell infiltration and growth in a low density, uncompressed three-dimensional electrospun nanofibrous scaffold. *Biomaterials*, 2011. 32(6): p. 1583-1590.
128. Shabani, I., et al., Cellular infiltration on nanofibrous scaffolds using a modified electrospinning technique. *Biochemical and Biophysical Research Communications*, 2012. 423(1): p. 50-54.
129. Sundararaghavan, H.G. and J.A. Burdick, Gradients with Depth in Electrospun Fibrous Scaffolds for Directed Cell Behavior. *Biomacromolecules*, 2011. 12(6): p. 2344-2350.
130. Zhong, S.P., Y.Z. Zhang, and C.T. Lim, Fabrication of Large Pores in Electrospun Nanofibrous Scaffolds for Cellular Infiltration: A Review. *Tissue Engineering Part B-Reviews*, 2012. 18(2): p. 77-87.
131. Chen, M., et al., Role of fiber diameter in adhesion and proliferation of NIH 3T3 fibroblast on electrospun polycaprolactone scaffolds. *Tissue Engineering*, 2007. 13(3): p. 579-587.
132. Badami, A.S., et al., Effect of fiber diameter on spreading, proliferation, and differentiation of osteoblastic cells on electrospun poly(lactic acid) substrates. *Biomaterials*, 2006. 27(4): p. 596-606.
133. Whited, B.M. and M.N. Rylander, The Influence of Electrospun Scaffold Topography on Endothelial Cell Morphology, Alignment, and Adhesion in Response to Fluid Flow. *Biotechnology and Bioengineering*, 2014. 111(1): p. 184-195.
134. Christopherson, G.T., H. Song, and H.Q. Mao, The influence of fiber diameter of electrospun substrates on neural stem cell differentiation and proliferation. *Biomaterials*, 2009. 30(4): p. 556-564.
135. Hsia, H.C., et al., The Fiber Diameter of Synthetic Bioresorbable Extracellular Matrix Influences Human Fibroblast Morphology and Fibronectin Matrix Assembly. *Plastic and Reconstructive Surgery*, 2011. 127(6): p. 2312-2320.
136. Noriega, S.E., et al., Effect of Fiber Diameter on the Spreading, Proliferation and Differentiation of Chondrocytes on Electrospun Chitosan Matrices. *Cells Tissues Organs*, 2012. 195(3): p. 207-221.
137. Bashur, C.A., M.J. Egleton, and A. Ramamurthi, Impact of Electrospun Conduit Fiber Diameter and Enclosing Pouch Pore Size on Vascular Constructs Grown Within Rat Peritoneal Cavities. *Tissue Engineering Part A*, 2013. 19(7-8): p. 809-823.
138. Pham, Q.P., U. Sharma, and A.G. Mikos, Electrospun poly(epsilon-caprolactone) microfiber and multilayer nanofiber/microfiber scaffolds: Characterization of scaffolds

- and measurement of cellular infiltration. *Biomacromolecules*, 2006. 7(10): p. 2796-2805.
139. Li, Y., et al., Effects of filtration seeding on cell density, spatial distribution, and proliferation in nonwoven fibrous matrices. *Biotechnology Progress*, 2001. 17(5): p. 935-944.
140. Milczarek, M.A., et al., Dynamic seeding and culture of urothelial cells on tubular type I collagen scaffolds for urogenital tissue engineering applications. *Tissue Engineering Part A*, 2008. 14(5): p. 841-841.
141. Sailon, A.M., et al., A Novel Flow-Perfusion Bioreactor Supports 3D Dynamic Cell Culture. *Journal of Biomedicine and Biotechnology*, 2009.
142. Reichardt, A., R. Hetzer, and C. Lueders, Construction of a new bioreactor system combining dynamic cell seeding and *in vitro* conditioning for tissue engineering of heart valves: first standards in cardiovascular tissue engineering. *European Journal of Medical Research*, 2010. 15: p. 26-27.
143. Zhao, F. and T. Ma, Perfusion bioreactor system for human mesenchymal stem cell tissue engineering: Dynamic cell seeding and construct development. *Biotechnology and Bioengineering*, 2005. 91(4): p. 482-493.
144. Rockwood, D.N., et al., Culture on electrospun polyurethane scaffolds decreases atrial natriuretic peptide expression by cardiomyocytes *in vitro*. *Biomaterials*, 2008. 29(36): p. 4783-4791.
145. Dzenis, Y., Spinning continuous fibers for nanotechnology. *Science*, 2004. 304(5679): p. 1917-1919.
146. Teo, W.E., R. Inai, and S. Ramakrishna, Technological advances in electrospinning of nanofibers. *Science and Technology of Advanced Materials*, 2011. 12(1).
147. Wang, X., B. Ding, and B. Li, Biomimetic electrospun nanofibrous structures for tissue engineering. *Materials Today*, 2013. 16(6): p. 229-241.
148. Tong, H.W. and M. Wang, Electrospinning of aligned biodegradable polymer fibers and composite fibers for tissue engineering applications. *Journal of Nanoscience and Nanotechnology*, 2007. 7(11): p. 3834-3840.
149. Ayres, C., et al., Modulation of anisotropy in electrospun tissue-engineering scaffolds: Analysis of fiber alignment by the fast Fourier transform. *Biomaterials*, 2006. 27(32): p. 5524-5534.
150. Matthews, J.A., et al., Electrospinning of collagen nanofibers. *Biomacromolecules*, 2002. 3(2): p. 232-238.
151. Yang, F., et al., Electrospinning of nano/micro scale poly(L-lactic acid) aligned fibers and their potential in neural tissue engineering. *Biomaterials*, 2005. 26(15): p. 2603-2610.
152. Li, W.J., et al., Engineering controllable anisotropy in electrospun biodegradable nanofibrous scaffolds for musculoskeletal tissue engineering. *Journal of Biomechanics*, 2007. 40(8): p. 1686-1693.
153. Kessick, R., J. Fenn, and G. Tepper, The use of AC potentials in electrospinning and electrospinning processes. *Polymer*, 2004. 45(9): p. 2981-2984.
154. Baker, B.M. and R.L. Mauck, The effect of nanofiber alignment on the maturation of engineered meniscus constructs. *Biomaterials*, 2007. 28(11): p. 1967-1977.
155. Bashur, C.A. and A. Ramamurthi, Aligned electrospun scaffolds and elastogenic factors for vascular cell-mediated elastic matrix assembly. *Journal of Tissue Engineering and Regenerative Medicine*, 2012. 6(9): p. 673-686.
156. Dong, Y.X., et al., Distinctive Degradation Behaviors of Electrospun Polyglycolide, Poly(DL-Lactide-co-Glycolide), and Poly(L-Lactide-co-epsilon-Caprolactone) Nanofibers Cultured With/Without Porcine Smooth Muscle Cells. *Tissue Engineering Part A*, 2010. 16(1): p. 283-298.
157. Ghasemi-Mobarakeh, L., et al., Electrical Stimulation of Nerve Cells Using Conductive Nanofibrous Scaffolds for Nerve Tissue Engineering. *Tissue Engineering Part A*, 2009. 15(11): p. 3605-3619.
158. Prabhakaran, M.P., J.R. Venugopal, and S. Ramakrishna, Mesenchymal stem cell differentiation to neuronal cells on electrospun nanofibrous substrates for nerve tissue engineering. *Biomaterials*, 2009. 30(28): p. 4996-5003.
159. Ma, Z.W., et al., Grafting of gelatin on electrospun poly(caprolactone) nanofibers to improve endothelial cell spreading and proliferation and to control cell orientation. *Tissue Engineering*, 2005. 11(7-8): p. 1149-1158.

160. Chen, Z.G., et al., Electrospun collagen-chitosan nanofiber: A biomimetic extracellular matrix for endothelial cell and smooth muscle cell. *Acta Biomaterialia*, 2010. 6(2): p. 372-382.
161. Zhu, Y.B., et al., Macro-Alignment of Electrospun Fibers For Vascular Tissue Engineering. *Journal of Biomedical Materials Research Part B-Applied Biomaterials*, 2010. 92B(2): p. 508-516.
162. Kai, D., et al., Guided orientation of cardiomyocytes on electrospun aligned nanofibers for cardiac tissue engineering. *Journal of Biomedical Materials Research Part B-Applied Biomaterials*, 2011. 98B(2): p. 379-386.
163. Zong, X.H., et al., Electrospun fine-textured scaffolds for heart tissue constructs. *Biomaterials*, 2005. 26(26): p. 5330-5338.
164. Thomas, V., et al., Mechano-morphological studies of aligned nanofibrous scaffolds of polycaprolactone fabricated by electrospinning. *Journal of Biomaterials Science-Polymer Edition*, 2006. 17(9): p. 969-984.
165. Discher, D.E., P. Janmey, and Y.L. Wang, Tissue cells feel and respond to the stiffness of their substrate. *Science*, 2005. 310(5751): p. 1139-1143.
166. Nam, J., et al., Modulation of embryonic mesenchymal progenitor cell differentiation via control over pure mechanical modulus in electrospun nanofibers. *Acta Biomaterialia*, 2011. 7(4): p. 1516-1524.
167. He, W., et al., Fabrication of collagen-coated biodegradable polymer nanofiber mesh and its potential for endothelial cells growth. *Biomaterials*, 2005. 26(36): p. 7606-7615.
168. Jin, H.J., et al., Human bone marrow stromal cell responses on electrospun silk fibroin mats. *Biomaterials*, 2004. 25(6): p. 1039-1047.
169. Min, B.M., et al., Electrospinning of silk fibroin nanofibers and its effect on the adhesion and spreading of normal human keratinocytes and fibroblasts *in vitro*. *Biomaterials*, 2004. 25(7-8): p. 1289-1297.
170. Mo, X.M., et al., Electrospun P(LLA-CL) nanofiber: a biomimetic extracellular matrix for smooth muscle cell and endothelial cell proliferation. *Biomaterials*, 2004. 25(10): p. 1883-1890.
171. Venugopal, J.R., Y.Z. Zhang, and S. Ramakrishna, *In vitro* culture of human dermal fibroblasts on electrospun polycaprolactone collagen nanofibrous membrane. *Artificial Organs*, 2006. 30(6): p. 440-446.
172. Leong, M.F., et al., *In vitro* cell infiltration and *in vivo* cell infiltration and vascularization in a fibrous, highly porous poly(D,L-lactide) scaffold fabricated by cryogenic electrospinning technique. *Journal of Biomedical Materials Research Part A*, 2009. 91A(1): p. 231-240.
173. Balguid, A., et al., Tailoring Fiber Diameter in Electrospun Poly(epsilon-Caprolactone) Scaffolds for Optimal Cellular Infiltration in Cardiovascular Tissue Engineering. *Tissue Engineering Part A*, 2009. 15(2): p. 437-444.
174. Fioretta, E.S., et al., Differential Response of Endothelial and Endothelial Colony Forming Cells on Electrospun Scaffolds with Distinct Microfiber Diameters. *Biomacromolecules*, 2014. 15(3): p. 821-829.
175. Leong, M.F., et al., Effect of electrospun poly(D,L-lactide) fibrous scaffold with nanoporous surface on attachment of porcine esophageal epithelial cells and protein adsorption. *Journal of Biomedical Materials Research Part A*, 2009. 89A(4): p. 1040-1048.
176. Horst, M., et al., Increased porosity of electrospun hybrid scaffolds improved bladder tissue regeneration. *Journal of Biomedical Materials Research Part A*, 2014. 102(7): p. 2116-2124.
177. Zhu, X.L., et al., Electrospun fibrous mats with high porosity as potential scaffolds for skin tissue engineering. *Biomacromolecules*, 2008. 9(7): p. 1795-1801.
178. Lee, J.B., et al., Highly Porous Electrospun Nanofibers Enhanced by Ultrasonication for Improved Cellular Infiltration. *Tissue Engineering Part A*, 2011. 17(21-22): p. 2695-2702.
179. Nam, J., et al., Improved cellular infiltration in electrospun fiber via engineered porosity. *Tissue Engineering*, 2007. 13(9): p. 2249-2257.
180. Ekaputra, A.K., et al., Combining electrospun scaffolds with electrosprayed hydrogels leads to three-dimensional cellularization of hybrid constructs. *Biomacromolecules*, 2008. 9(8): p. 2097-2103.

181. Rnjak-Kovacina, J. and A.S. Weiss, Increasing the Pore Size of Electrospun Scaffolds. *Tissue Engineering Part B-Reviews*, 2011. 17(5): p. 365-372.
182. Rnjak, J., et al., Primary human dermal fibroblast interactions with open weave three-dimensional scaffolds prepared from synthetic human elastin. *Biomaterials*, 2009. 30(32): p. 6469-6477.
183. Powell, D.W., et al., Myofibroblasts. I. Paracrine cells important in health and disease. *American Journal of Physiology-Cell Physiology*, 1999. 277(1): p. C1-C19.
184. Sisson, K., et al., Fiber diameters control osteoblastic cell migration and differentiation in electrospun gelatin. *Journal of Biomedical Materials Research Part A*, 2010. 94A(4): p. 1312-1320.
185. Soliman, S., et al., Controlling the porosity of fibrous scaffolds by modulating the fiber diameter and packing density. *Journal of Biomedical Materials Research Part A*, 2011. 96A(3): p. 566-574.
186. Eichhorn, S.J. and W.W. Sampson, Statistical geometry of pores and statistics of porous nanofibrous assemblies. *Journal of the Royal Society Interface*, 2005. 2(4): p. 309-318.
187. Rnjak-Kovacina, J., et al., Tailoring the porosity and pore size of electrospun synthetic human elastin scaffolds for dermal tissue engineering. *Biomaterials*, 2011. 32(28): p. 6729-6736.
188. Teo, W.E. and S. Ramakrishna, Electrospun fibre bundle made of aligned nanofibres over two fixed points. *Nanotechnology*, 2005. 16(9): p. 1878-1884.
189. Vaquette, C. and J.J. Cooper-White, Increasing electrospun scaffold pore size with tailored collectors for improved cell penetration. *Acta Biomaterialia*, 2011. 7(6): p. 2544-2557.
190. Hong, J.K., et al., Analysis of void shape and size in the collector plate and polycaprolactone molecular weight on electrospun scaffold pore size. *Journal of Applied Polymer Science*, 2013. 128(3): p. 1583-1591.
191. Li, D., et al., Collecting electrospun nanofibers with patterned electrodes. *Nano Letters*, 2005. 5(5): p. 913-916.
192. Zhang, D.M. and J. Chang, Electrospinning of Three-Dimensional Nanofibrous Tubes with Controllable Architectures. *Nano Letters*, 2008. 8(10): p. 3283-3287.
193. Simonet, M., et al., Ultraporous 3D polymer meshes by low-temperature electrospinning: Use of ice crystals as a removable void template. *Polymer Engineering & Science*, 2007. 47(12): p. 2020-2026.
194. Bulysheva, A.A., et al., Low-temperature electrospun silk scaffold for *in vitro* mucosal modeling. *Journal of Biomedical Materials Research Part A*, 2012. 100A(3): p. 757-767.
195. Simonet, M., et al., Tailoring the void space and mechanical properties in electrospun scaffolds towards physiological ranges. *Journal of Materials Chemistry B*, 2014. 2(3): p. 305-313.
196. Gentsch, R., et al., Single-Step Electrospinning of Bimodal Fiber Meshes for Ease of Cellular Infiltration. *Macromolecular Rapid Communications*, 2010. 31(1): p. 59-64.
197. Soliman, S., et al., Multiscale three-dimensional scaffolds for soft tissue engineering via multimodal electrospinning. *Acta Biomaterialia*, 2010. 6(4): p. 1227-1237.
198. Tuzlakoglu, K., et al., Nano- and micro-fiber combined scaffolds: A new architecture for bone tissue engineering. *Journal of Materials Science-Materials in Medicine*, 2005. 16(12): p. 1099-1104.
199. Santos, M.I., et al., Endothelial cell colonization and angiogenic potential of combined nano- and micro-fibrous scaffolds for bone tissue engineering. *Biomaterials*, 2008. 29(32): p. 4306-4313.
200. Ju, Y.M., et al., Bilayered scaffold for engineering cellularized blood vessels. *Biomaterials*, 2010. 31(15): p. 4313-4321.
201. Suh, S.W., et al., Effect of different particles on cell proliferation in polymer scaffolds using a solvent-casting and particulate leaching technique. *Asaio Journal*, 2002. 48(5): p. 460-464.
202. Wang, Y.Z., et al., A novel method for preparing electrospun fibers with nano-/micro-scale porous structures. *Polymer Bulletin*, 2009. 63(2): p. 259-265.
203. Wulkersdorfer, B., et al., Bimodal Porous Scaffolds by Sequential Electrospinning of Poly(glycolic acid) with Sucrose Particles. *International Journal of Polymer Science*, 2010.



204. Sasmazel, H.T., et al., Comparison of cellular proliferation on dense and porous PCL scaffolds. *Bio-Medical Materials and Engineering*, 2008. 18(3): p. 119-128.
205. Zhang, X., V. Thomas, and Y.K. Vohra, *In Vitro* Biodegradation of Designed Tubular Scaffolds of Electrospun Protein/Polyglyconate Blend Fibers. *Journal of Biomedical Materials Research Part B-Applied Biomaterials*, 2009. 89B(1): p. 135-147.
206. Gong, Y.H., et al., *In vitro* and *in vivo* degradability and cytocompatibility of poly(L-lactic acid) scaffold fabricated by a gelatin particle leaching method. *Acta Biomaterialia*, 2007. 3(4): p. 531-540.
207. Ji, Y., et al., Dual-syringe reactive electrospinning of cross-linked hyaluronic acid hydrogel nanofibers for tissue engineering applications. *Macromolecular Bioscience*, 2006. 6(10): p. 811-817.
208. Shin, J.W., et al., Manufacturing of Multi-Layered Nanofibrous Structures Composed of Polyurethane and Poly(ethylene oxide) as Potential Blood Vessel Scaffolds. *Journal of Biomaterials Science-Polymer Edition*, 2009. 20(5-6): p. 757-771.
209. Skotak, M., et al., Improved cellular infiltration into nanofibrous electrospun cross-linked gelatin scaffolds templated with micrometer-sized polyethylene glycol fibers. *Biomedical Materials*, 2011. 6(5).
210. Baker, B.M., et al., The potential to improve cell infiltration in composite fiber-aligned electrospun scaffolds by the selective removal of sacrificial fibers. *Biomaterials*, 2008. 29(15): p. 2348-2358.
211. Shin, J.W., et al., Hybrid nanofiber scaffolds of polyurethane and poly(ethylene oxide) using dual-electrospinning for vascular tissue engineering. 3rd Kuala Lumpur International Conference on Biomedical Engineering 2006, 2007. 15: p. 692-695.
212. You, Y., et al., Preparation of porous ultrafine PGA fibers via selective dissolution of electrospun PGA/PLA blend fibers. *Materials Letters*, 2006. 60(6): p. 757-760.
213. Zhang, Y.Z., et al., Electrospinning of gelatin fibers and gelatin/PCL composite fibrous scaffolds. *Journal of Biomedical Materials Research Part B-Applied Biomaterials*, 2005. 72B(1): p. 156-165.
214. Milleret, V., et al., Tuning Electrospinning Parameters for Production of 3d-Fiber-Fleeces with Increased Porosity for Soft Tissue Engineering Applications. *European Cells & Materials*, 2011. 21: p. 286-303.
215. Kim, G., H. Yoon, and Y. Park, Drug release from various thicknesses of layered mats consisting of electrospun polycaprolactone and polyethylene oxide micro/nanofibers. *Applied Physics A*, 2010. 100(4): p. 1197-1204.
216. Kim, T.G., D.S. Lee, and T.G. Park, Controlled protein release from electrospun biodegradable fiber mesh composed of poly( $\epsilon$ -caprolactone) and poly(ethylene oxide). *International Journal of Pharmaceutics*, 2007. 338(1-2): p. 276-283.
217. Phipps, M.C., et al., Increasing the pore sizes of bone-mimetic electrospun scaffolds comprised of polycaprolactone, collagen I and hydroxyapatite to enhance cell infiltration. *Biomaterials*, 2012. 33(2): p. 524-534.
218. Zander, N.E., et al., Electrospun polycaprolactone scaffolds with tailored porosity using two approaches for enhanced cellular infiltration. *Journal of Materials Science-Materials in Medicine*, 2013. 24(1): p. 179-187.
219. Lehuec, J.C., et al., Influence of Porosity on the Mechanical Resistance of Hydroxyapatite Ceramics under Compressive Stress. *Biomaterials*, 1995. 16(2): p. 113-118.
220. Athanasiou, K.A., J.P. Schmitz, and C.M. Agrawal, The effects of porosity on *in vitro* degradation of polylactic acid polyglycolic acid implants used in repair of articular cartilage. *Tissue Engineering*, 1998. 4(1): p. 53-63.
221. Lu, L., et al., *In vitro* and *in vivo* degradation of porous poly(DL-lactic-co-glycolic acid) foams. *Biomaterials*, 2000. 21(18): p. 1837-1845.
222. Karageorgiou, V. and D. Kaplan, Porosity of 3D biomaterial scaffolds and osteogenesis. *Biomaterials*, 2005. 26(27): p. 5474-5491.
223. Hasan, A., et al., Electrospun scaffolds for tissue engineering of vascular grafts. *Acta Biomaterialia*, 2014. 10(1): p. 11-25.
224. Kwon, I.K., S. Kidoaki, and T. Matsuda, Electrospun nano- to microfiber fabrics made of biodegradable copolyesters: structural characteristics, mechanical properties and cell adhesion potential. *Biomaterials*, 2005. 26(18): p. 3929-3939.

- 
225. Sawalha, H., K. Schroen, and R. Boom, Mechanical properties and porosity of polylactide for biomedical applications. *Journal of Applied Polymer Science*, 2008. 107(1): p. 82-93.
226. Lee, S.J., et al., The use of thermal treatments to enhance the mechanical properties of electrospun poly( $\epsilon$ -caprolactone) scaffolds. *Biomaterials*, 2008. 29(10): p. 1422-1430.
227. Pan, Z. and J.D. Ding, Poly(lactide-co-glycolide) porous scaffolds for tissue engineering and regenerative medicine. *Interface Focus*, 2012. 2(3): p. 366-377.
228. Zhang, K., et al., Processing and properties of porous poly(L-lactide)/bioactive glass composites. *Biomaterials*, 2004. 25(13): p. 2489-2500.
229. Asran, A.S., et al., Solvent Influences the Morphology and Mechanical Properties of Electrospun Poly(L-lactic acid) Scaffold for Tissue Engineering Applications. *Layered Nanostructures - Polymers with Improved Properties*, 2010. 294-I: p. 153-161.
230. Boland, E.D., et al., Tailoring tissue engineering scaffolds using electrostatic processing techniques: A study of poly(glycolic acid) electrospinning. *Journal of Macromolecular Science-Pure and Applied Chemistry*, 2001. 38(12): p. 1231-1243.
231. Meng, Z.X., et al., Electrospinning of PLGA/gelatin randomly-oriented and aligned nanofibers as potential scaffold in tissue engineering. *Materials Science and Engineering: C*, 2010. 30(8): p. 1204-1210.
232. McClure, M.J., et al., The use of air-flow impedance to control fiber deposition patterns during electrospinning. *Biomaterials*, 2012. 33(3): p. 771-779.
233. Johnson, J., et al., Electrospun PCL *in Vitro*: a Microstructural Basis for Mechanical Property Changes. *Journal of Biomaterials Science-Polymer Edition*, 2009. 20(4): p. 467-481.
234. Thomas, V., et al., Functionally graded electrospun scaffolds with tunable mechanical properties for vascular tissue regeneration. *Biomedical Materials*, 2007. 2(4): p. 224-232.
235. Chew, S.Y., et al., Mechanical properties of single electrospun drug-encapsulated nanofibres. *Nanotechnology*, 2006. 17(15): p. 3880-3891.
236. Li, P., et al., Influences of tensile load on *in vitro* degradation of an electrospun poly(L-lactide-co-glycolide) scaffold. *Acta Biomaterialia*, 2010. 6(8): p. 2991-2996.
237. Fan, Y.B., P. Li, and X.Y. Yuan, Influence of Mechanical Loads on Degradation of Scaffolds. 6th World Congress of Biomechanics (Wcb 2010), Pts 1-3, 2010. 31: p. 549-552.
238. Yeganegi, M., R.A. Kandel, and J.P. Santerre, Characterization of a biodegradable electrospun polyurethane nanofiber scaffold: Mechanical properties and cytotoxicity. *Acta Biomaterialia*, 2010. 6(10): p. 3847-3855.
239. Babensee, J.E., et al., Host response to tissue engineered devices. *Advanced Drug Delivery Reviews*, 1998. 33(1-2): p. 111-139.
240. Sung, H.J., et al., The effect of scaffold degradation rate on three-dimensional cell growth and angiogenesis. *Biomaterials*, 2004. 25(26): p. 5735-5742.
241. Tao Jiang, G.Z., Wentong He, Hui Li, and Xun Jin, The Tissue Response and Degradation of Electrospun Poly( $\epsilon$ -caprolactone)/Poly(trimethylene-carbonate) Scaffold in Subcutaneous Space of Mice. *Journal of Nanomaterials*. 2014.
242. Ji, W., et al., Biocompatibility and degradation characteristics of PLGA-based electrospun nanofibrous scaffolds with nanoapatite incorporation. *Biomaterials*, 2012. 33(28): p. 6604-6614.
243. Dong, Y.X., et al., Degradation Behaviors of Electrospun Resorbable Polyester Nanofibers. *Tissue Engineering Part B-Reviews*, 2009. 15(3): p. 333-351.
244. Lam, C.X.F., et al., Dynamics of *in vitro* polymer degradation of polycaprolactone-based scaffolds: accelerated versus simulated physiological conditions. *Biomedical Materials*, 2008. 3(3).
245. Bawolin, N.K., et al., Modeling Material-Degradation-Induced Elastic Property of Tissue Engineering Scaffolds. *Journal of Biomechanical Engineering-Transactions of the Asme*, 2010. 132(11).
246. Kim, K., et al., Control of degradation rate and hydrophilicity in electrospun non-woven poly(D,L-lactide) nanofiber scaffolds for biomedical applications. *Biomaterials*, 2003. 24(27): p. 4977-4985.

247. Liu, H., S.D. Wang, and N. Qi, Controllable structure, properties, and degradation of the electrospun PLGA/PLA-blended nanofibrous scaffolds. *Journal of Applied Polymer Science*, 2012. 125: p. E468-E476.
248. Hong, Y., et al., Tailoring the degradation kinetics of poly(ester carbonate urethane)urea thermoplastic elastomers for tissue engineering scaffolds. *Biomaterials*, 2010. 31(15): p. 4249-4258.
249. Liao, G.Y., et al., Electrospun aligned PLLA/PCL/HA composite fibrous membranes and their *in vitro* degradation behaviors. *Materials Letters*, 2012. 82: p. 159-162.
250. Jay, S.M., et al., Dual delivery of VEGF and MCP-1 to support endothelial cell transplantation for therapeutic vascularization. *Biomaterials*, 2010. 31(11): p. 3054-3062.
251. Roh, J.D., et al., Tissue-engineered vascular grafts transform into mature blood vessels via an inflammation-mediated process of vascular remodeling. *Proceedings of the National Academy of Sciences of the United States of America*, 2010. 107(10): p. 4669-4674.
252. Sarkar, S., et al., The Mechanical Properties of Infrainguinal Vascular Bypass Grafts: Their Role in Influencing Patency. *European Journal of Vascular and Endovascular Surgery*, 2006. 31(6): p. 627-636.
253. Jeong, C.G. and S.J. Hollister, Mechanical, permeability, and degradation properties of 3D designed poly(1,8 octanediol-co-citrate) scaffolds for soft tissue engineering. *Journal of Biomedical Materials Research Part B: Applied Biomaterials*, 2010. 93B(1): p. 141-149. Wissing, T.B., et al., *Biomaterial-driven in situ cardiovascular tissue engineering—a multi-disciplinary perspective*. *npj Regenerative Medicine*, 2017. 2(1): p. 18.



Chapter 3

Decellularized human  
mesenchymal stem cell  
derived matrix skews  
macrophages towards a  
regenerative phenotype

Shraddha Thakkar, Marloes W.J.T. Janssen-van den Broek, Marina van Doeselaar, Anthal I.P.M. Smits and Carlijn V.C. Bouten  
(Submitted)

## Abstract

Extracellular matrix (ECM) derived from different tissues and organs has shown to play an important role in influencing immune cell behaviour. As such, the native ECM is an attractive material for *in situ* tissue engineering applications. In this study, we investigated the immunomodulatory properties of ECM, derived from human mesenchymal stem cells (hMSCs), with respect to human monocyte recruitment and macrophage polarization, both in 2D and 3D; the latter in the form of a hybrid electrospun scaffold. In 2D, the decellularized ECM (dECM) elicited a strong chemotactic effect on human monocytes, as determined via migration assays. Direct culture of human monocytes on the dECM led to an increased expression of M2-associated cell surface proteins (CD163 and CD206), a decreased expression of M1-associated surface proteins (CD64 and CCR7), and a corresponding gene expression profile. To create 3D scaffolds, the dECM was lyophilized (LECM) and electrospun into hybrid microfibrillar scaffold with poly ( $\epsilon$ -caprolactone) (PCL). The LECM maintained its chemoattractant properties both before and after electrospinning. Cells seeded on hybrid scaffolds acquired an elongated morphology and showed increased expression of M2 markers (CD163 and CD206) and decreased expression of M1 markers (CD64 and CCR7), when compared to PCL only scaffolds, suggesting macrophage polarization towards an M2 phenotype. This study highlights the potential of hMSC-derived decellularized ECM as a bioactive material to design hybrid scaffolds with off-the-shelf availability for *in situ* tissue engineering applications.

### 3.1 Introduction

*In situ* tissue engineering builds on the regenerative potential of the body to repair and regenerate damaged tissues. This innovative technique relies on biomaterial-driven tissue regeneration, in which an implanted porous scaffold is infiltrated by immune cells, followed by subsequent initiation of an inflammatory response by the host [1]. Amongst the infiltrated immune cells, macrophages play an important role in modulating the inflammatory response due to their ability to polarize towards a pro-inflammatory (M1) or a reparative (M2) phenotype in response to the changing environmental stimuli [2]. The balance between M1 and M2 macrophages, plays a decisive role in tissue repair and regeneration [3]. The regenerative process is succeeded by attracting the endogenous cells from the host body, followed by cell adhesion and proliferation to eventually create a living and functional tissue at the site of implantation [4].

For *in situ* TE applications, the type of biomaterial is one of the most crucial elements of the implant. Currently available biomaterials are either synthetic or natural by origin. Synthetic materials are abundantly available, mechanically tuneable, and offer the ability to fabricate scaffolds using a variety of techniques [5-7]. However, these materials lack intrinsic bioactivity and may induce a pro-inflammatory response upon implantation, eventually leading to scar formation. Natural materials, including decellularized extracellular matrix (ECM) or components of ECM such as collagen [8] or glycosaminoglycan's (GAGs) [9], have the advantage of being inherently bioactive, but lack the tenability and processibility compared to their synthetic counterparts [10]. Furthermore, a major drawback of using natural materials is risk of zoonoses transfer in case of ECM from animal origin, or limited availability of and variability in tissue or organ sourced ECM. Nevertheless, solubilized ECM scaffolds have shown to positively influence macrophage behaviour and promote M2 macrophage polarization [11-12]. Thus, the goal of this study was to investigate the immunomodulatory properties of cell-derived ECM and combine the beneficial properties of ECM with those of

synthetic materials, thereby creating a hybrid scaffold that acquires the bioactivity of ECM and processibility of synthetic materials.

Here, we selected human bone marrow-derived mesenchymal stem cells (hMSCs) as the cell source due to their favourable immunomodulatory properties [13-16]. Previous research has demonstrated the ability of hMSCs to modulate monocyte-to-macrophages differentiation [17]. We hypothesized that hMSC-derived ECM can skew macrophages to a reparative, anti-inflammatory M2 phenotype and that these properties would be maintained upon processing (i.e. lyophilizing and electrospinning) into a hybrid scaffold. To test the proposed hypothesis, the immunomodulatory properties of ECM were investigated with respect to human monocyte recruitment and macrophage polarization, both before and after processing it into a hybrid 3D scaffold in combination with poly( $\epsilon$ -caprolactone) (PCL). In the first step, the ECM deposited by hMSC was decellularized (dECM) and its chemotactic properties were investigated. Subsequently, primary human monocytes were seeded onto the dECM and analysed for macrophage differentiation and polarization in terms of gene expression and expression of cell surface markers. In the second step, the feasibility of processing the dECM in lyophilized form (LECM), and further into a 3D hybrid scaffold via electrospinning LECM with PCL, was evaluated, and the retainment of immunomodulatory properties of the LECM after processing was analysed.

## **3.2 Materials & Methods**

### **3.2.1 Human mesenchymal stem cell isolation and ECM synthesis**

Human bone marrow was obtained from Lonza Group Ltd. (Maryland). hMSCs were isolated from the obtained bone marrow by cell adhesion on tissue culture plastic as previously described [18]. Briefly, 7 ml of bone marrow aliquots were diluted in 10 ml RPMI medium (Life Technologies) along with 5% fetal bovine serum (FBS). Cells were centrifuged at 300 g for 10 minutes. The cell pellet was resuspended in proliferation medium consisting of Dulbecco's modified Eagle's medium (DMEM) with 10% (v/v) FBS, and 1%

---

(v/v) penicillin/streptomycin (P/S) (Life Technologies), 1% (v/v) non-essential amino acids (NEAA) (consisting of 8.9 mg/L L-alanine, 13.2 mg/L L-asparagine, 13.3 mg/L L-aspartic acid, 14.7 mg/L L-glutamic acid, 7.5 mg/L glycine, 11.5 mg/L L-proline, 10.5 mg/L L-serine); and 1 ng/mL basic fibroblast growth factor-2 (bFGF) solution.

To obtain cell-produced ECM, hMSCs of passage 2 - 4 were cultured in  $\alpha$ MEM with 10% (v/v) FBS, and 1% (v/v) P/S, 1% (v/v) Glutamax (100X, Sigma), 0.2 mM ascorbic acid (Sigma) and 0.1% (v/v) bFGF. The seeding density was 2500 cells/cm. Cells were cultured for 2 weeks during which the medium was refreshed every 3 days. Upon confluency, the cells secreted ECM (cECM), which was isolated by decellularization (n=9 using 3 donors).

### **3.2.2 Decellularized ECM processing and characterization**

The cECM was decellularized by 5 minutes incubation with 20mM ammonium hydroxide (NH<sub>4</sub>OH), as previously reported [19]. Cellular remnants were removed by adding distilled water followed by removal of diluted NH<sub>4</sub>OH. After washing away of NH<sub>4</sub>OH, deoxy ribonuclease 1 (50 units/mL) was added followed by 5 minutes incubation, to degrade the DNA. The deposited ECM was washed with PBS to remove the cell debris and degraded DNA, after which a thin transparent layer of decellularized ECM (dECM) was visible. The resulting dECM was washed once again with PBS and stained for Phalloidin and 4', 6-diamidino-2-phenylindole (DAPI) to verify removal of cellular components. This dECM was used for migration assays and macrophage polarization studies. For preparation of 3D scaffolds, the dECM was gently scraped from the culture substrate using a cell scraper. The detached dECM was translucent in colour and delicate jelly-like in structure. To ensure complete water removal, dECM was frozen in liquid nitrogen followed by lyophilisation in a freeze drier, yielding lyophilized ECM (LECM). The dECM and LECM were characterized in terms of structure and composition, and the LECM was used for migration assays and for preparation of 3D electrospun scaffolds.



### 3.2.3 Biochemical assays

The cECM, dECM and LECM (n=9 per group, 3 different donors) were characterized for sulphated GAG content and hydroxyproline (HYP) content as an indicator of collagen. To this end, all ECM samples were digested in papain buffer (100 mM phosphate buffer, 5 mM l-cysteine, 5 mM ethylene diamine tetra-acetic acid, and 140 mg/mL papain) for 16 hours at 60°C. From the digested samples, the GAG content was analysed using a dimethyl-methylene blue (DMMB) assay, modified from a previous protocol [20], with shark cartilage chondroitin sulphate (Sigma) as a reference. HYP content was measured with a Chloramin-T assay as previously described [21]. The GAG & HYP concentrations were calculated using their respective standard curves.

### 3.2.4 Elastin Assay

The concentrations of elastin in cECM and dECM were measured using the Fastin Elastin Assay (Biocolor), following the manufacturer's protocol (n=9 per group with 3 different donors). LECM was excluded for this assay as the manufacturer's protocol specifies use of wet samples. Briefly, elastin was extracted by incubating samples in anhydrous oxalic acid (0.25M, Fluka Chemie) for one hour at 100 °C, which converts the insoluble elastin from samples into water soluble  $\alpha$  elastin. The oxalic acid treatment was repeated three times and the solubilized extract was collected. The extract was treated as described by the manufacturer's protocol, and dye absorbance was measured at 513 nm using a plate reader. The elastin concentration was calculated in  $\mu\text{g}$  per mg wet sample.

### 3.2.5 Collagen staining

The collagen architecture of various ECM samples was stained using a collagen binding protein CNA-mcherry fluorescent probe, as previously reported by our group [22]. Samples were incubated with the CNA-mcherry probe for 60 mins at 37°C and washed with PBS for 15 mins on a plate shaker. The samples were visualized using a fluorescent microscope (Zeiss Axiovert

200M microscope), with excitation and emission wavelengths of 587 and 610 nm, respectively (n=9 per group).

### **3.2.6 Preparation and characterization of 3D electrospun scaffolds**

A polymer solution was prepared by dissolving 15% w/w of PCL in a solution consisting of 9:1 w/w ratio of hexafluoroisopropanol (Acros Organics) and 1M Acetic acid (Sigma Aldrich). The solution was sealed and kept on a magnetic stirrer overnight at room temperature. Polymeric solutions including ECM were prepared by adding 3% w/w of LECM (maximum soluble concentration) to the PCL solution. The solution was mixed for 5 hours prior to spinning. Electrospinning was performed in a climate-controlled chamber (IME Technologies) in which temperature and humidity were maintained at 23 °C and 30%, respectively. The grounded cylindrical target with rotation speed of 500 rpm was positioned at a distance of 10 cm from the spinneret. A potential difference of 18 kV was applied between the spinneret and the target. The flow rate of the polymeric solution was maintained at 20  $\mu$ l/min to fabricate electrospun meshes. All the meshes were electrospun with the same conditions to maintain the fiber diameter and porosity of the scaffolds. The spun meshes were kept overnight in the oven for drying. For all experiments, scaffolds of same dimensions (diameter 10 mm) were punched from the respective electrospun meshes. Bare PCL was used as a control group along with collagen coated scaffolds (CoIPCL).

CoIPCL scaffolds (control group) were prepared from sterilized bare electrospun PCL scaffolds (n=3). Type I bovine collagen (Advanced BioMatrix) at a concentration of 31  $\mu$ g/scaffold was added onto the scaffold to cover the entire surface area of the scaffold, followed by 2 hour incubation at room temperature. The excess collagen was washed with PBS and samples were stored at 4 °C until further use. The samples were used within 6 days to avoid degradation of the collagen.

### **3.2.7 Scanning electron microscopy**

The fabricated scaffolds were visualised using scanning electron microscopy (SEM) to analyse the fiber diameter and the morphology of the fibers. The SEM images were taken with a 2kV beam using a Quanta 600F field emission scanning electron microscope (FEI Company). The fiber diameter was quantified by measuring 20 fibers per scaffold type, using Image J software [23] (Image J 1.48v, National Institutes of Health). Reported values represent the average  $\pm$  standard deviation.

The cell-seeded scaffolds were also visualised under SEM. The samples to be imaged were fixated in glutaraldehyde (2.5% grade I) solution for 24 hours. The fixated samples were washed and stored in PBS at 4°C until further use. The stored samples were first washed with PBS for 10 minutes (twice). Subsequently the samples were dehydrated using a dehydration series with increasing ethanol concentration (50, 60, 70, 80, 90, 96 and 100%) each for 10 minutes. Lastly the samples were kept overnight for drying and mounted onto an aluminium holder and visualized using SEM.

### **3.2.8 Human peripheral mononuclear cell isolation**

Human peripheral blood mononuclear cells (hPBMCs) were isolated from buffy coats obtained from healthy human donors (9 donors) under informed consent (Sanquin). The obtained buffy coats were diluted in 0.6% (w/v) sodium citrate in PBS, carefully layered onto iso-osmotic medium with a density of 1.077 g/ml (Lymphoprep, Axis-Shield), and centrifuged for 30 mins at 350 g. After thorough washing, the resulting hPBMCs pellet was resuspended in freezing medium consisting of RPMI, supplemented with 20% (v/v) fetal bovine serum (FBS) and 10% (v/v) Dimethyl Sulfoxide (DMSO; Merck Millipore), and cryopreserved in liquid nitrogen until use.

Monocytes were isolated from hPBMCs according to previous protocol [24]. Briefly, a hyper-osmotic solution using Percoll (GE Healthcare) was prepared by mixing 48.5 ml Percoll, 41.5 ml of water and 10 ml of 1.6M sodium chloride. The stored hPBMCs were thawed and centrifuged at 350 g for 7 minutes to remove DMSO. Subsequently, the cells were resuspended in medium and

---

counted. The hPBMC concentration was set to  $150\text{-}200 \times 10^6$  cells in 3 ml, carefully layered onto 10 ml of hyper-osmotic solution and centrifuged at 580 g for 15 minutes with the brake off. The interface was collected using a Pasteur pipette (combined up to 3 tubes), resuspended in RPMI at final volume of 45 ml of RPMI, and centrifuged again. The resulting supernatant was discarded and the cell suspension was referred to as monocyte suspension, used for seeding on dECM and on 3D scaffolds.

### **3.2.9 Monocyte migration assay**

Boyden chambers (ThinCerts, Griner Bio-One) with a PET membrane consisting of 3  $\mu\text{m}$  pores were fitted into each well of a 24-wells plate. The samples were placed at the bottom compartment of Boyden chamber and covered with medium. An hPBMCs suspension was placed in the upper compartment at a concentration of  $1 \times 10^6$  cells per mL. dECM and LECM were used as the 2D samples. Slides coated with 31  $\mu\text{g}/\text{sample}$  of collagen (Collagen) and medium with Monocyte Chemoattractant Protein-1 (MCP1; 20 ng/ml) were used as control samples. Electrospun PCL with and without LECM was used as 3D samples, with PCL scaffold coated with collagen (ColPCL) as a reference group. After 4 hours of incubation, the migrated cells in the medium were counted using a haemocytometer.

### **3.2.10 Macrophage polarization experiments**

Freshly isolated monocytes were seeded on dECM, FBS and collagen slides ( $n=3$  per experimental group at day 3 and day 9) at a density of  $1.5 \times 10^5$  cells/cm<sup>2</sup>. The experiment was repeated using 3 different donors. For this, glass slides (diameter 14 mm) were UV sterilized for 5 mins, followed by coating with FBS or collagen I. FBS at a concentration of 50  $\mu\text{l}/\text{well}$  (required concentration to cover the surface area of a well) was added to the well plate and incubated overnight. Excess of FBS was removed and the wells were washed with PBS. Type I collagen solution (Advance Biomatrix) at concentration of 31  $\mu\text{g}/\text{well}$  (required concentration to cover the surface area of a well) was incubated at room temperature for 2 hours, for coating the glass

slides with collagen. After washing with PBS, the collagen-coated slides were stored at 4 °C until further use. During the experiment, medium was refreshed at day 3 and day 6. Samples were sacrificed for analysis at day 3 and day 9. The positive control group (FBS) was treated with medium containing 100 ng/ml stimulant macrophage colony-stimulating factor (MCSF), to differentiate the seeded monocytes into macrophages.

The 3D experiments were performed by seeding 3 different donors on electrospun scaffolds (diameter of 10 mm) punched out from the electrospun mesh fabricated with and without LECM (n=3 per group). The discs were UV sterilized for 5 mins, washed with PBS and transferred to non-culture-treated 24-wells plates. All the scaffolds were soaked in medium overnight.  $1 \times 10^6$  cells per scaffold were seeded on LECM scaffold and PCL scaffold in 50  $\mu$ l of medium followed by an hour of incubation at 37 °C and 5% CO<sub>2</sub>, to allow for cell attachment onto the scaffolds. Finally, 1 ml of medium was added to each well, refreshed every 3 days. The samples were sacrificed for analysis at day 3 and day 9.

### **3.2.11 Immunohistochemistry**

The samples sacrificed at day 3 and day 9 were fixated in 10% (v/v) formalin and washed twice with PBS. Subsequent to fixation, the samples were permeabilized in 0.5% (v/v) Triton X-100 (Merck Serono), followed by blocking with serum albumin for nonspecific binding. The samples were stained against the primary antibodies as reported in Table 3.1 (1:200 dilution). Double-label immunohistochemistry was performed by incubating the samples for 1 hour at room temperature with a mix of either CD64 and CD163, or CCR7 and CD206. After removal of the primary antibodies and washing with PBS, the samples were incubated for 1 hour with the secondary antibodies as specified in Table 3.1 (1:400 dilution), and cell nuclei were counterstained with DAPI. The stained samples were imaged with a confocal microscope (TCS SP5X, Leica Microsystems).

**Table 3.1: Antibodies used for immunohistochemistry.**

Protein	Marker	Primary Antibody	Secondary Antibody
CD64	M1 marker	Mouse anti-Human IgG <sub>1</sub>	Alexa 647 Goat anti-Mouse IgG <sub>1</sub>
CD163	M2 marker	Mouse anti-Human IgG <sub>2a</sub>	Alexa 555 Goat anti-Mouse IgG <sub>2a</sub>
CCR7	M1 marker	Goat anti-Human IgG	Alexa 555 Donkey anti-Goat IgG
CD206	M2 marker	Mouse anti-Human IgG <sub>1</sub>	Alexa 647 Donkey anti-Mouse IgG <sub>1</sub>

### 3.2.12 qPCR

The sacrificed scaffolds (day 3 and day 9) were washed in PBS, followed by snap-freezing the samples and subsequently storing at -80 °C in Nalgene® cryogenic vials (Sigma). Samples were disrupted using RNA-free metal beads with a microdismembrator (Sartorius) 3 times for 30 sec at 3000 rpm. Cells were lysed using RLT buffer and subsequently RNA was isolated using Qiagen RNeasy kit (Qiagen) according to manufacturer's protocol. The isolated RNA purity and quantity was determined with a spectrophotometer (Nanodrop®, Isogen Life science). cDNA was synthesized from 100 ng RNA in 20 µl volume consisting of random primers (Promega, USA), dNTPs (Invitrogen), 5x first strand buffer (Invitrogen), DTT (Invitrogen), M-MLV enzyme (Invitrogen), and double autoclaved water. cDNA was synthesized in Thermal cycler (c1000 Touch™, Bio Rad) by heating at 65 °C for 5 mins, 2 min on ice, 2 mins at 37 °C, added M-MLV enzyme followed by 10 mins at 37 °C, 50 mins at 37°C, and 15 mins at 70 °C. The cDNA was stored at -20 °C until used for qPCR.

qPCR was performed for the primers as specified in Table 3.2. The efficiency was checked for each primer. Glyceraldehyde-3-phosphate dehydrogenase (GAPDH) and cyclophilin (CYC-1) were selected as reference genes, as they were the most stable for the experimental conditions. Gene expression was determined by adding primer mix (end concentration of 1000 mM for GAPDH, CYC-1, and MMP9, and end concentration of 500 mM for all other primers) to cDNA samples, together with SYBR green mix (Biorad) and double autoclaved water. The real time PCR reaction was carried out for 3 min at 95 °C, 40x (20 s at 95 °C, 20 s at 60 °C, 30 s at 72 °C), 1 min at 95 °C, 1 min at

65 °C followed by melting curve analysis. Data was analysed using Biorad software. Fold induction was calculated using the delta Ct method after normalizing to the geometric mean of the reference genes.

### **3.2.13 Statistical analysis**

All data from fiber diameter, migration assay, HYP, GAG and DNA assay were expressed as mean and standard deviation. Quantitative assays were performed with 9 samples (n=9 per condition from 3 different donors). Two-way ANOVA followed by Bonferroni post-hoc test was performed to detect statistical differences between the groups with  $p < 0.05$  being considered statistically significant.

Table 3.2: Primer sequences for qPCR analysis.

Primer	Symbol	Amplification size (bp)	Accession Number	Primer sequence (5' – 3')
Chemokine (C-C motif) receptor 7	CCR7	106	NM_001838	Fw: AAGCCTGGTTCCTCCCTATC RV: ATGGTCTTGAGCCTCTTGAAATA
Monocytes chemotactic protein 1	MCP1	190	NM_002982	Fw: CAGCCAGATGCAATCAATGCC RV: TGGAATCCTGAACCCACTTCT
Tumor necrosis factor $\alpha$	TNF $\alpha$	91	NM_000594	Fw: GAGGCCAAGCCCTGGTATG RV: CGGGCCGATTGATCTCAGC
Interleukin 6	IL6	45	NM_000600	Fw: ACTCACCTCTTCAGAACGAATTG RV: GTCGAGGATGTACCGAATTTGT
Interleukin 10	IL10	112	NM_000572	Fw: GACTTTAAGGGTTACCTGGGTTG RV: TCACATGCGCCTTGATGTCTG
Matrix metalloproteinase 9	MMP9	224	NM_004994	Fw: TGGGGGGCAACTCGGC RV: GGAATGATCTAAGCCCAG
CD163 molecule	CD163	137	NM_004244	Fw: CACTATGAAGAAGCCAAAATTACCCT RV: AGAGAGAAGTCCGAATCACAGA
Transforming growth factor $\beta$	TGF $\beta$	127	NM_000660	Fw: GCAACAATTCCTGGCGATACCTC RV: AGTTCTTCTCCGTGGAGCTGAAG
Mannose receptor C-type 1	CD206	114	NM_002438.3	Fw: CAACATTTCTGAACAATCCTATCCA RV: TGGGTTCTCTCTGGTTTCC
CD200 receptor 1 (transcript variant 4)	CD200R1	73	NM_170780.2	Fw: GAGCAATGGCACAGTGACTGTT RV: GTGGCAGGTCACGGTAGACA



## **3.3 Results**

### **3.3.1 Characterization of ECM**

Collagen staining revealed a well-organized collagen structure for cECM, dECM and LECM, with a more dense matrix in LECM (Figure 3.1A). Biochemical analysis revealed a significant decrease in GAG, HYP and elastin content in the dECM samples when compared to the cECM samples (Figure 3.1B). No significant differences were detected between dECM and LECM samples. Cellular components were not detected on dECM when decellularized with  $\text{NH}_4\text{OH}$  and stained with DAPI and Phalloidin (Figure 3.S1, pg 154).

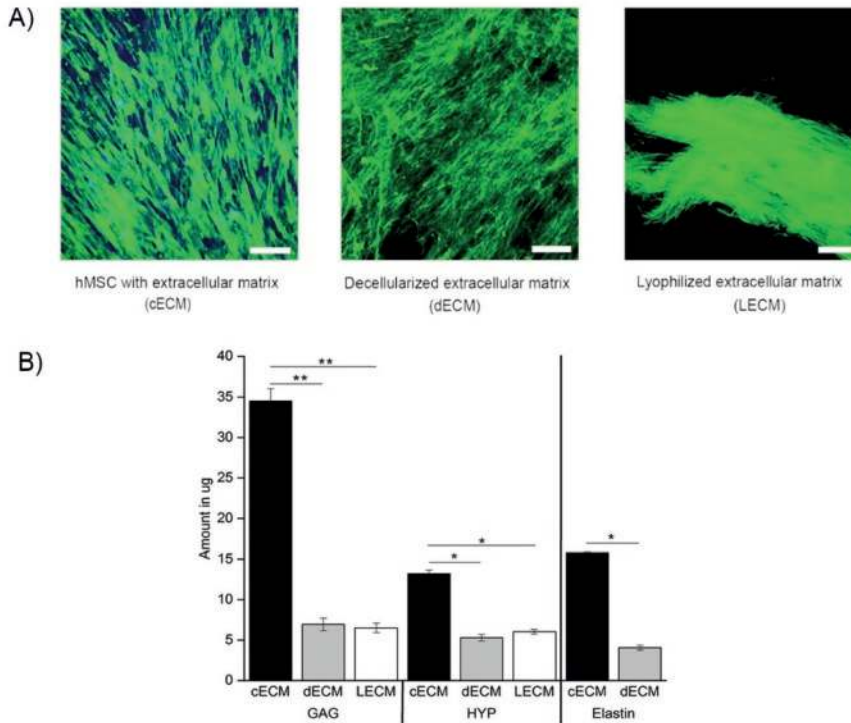


**Figure 3.1: Characterization of human mesenchymal stem cells (hMSC) derived extracellular matrix.** A) Fluorescent images showing hMSC with extracellular matrix (cECM) (cell nuclei in blue and extracellular matrix in green), the matrix after decellularization (dECM) and matrix after lyophilisation (LECM). Scale bars 100  $\mu\text{m}$ . B) Glycosaminoglycan (GAG), hydroxyproline (HYP) and elastin contents in cECM, dECM and LECM. A significantly higher amount of GAG and HYP was measured for cECM group compared to dECM and LECM. cECM also demonstrated significantly higher amount of elastin before decellularization compared to dECM. \*,\*\* indicate significant difference with  $p < 0.05$  and  $p < 0.01$  respectively;  $n = 9$  for 3 donors.

### 3.3.2 dECM and LECM experiments in 2D

- **Bioactivity of ECM assessed by migration assay**

The migration of monocytes towards dECM, LECM, collagen samples, and control media was analysed, with direct addition of MCP1 (concentration 20 ng/ml) to medium representing a positive control. After 4 hrs, significantly more cells had migrated towards the dECM when compared to collagen samples and the bare control medium, with cell counts comparable to the MCP1-enriched medium (Figure 3.2). Cell migration towards LECM was comparable to dECM and MCP1-enriched medium.

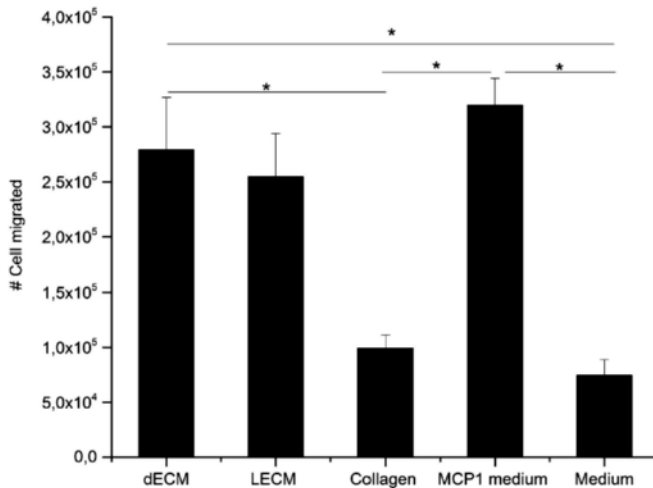


**Figure 3.2: The chemotactic properties of dECM and LECM.** The chemotaxis of monocytes was analysed after 4 hours (n=9 using 3 donors for each group). Direct addition of monocyte chemoattractant protein-1 in medium (MCP1 medium) was included as a positive control. Monocyte migration towards dECM and LECM was comparable to the MCP1 medium, while a significantly lower number of monocytes migrated towards collagen samples. \*indicates significant difference with  $p < 0.05$ .

- **Macrophage phenotype assessment via immunostaining**

Immunofluorescent staining revealed that MCSF-stimulated monocytes seeded on FBS samples differentiated into macrophages, with coexpression of CD64 and CD163, and CCR7 and CD206 on both days 3 and 9 (Figure 3.3). Cells positive to CCR7 and CD64 retained a small and rounded shape, while the majority of CD206 and CD163 positive cells showed an elongated morphology. Cells on collagen samples showed higher expression of CD64 and CCR7 and lower expression of CD163 and CD206, with a predominantly rounded morphology (Figure 3.3). In contrast, cells cultured on dECM displayed a predominantly elongated phenotype, with increased expression of CD163 and CD206 (Figure 3.3). Furthermore, increased cell attachment was observed on dECM samples compared to FBS samples, as determined by DNA assay (Figure 3.S2A, pg 155).

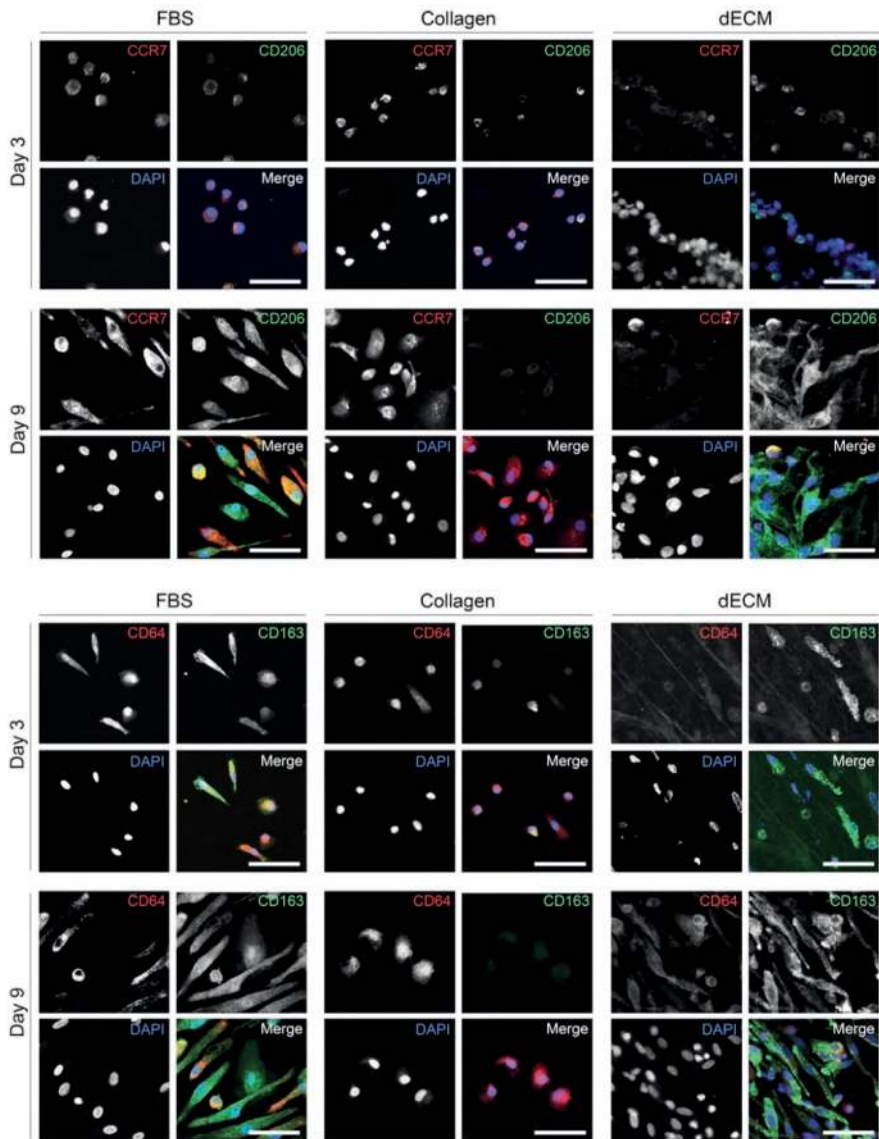


**Figure 3.3: Cell morphology and macrophage phenotype on decellularized extracellular matrix.** All the samples were immunofluorescently double-labelled with either CCR7 (red) and CD206 (green) (top panel) or CD64 (red) and CD163 (green) (bottom panel). Cell nuclei were stained blue with DAPI. An increase in M2 markers (green) at day 9 with few co-localised M1 markers (red) was observed for dECM group. At day 9, co-localized staining was observed for the FBS group, while the collagen group showed a clear increase in M1 (red) markers. Overall, a higher number of cell nuclei was observed on dECM than FBS and collagen groups. Scale bar 50 $\mu$ m.

---

- **Macrophage polarization assessment using gene expression analysis**

At day 3, gene expression of MCP1 and IL6 was significantly increased for cells cultured on dECM when compared to the other groups (Figure 3.4B, D). Cells cultured on collagen showed a significant increase for CCR7 and TNF $\alpha$  expression compared to both other groups and the dECM group, respectively (Figure 3.4A, C). A significant downregulation of CD206 expression was observed at day 3 for the dECM group in comparison to collagen, while at day 9 the CD206 expression was significantly higher in the dECM group compared to both other groups (Figure 3.4I). TGF $\beta$  expression showed a significant downregulation for dECM group with respect to the controls at both day 3 and day 9 (Figure 3.4H). MMP9 gene expression was significantly higher at day 9 for the FBS group compared to the collagen and dECM groups (Figure 3.4F). No significant differences were detected for expression of IL10 and CD163 (Figure 3.4E, G).

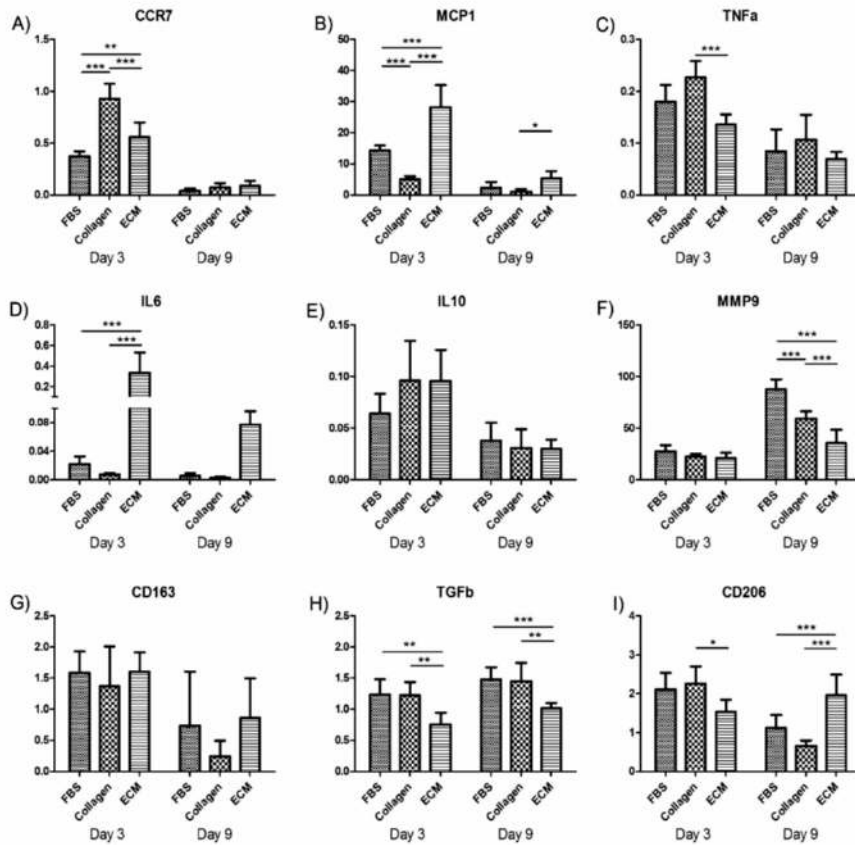


**Figure 3.4: Gene expression analysis (2D).** Gene expression of seeded monocytes on dECM, FBS and collagen samples at day 3 and 9 for (A) CCR7, (B) MCP1, (C) TNF $\alpha$ , (D) IL6, (E) IL10, (F) MMP9, (G) CD163, (H) TGF $\beta$  and (I) CD206. \*, \*\* indicate significant differences with  $p < 0.05$  and  $p < 0.01$  respectively;  $n = 9$  using 3 donors.

### 3.3.3 LECM experiments in 3D

The LECM was mixed with PCL to fabricate a hybrid LECM 3D electrospun scaffolds. The fabricated scaffolds were  $250 \pm 78 \mu\text{m}$  in thickness with an average fiber diameter of  $3.2 \pm 0.9 \mu\text{m}$  for PCL scaffolds and  $2.8 \pm 0.6 \mu\text{m}$  for hybrid LECM (i.e. LECM with PCL) scaffolds (Figure 3.5A). Collagen staining revealed a homogenous distribution of the LECM on the PCL scaffold fibers (Figure 3.5B).

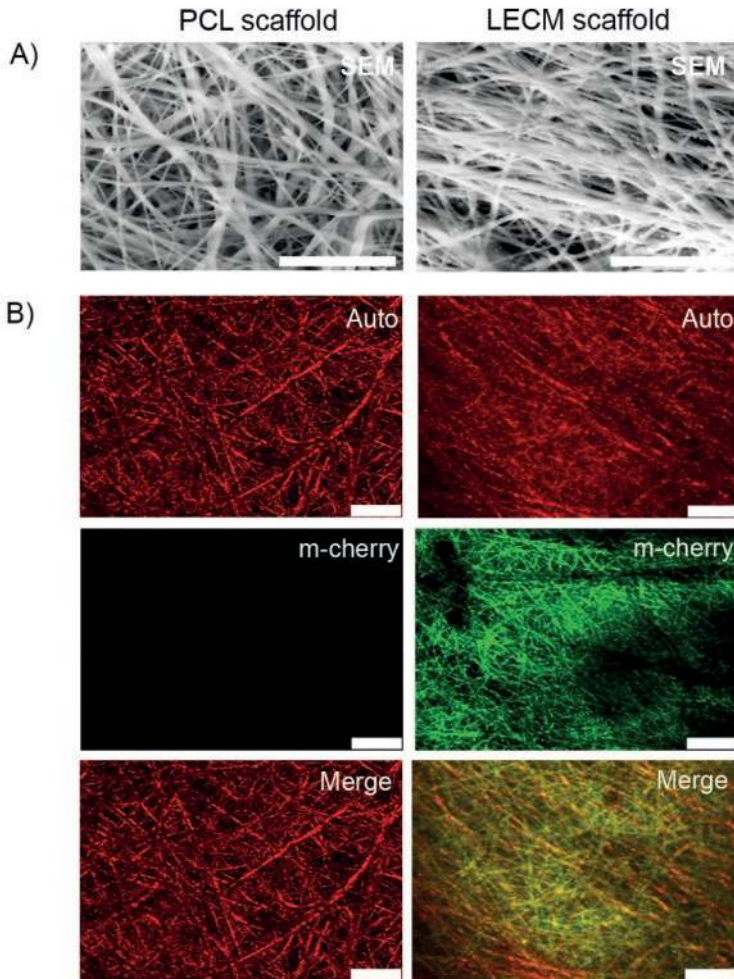


**Figure 3.5: Structure and morphology of 3D hybrid electrospun scaffolds.** (A) Scanning electron micrographs of LECM scaffold showed a comparable fiber diameter between hybrid LECM and bare PCL scaffolds. Scale bars 10  $\mu\text{m}$ . (B) Confocal microscopy (m-cherry staining for collagen in green, scaffold auto fluorescence in red) revealed a homogenous presence of collagen on LECM scaffolds, while PCL scaffolds showed no fluorescent green staining. Scale bars 10  $\mu\text{m}$ .

- **Bioactivity of ECM assessed by migration assay**

The cell migration assay was conducted to investigate the retention of bioactivity of LECM after electrospinning. Significantly more cells migrated to LECM hybrid scaffolds compared to PCL-only scaffolds and collagen-coated



PCL (ColPCL) scaffolds (Figure 3.6). However, significantly less cell migration was observed towards LECM hybrid scaffolds compared to MCP1-enriched control medium.

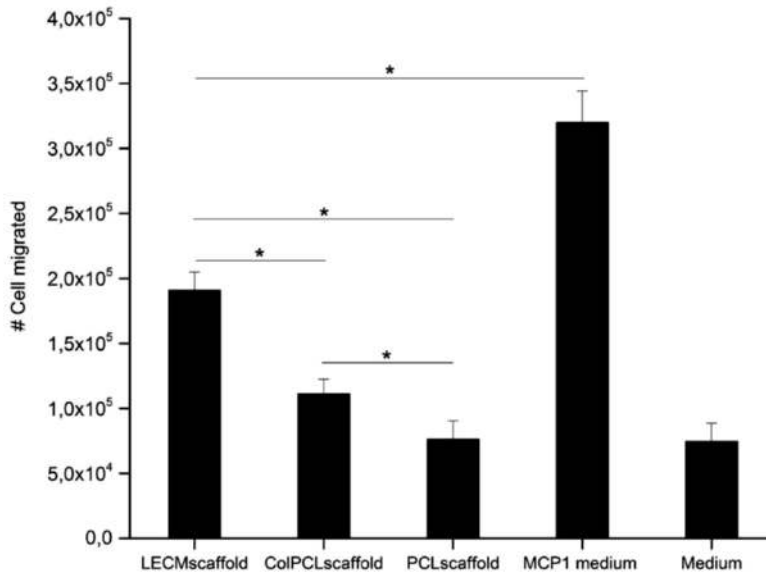


**Figure 3.6: Chemotaxis towards 3D electrospun scaffolds.** Significantly more monocyte migration was detected towards LECM hybrid scaffolds compared to collagen-coated PCL (ColPCL) and bare PCL scaffolds, but significantly less than monocyte chemoattractant protein-1 (MCP1)-enriched control medium (n=9 per group, using 3 different donors). Significantly more cells were attracted towards ColPCL scaffold than PCL scaffolds. \*indicates significant difference with  $p < 0.05$ .

- **Cell morphology assessment and immunostaining**

The cell morphology on electrospun scaffolds at day 3 and day 9 was visualized by SEM (Figure 3.7). Clusters of cells and small rounded cells were detected on PCL scaffolds at both day 3 and day 9. Large, irregular shaped cells, spreading on LECM fibers were visible at day 3 and day 9 (Figure 3.7). Fluorescent microscopy images reveal a change in morphology of cells in time when cultured on hybrid LECM scaffolds (Figure 3.8). Co-localization of CD64 -CD163, and CCR7 - CD206 was observed on LECM scaffolds at day 3, while expression of CD163 and CD206 was predominant at day 9. Cells cultured on

PCL scaffolds maintained a rounded morphology at both time points with predominant expression of CCR7 and CD64. A higher number of cells adhered to hybrid LECM scaffold compared to PCL scaffolds, as determined by DNA assay (Figure 3.S2B, pg 155).

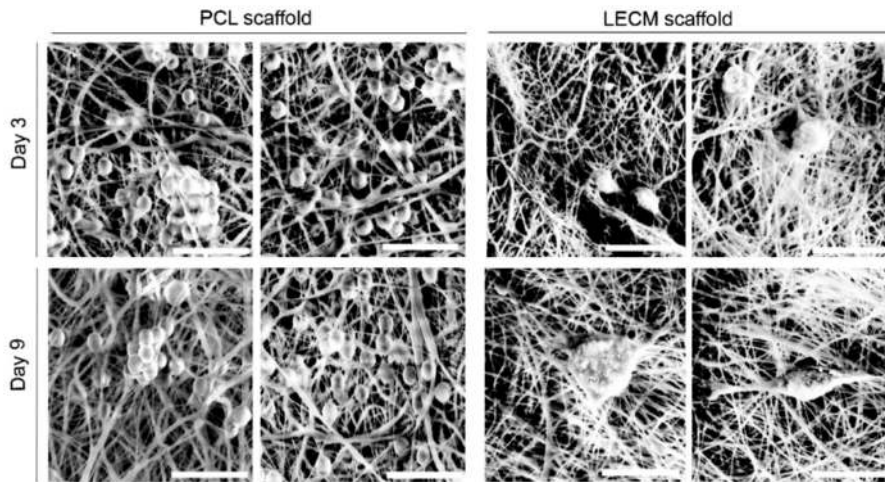


**Figure 3.7: Cell distribution and morphology on 3D hybrid electrospun scaffolds.** Scanning electron micrographs demonstrated rounded cells and cell clusters on PCL scaffolds at both day 3 and day 9 (left panel). Cells seeded on LECM scaffolds (right panel) were spreading on the surface of the scaffold (day 3) and an elongated or flat cell morphology was observed at day 9 (scale bars 20  $\mu\text{m}$ ).

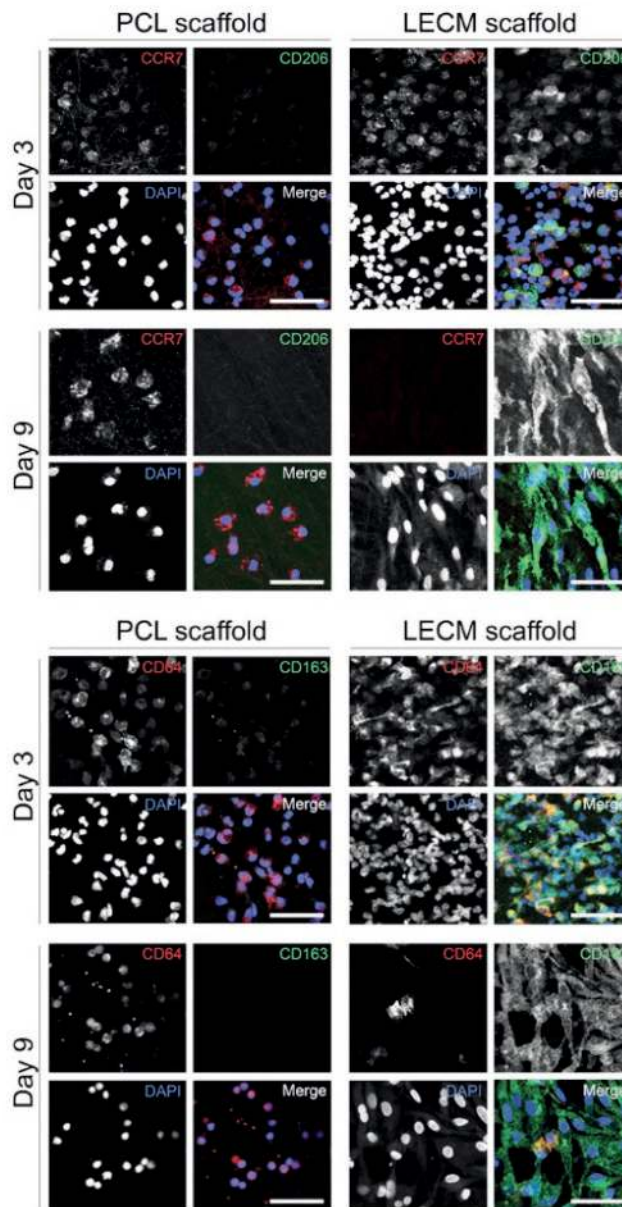


**Figure 3.8: Macrophage phenotype and morphology on 3D scaffolds.** More cell attachment was observed on LECM scaffolds compared to PCL scaffolds. At day 9, cells on LECM hybrid scaffolds expressed M2 surface markers (green) indicating polarization towards M2 macrophages, while cells on PCL-only scaffolds maintained a rounded morphology with M1 macrophage protein expression. Scale bars 50  $\mu$ m.

---

### 3.4 Discussion

ECM derived from different tissue sources has been employed as an immunomodulatory biomaterial that is able to promote constructive tissue regeneration, more favourably than synthetic materials [11-12]. In this study, we investigated the immunomodulatory properties of hMSC-derived ECM, before and after processing into 3D electrospun hybrid scaffolds with PCL. Our results demonstrated that hMSC-derived dECM had a strong chemotactic effect on human monocytes, and it promoted macrophage polarization towards an M2 phenotype. These immunomodulatory properties were maintained after processing by lyophilisation and electrospinning.

MSC-derived dECM is composed of a range of ECM proteins, including collagens, elastin and matricellular proteins (e.g. thrombospondin 1, periostin) [25-27]. The decellularization technique applied in this study affects the biochemical composition of the dECM significantly, leading to the loss of bulk proteins, similar to previous reports [28-29]. Nevertheless, our findings show that the ECM maintains its beneficial bioactive functions after decellularization, lyophilisation treatment and electrospinning. Moreover, no significant difference in biochemical composition of dECM and LECM was observed, suggesting that LECM could be a suitable material for making off-the-shelf available hybrid scaffolds for *in situ* TE applications. The strong chemotactic effects of hMSC-derived ECM in our study suggest a retention of intrinsic chemokines in the dECM matrix. Previous research by Vorotnikova et al. has shown that blastemal cells ECM derived factors promoted migration and proliferation of progenitor cells *in vitro* [30]. Here, we focused on human monocytes, as monocyte recruitment and infiltration is a prerequisite for initiation an *in situ* regenerative response. Several chemokines have shown to be involved in migration and recruitment of monocytes [31]. Ballotta et al. demonstrated abundant secretion of trophic factors, such as MCP1, by hMSCs after seeding into 3D electrospun scaffolds [32]. In our study, it could thereby be speculated that a chemokine such as MCP1 (secreted and maintained in the dECM) is driving the observed monocyte migration towards

the dECM. An alternate explanation could be that structural proteins or fragments of structural proteins, such as collagen and elastin, induce the observed chemotaxis of monocytes [33-35].

Both on protein and on gene level, the monocytes seeded on dECM expressed markers for both the M1 and the M2 profile simultaneously. This is in agreement with previous studies, defining phenotypic switching of macrophages as a continuous spectrum, rather than a bidirectional event [36]. Overall, our results demonstrate that the hMSC-derived dECM predominantly favors an M2-like macrophage phenotype, in comparison to collagen-only groups. However, the exact mechanism by which dECM modulates the polarization is not clear. Potentially, cytokines and signalling molecules residing in dECM create an appropriate biochemical microenvironment to guide macrophage polarization towards an M2 state. Additionally, the sulphated hyaluronan in ECM produced by hMSCs could interact with monocyte receptors, thereby inducing a reduction in pro-inflammatory cytokines, as previously reported [37-38]. Alternately, the GAGs in dECM can bind to pro-inflammatory cytokines, such as MCP1 and IL6, and thereby alter the bioactivity of these cytokines, leading to polarization towards an M2 phenotype [38-39]. In addition, structural proteins such as collagen and elastin, along with matricellular proteins residing in dECM, have been reported to be able to regulate inflammatory cell behaviour directly [40-41]. A major advantage of using dECM for scaffold functionalization over single-factor functionalization methods is that the dECM inherently contains a plethora of factors (e.g. cytokine, growth factors) and co-stimulatory factors. All our experiments were conducted with primary hMSCs from 3 different donors and hPBMCs from 3 different donors (9 donors in total), the observed immunomodulatory effects proved to be consistent and reproducible for all donors. This underlines the robustness of the immunomodulatory potency of hMSC-derived dECM for scaffold functionalization.

Since we aimed to incorporate the beneficial immunomodulatory effects of the hMSC-derived dECM into hybrid scaffolds, retainment of the analysed bioactive properties after lyophilisation treatment is an essential finding. This

enables the production of hybrid scaffolds, functionalized with hMSC-derived LECM, for which we used electrospun PCL as a model scaffold. The production of hybrid natural/synthetic scaffolds with cell-derived ECM has been pursued via various alternative routes. Levenson et al. cultured cells on electrospun scaffolds to deposit ECM directly on the scaffolds [47-48]. Upon decellularization, these cell-deposited ECM scaffolds were employed as 3D ECM scaffolds to enhance the chondroinductive properties of the scaffold. Mao et al. seeded primary animal cells on electrospun scaffolds to deposit ECM by infiltrating the pores of the scaffold [49]. The ECM-deposited decellularized scaffolds were demonstrated to drive hMSCs differentiation towards the lineage of the source tissue. While the above studies demonstrate a proof of concept for 3D ECM scaffolds, complete decellularization of the scaffolds in terms of cell remnants and removal of decellularization agents may be complicated, causing detrimental effects to both the ECM and the repopulating cells [50-52]. Since in our study we decellularized the ECM prior to processing it into a 3D scaffolds, removal of cellular debris and nuclei from dECM (Figure 3.S1, pg 154) was ensured, thereby circumventing the above mentioned complications. Moreover, the structure in our hybrid scaffolds is predominantly governed by the electrospinning parameters, and as such is fully tuneable.

The immunomodulatory effects of the hMSC-derived LECM were preserved after electrospinning into 3D scaffolds. In 3D, in addition to biological cues in the ECM, the scaffold architecture or microstructure can influence cell infiltration and cell behaviour [42-44]. More specifically, the scaffold microstructure, in terms of fiber diameter and pore size, can regulate macrophage polarization, as previously reported by Wang et al. [45]. In that study, *in vitro* culture of macrophages on electrospun meshes with thin fibers (diameter less than 1  $\mu\text{m}$ ) polarized towards a pro-inflammatory phenotype, while macrophages cultured on thick fibers (diameter larger than 5  $\mu\text{m}$ ) polarizes towards M2 phenotype [45]. In contrast, Saino et al. demonstrated a minimized inflammatory response on nanofibrous electrospun scaffolds, when compared to microfibrillar electrospun scaffolds and 2D surfaces [46].

Here, we electrospun scaffolds in the microfibrinous range (fiber diameter of approximately 3  $\mu\text{m}$ ), and importantly the fiber diameters between the bare PCL and the LECM hybrid scaffold were not significantly different from each other. Although the precise fiber diameter that directly correlates to positive M2 polarization is ambiguous, it is clear that the microstructure of the electrospun scaffold is an additional cue that can skew macrophage phenotypic profile.

### **3.5 Conclusion**

This study demonstrates that hMSC-derived dECM has a positive influence on human monocyte recruitment and macrophage polarization, intrinsically providing a biological microenvironment that favors macrophage polarization towards a pro-regenerative M2 phenotype. Moreover, hMSC-derived ECM maintains its beneficial immunomodulatory functions, after decellularization, lyophilisation, and electrospinning. These findings offer opportunities to combine cell-derived ECM with synthetic materials to create a 3D hybrid scaffold. These results indicate the potential of ECM as an off-the-shelf material to design hybrid scaffolds for *in situ* TE applications.

### **Acknowledgements**

The authors would like to thank Dr. Noortje Bax for her input on decellularization treatments and analysis. This research was supported by a grant from the Dutch government to the Netherlands Institute for Regenerative Medicine (NIRM) and their contribution is gratefully acknowledged.

---

## References

1. Wissing, T.B., et al., *Biomaterial-driven in situ cardiovascular tissue engineering—a multi-disciplinary perspective*. npj Regenerative Medicine, 2017. **2**(1): p. 18.
2. Martinez, F.O., et al., *Macrophage activation and polarization*. Frontiers in Bioscience, 2008. **13**: p. 453-61.
3. Brown, B.N., et al., *Macrophage polarization: An opportunity for improved outcomes in and regenerative medicine*. Biomaterials, 2012. **33**(15): p. 3792-3802.
4. Keane, T.J. and S.F. Badylak, *Biomaterials for tissue engineering applications*. Seminars in Pediatric Surgery, 2014. **23**(3): p. 112-118.
5. Dhandayuthapani, B., et al., *Polymeric Scaffolds in Tissue Engineering Application: A Review*. International Journal of Polymer Science, 2011.
6. Ma, P.X., *Scaffolds for tissue fabrication*. Materials Today, 2004. **7**(5): p. 30-40.
7. Lu, T.L., Y.H. Li, and T. Chen, *Techniques for fabrication and construction of three-dimensional scaffolds for tissue engineering*. International Journal of Nanomedicine, 2013. **8**: p. 337-350.
8. Parenteau-Bareil, R., R. Gauvin, and F. Berthod, *Collagen-Based Biomaterials for Tissue Engineering Applications*. Materials, 2010. **3**(3): p. 1863-1887.
9. Ellis, D.L. and I.V. Yannas, *Recent advances in tissue synthesis in vivo by use of collagen-glycosaminoglycan copolymers*. Biomaterials, 1996. **17**(3): p. 291-299.
10. Badylak, S.F., *The extracellular matrix as a biologic scaffold material*. Biomaterials, 2007. **28**(25): p. 3587-3593.
11. Dziki, J.L., et al., *Solubilized extracellular matrix bioscaffolds derived from diverse source tissues differentially influence macrophage phenotype*. Journal of Biomedical Materials Research Part A, 2017. **105**(1): p. 138-147.
12. Sicari, B.M., et al., *The promotion of a constructive macrophage phenotype by solubilized extracellular matrix*. Biomaterials, 2014. **35**(30): p. 8605-8612.
13. Ben-Ami, E., S. Berrih-Aknin, and A. Miller, *Mesenchymal stem cells as an immunomodulatory therapeutic strategy for autoimmune diseases*. Autoimmunity Reviews, 2011. **10**(7): p. 410-415.
14. Yi, T. and S.U. Song, *Immunomodulatory Properties of Mesenchymal Stem Cells and Their Therapeutic Applications*. Archives of Pharmacal Research, 2012. **35**(2): p. 213-221.
15. Zhao, Q., H. Ren, and Z. Han, *Mesenchymal stem cells: Immunomodulatory capability and clinical potential in immune diseases*. Journal of Cellular Immunotherapy, 2016. **2**(1): p. 3-20.
16. Pei, M., et al., *A review of decellularized stem cell matrix: a novel cell expansion system for cartilage tissue engineering*. Eur Cell Mater, 2011. **22**: p. 333-43; discussion 343.
17. Abumaree, M.H., et al., *Human Placental Mesenchymal Stem Cells (pMSCs) Play a Role as Immune Suppressive Cells by Shifting Macrophage Differentiation from Inflammatory M1 to Anti-inflammatory M2 Macrophages*. Stem Cell Reviews and Reports, 2013. **9**(5): p. 620-641.
18. Both, S.K., et al., *A rapid and efficient method for expansion of human mesenchymal stem cells*. Tissue Engineering, 2007. **13**(1): p. 3-9.
19. Gilbert, T.W., T.L. Sellaro, and S.F. Badylak, *Decellularization of tissues and organs*. Biomaterials, 2006. **27**(19): p. 3675-3683.
20. Farndale, R.W., C.A. Sayers, and A.J. Barrett, *A Direct Spectrophotometric Micro-Assay for Sulfated Glycosaminoglycans in Cartilage Cultures*. Connective Tissue Research, 1982. **9**(4): p. 247-248.
21. Mol, A., et al., *Fibrin as a cell carrier in cardiovascular tissue engineering applications*. Biomaterials, 2005. **26**(16): p. 3113-3121.
22. Aper, S.J.A., et al., *Colorful Protein-Based Fluorescent Probes for Collagen Imaging*. Plos One, 2014. **9**(12).
23. Schneider, C.A., W.S. Rasband, and K.W. Eliceiri, *NIH Image to ImageJ: 25 years of image analysis*. Nat Meth, 2012. **9**(7): p. 671-675.
24. Repnik, U., M. Knezevic, and M. Jeras, *Simple and cost-effective isolation of monocytes from buffy coats*. Journal of Immunological Methods, 2003. **278**(1): p. 283-292.



25. Harvey, A., et al., *Proteomic Analysis of the Extracellular Matrix Produced by Mesenchymal Stromal Cells: Implications for Cell Therapy Mechanism*. Plos One, 2013. **8**(11): p. e79283.
26. Byron, A., J.D. Humphries, and M.J. Humphries, *Defining the extracellular matrix using proteomics*. International Journal of Experimental Pathology, 2013. **94**(2): p. 75-92.
27. Ragelle, H., et al., *Comprehensive proteomic characterization of stem cell-derived extracellular matrices*. Biomaterials, 2017. **128**: p. 147-159.
28. Crapo, P.M., T.W. Gilbert, and S.F. Badylak, *An overview of tissue and whole organ decellularization processes*. Biomaterials, 2011. **32**(12): p. 3233-43.
29. Zhao, Y., M. Yu, and S. Bai, *[Research progress of decellularization and application in tissue engineering]*. Zhongguo Xiu Fu Chong Jian Wai Ke Za Zhi, 2013. **27**(8): p. 950-4.
30. Vorotnikova, E., et al., *Extracellular matrix-derived products modulate endothelial and progenitor cell migration and proliferation in vitro and stimulate regenerative healing in vivo*. Matrix Biology, 2010. **29**(8): p. 690-700.
31. Shi, C. and E.G. Pamer, *Monocyte recruitment during infection and inflammation*. Nature reviews Immunology, 2011. **11**(11): p. 762-774.
32. Ballotta, V., et al., *Synergistic protein secretion by mesenchymal stromal cells seeded in 3D scaffolds and circulating leukocytes in physiological flow*. Biomaterials, 2014. **35**(33): p. 9100-9113.
33. Senior, R.M., et al., *Val-Gly-Val-Ala-Pro-Gly, a Repeating Peptide in Elastin, Is Chemotactic for Fibroblasts and Monocytes*. Journal of Cell Biology, 1984. **99**(3): p. 870-874.
34. O'Reilly, P.J., A. Gaggar, and J.E. Blalock, *Interfering with extracellular matrix degradation to blunt inflammation*. Current Opinion in Pharmacology, 2008. **8**(3): p. 242-248.
35. Postlethwaite, A.E. and A.H. Kang, *Collagen-and collagen peptide-induced chemotaxis of human blood monocytes*. Journal of Experimental Medicine, 1976. **143**(6): p. 1299-307.
36. Mosser, D.M. and J.P. Edwards, *Exploring the full spectrum of macrophage activation*. Nature Reviews Immunology, 2008. **8**(12): p. 958-969.
37. Franz, S., et al., *Modulation of inflammatory macrophage functions by artificial extracellular matrices composed of collagen and sulfated hyaluronan*. Experimental Dermatology, 2012. **21**(3): p. e26-e26.
38. Franz, S., et al., *Artificial extracellular matrices composed of collagen I and high-sulfated hyaluronan promote phenotypic and functional modulation of human pro-inflammatory M1 macrophages*. Acta Biomaterialia, 2013. **9**(3): p. 5621-5629.
39. Bornstein, P. and E.H. Sage, *Matricellular proteins: extracellular modulators of cell function*. Curr Opin Cell Biol, 2002. **14**(5): p. 608-16.
40. Lopez-Dee, Z., K. Pidcock, and L.S. Gutierrez, *Thrombospondin-1: multiple paths to inflammation*. Mediators Inflamm, 2011. **2011**: p. 296069.
41. Adair-Kirk, T.L. and R.M. Senior, *Fragments of extracellular matrix as mediators of inflammation*. International Journal of Biochemistry & Cell Biology, 2008. **40**(6-7): p. 1101-1110.
42. Kianoush, F., et al., *Regulation of RAW264.7 macrophage polarization on smooth and rough surface topographies by galectin-3*. Journal of Biomedical Materials Research Part A, 2017. **105**(9): p. 2499-2509.
43. Chen, Z., et al., *Nanoporous microstructures mediate osteogenesis by modulating the osteo-immune response of macrophages*. Nanoscale, 2017. **9**(2): p. 706-718.
44. Silva, M.M.C.G., et al., *The effect of anisotropic architecture on cell and tissue infiltration into tissue engineering scaffolds*. Biomaterials, 2006. **27**(35): p. 5909-5917.
45. Wang, Z., et al., *The effect of thick fibers and large pores of electrospun poly(epsilon-caprolactone) vascular grafts on macrophage polarization and arterial regeneration*. Biomaterials, 2014. **35**(22): p. 5700-10.
46. Saino, E., et al., *Effect of electrospun fiber diameter and alignment on macrophage activation and secretion of proinflammatory cytokines and chemokines*. Biomacromolecules, 2011. **12**(5): p. 1900-11.
47. Levorson, E.J., et al., *Cell-Derived Polymer/Extracellular Matrix Composite Scaffolds for Cartilage Regeneration, Part 2: Construct Devitalization and Determination of*

- 
- Chondroinductive Capacity*. Tissue Engineering Part C-Methods, 2014. **20**(4): p. 358-372.
48. Levorson, E.J., et al., *Cell-Derived Polymer/Extracellular Matrix Composite Scaffolds for Cartilage Regeneration, Part 1: Investigation of Cocultures and Seeding Densities for Improved Extracellular Matrix Deposition*. Tissue Engineering Part C-Methods, 2014. **20**(4): p. 340-357.
  49. Mao, Y., et al., *Cell type-specific extracellular matrix guided the differentiation of human mesenchymal stem cells in 3D polymeric scaffolds*. J Mater Sci Mater Med, 2017. **28**(7): p. 100.
  50. Gilpin, A. and Y. Yang, *Decellularization Strategies for Regenerative Medicine: From Processing Techniques to Applications*. Biomed Research International, 2017. **2017**: p. 9831534.
  51. Lu, H., et al., *Comparison of decellularization techniques for preparation of extracellular matrix scaffolds derived from three-dimensional cell culture*. Journal of Biomedical Materials Research Part A, 2012. **100**(9): p. 2507-16.
  52. He, M., et al., *Optimization of SDS exposure on preservation of ECM characteristics in whole organ decellularization of rat kidneys*. J Biomed Mater Res B Appl Biomater, 2017. **105**(6): p. 1352-1360.





Chapter 4

Mesoporous silica  
nanoparticles enhance  
loading efficiency of  
MCP1 on electrospun  
scaffolds

## Abstract

*In situ* tissue engineering utilizes the regenerative potential of the body to repair and reconstruct damaged tissues. This approach focuses on direct implantation of scaffolds and relies on the scaffold to provide the appropriate structural and biological microenvironment to guide the regenerative process. Electrospun scaffolds mimic the structure of native collagen bundles however, they lack bioactivity. Monocyte Chemoattractant Protein (MCP1) is one of the important cytokines that guides the inflammatory process, by enhancing monocyte migration and regulating macrophage polarization. Vascular grafts incorporated with MCP1 have demonstrated rapid influx of monocytes, leading to improved neo artery formation *in vivo*. Enhancing the total loading degree of MCP1 can enhance the amount of MCP1 released and accordingly increase the local MCP1 concentration. In this study, we employ animofunctionalized mesoporous silica nanoparticles (MSN) as depots of MCP1 to enhance the loading of the scaffold. MSNs physio adsorbed on electrospun polycaprolactone bisurea (PCLBU) scaffold enhanced the loading efficacy to  $38,5 \pm 1,1\%$  (i.e. [MSN + MCP1] scaffolds) compared to a loading efficacy of  $6,6 \pm 0,9 \%$  on scaffolds without MSNs (i.e. + MCP1 scaffolds). The developed [MSN + MCP1] scaffolds exhibit fast release profile by releasing approximately  $43 \pm 0,6 \%$  of total loaded MCP1 within 4h. The MCP1 release from [MSN + MCP1] scaffolds promoted selective migration of monocytes towards the scaffold. Further, high cell viability was observed on scaffolds with MSNs. These *in vitro* results demonstrate the potential of MSN as drug depots for improving the drug loading efficiency of the scaffolds.

## 4.1 Introduction

*In situ* tissue engineering is an emerging approach that utilizes the regenerative potential of the body to reconstruct damaged and diseased tissues. This approach focuses on using a synthetic scaffold mimicking the native microenvironment of the cell to attract and promote cell adhesion, enhance proliferation, and evoke a favorable regenerative response. Thus, the scaffold to be implanted should provide the necessary structural, mechanical and biological microenvironment to support tissue formation. Synthetic scaffolds lack the intrinsic biological cues which regulate the inflammatory process and stimulate tissue formation. Hence, incorporation of exogenous bioactive factors into the scaffold helps to mimic the cellular niche and modulate the immune response.

Throughout the process of the immune response, bioactive factors present in the surrounding tissue regulate the actions of infiltrating immune cells. One of the key mediators involved in the inflammatory process is monocyte chemoattractant protein 1 (MCP1) [1-6]. It is a CC chemokine that promotes migration of monocytes from the bone marrow towards an injured tissue [7]. MCP1 has been demonstrated as an immunomodulatory factor that promotes vessel remodelling and regeneration in mice [8]. Exogenous MCP1 at different concentrations (0ng/ml, 2ng/ml, 20ng/ml and 50ng/ml) has been directly incorporated into fibrin-polycaprolactone (PCL) scaffold. In this system, a burst release of MCP1 within the first 90 minutes was observed during static conditions while the release rate was accelerated to 45 minutes in flow conditions [9]. The released MCP1 created a local gradient which resulted in migration of specific monocyte subsets towards the scaffolds [9]. Furthermore, enhanced migration of monocytes was observed with MCP1 concentrations of 20ng/ml and 50 ng/ml [9]. Improved neotissue formation was observed in MCP1 loaded fibrin-PCL scaffolds implanted in rats compared to scaffolds without MCP1 [10]. Thus, in this study we wanted to incorporate MCP1 as a bioactive molecule inside an electrospun scaffold since it could be seen as a

beneficial treatment option to guide cell infiltration and regulate the healing process.

Mesoporous silica nanoparticles (MSNs) are frequently employed as a drug depots for biomedical applications [11-17]. The flexibility in tailoring the physiochemical properties of MSNs, such as shape, surface charge, particle size, surface area and pore volume, make them a potential candidate for delivery of drugs or biological moieties [18-19]. In addition, the properties of MSNs can be tuned to influence loading and release of drugs, cellular uptake, as well as cytotoxicity [20]. Furthermore, functionalization of MSNs with amino groups has been commonly employed to tune the properties of MSNs [28-31]. Manzano et al. demonstrated that amino functionalized mesoporous silica microspheres had a higher drug loading capacity of ibuprofen as compared to non-functionalized particles [21]. Morishige et al showed that surface modification of silica particles with functional groups ( $-\text{COOH}$ ,  $-\text{NH}_2$ ,  $-\text{SO}_3\text{H}$ ,  $-\text{CHO}$ ) suppresses inflammatory effects by reducing IL-1 $\beta$  production in THP1 cells [22]. Accordingly, the aim of this study was to employ amino functionalized MSNs as depots of MCP1, in order to improve MCP1 loading capacity of electrospun scaffolds.

In this study, we fabricated an electrospun polycaprolactone bisurea (PCLBU) scaffold functionalized with MCP1, using amino functionalized MSNs as carriers. We hypothesized that amino functionalized MSNs would enhance the loading efficiency and preserve the biological function of released MCP1. The higher MCP1 concentration would trigger a positive cell response and aid in the modulation of the early inflammatory process. To test this hypothesis, the chemoattractant property of the released MCP1 on human peripheral blood mononuclear cells (hPBMCs) was investigated. The loading efficiency of MCP1 on scaffolds with and without MSNs were determined by measuring the residual MCP1 concentration in the loading solution after loading MCP1. Subsequently, the MCP1 release kinetics from the scaffolds with MSN were investigated. In the final step, the biological response of the released MCP1 with respect to monocyte migration and infiltration was analysed.

---

## 4.2 Experimental

### 4.2.1 Particle synthesis

Amino functionalized mesoporous silica nanoparticles (MSNs) were synthesized according to Rosenholm et al [23]. A mixture of methanol (1440.0 g), deionized water (1750.0 g), 1M sodium hydroxide solution (9.1 g) and 43.9 mmol cetyltrimethylammoniumbromide (CTAB) (16.0 g;) was stirred for 1 h (400 rpm) in a 4L round bottom flask at room temperature. Then TMOS (4.76 mL; 32.2 mmol) and APTMS (0.62 mL; 2.6 mmol) were mixed under inert gas and added to the solution in a single step. The solution was further stirred at 400 rpm overnight. The particles were flocculated by addition of ammonium nitrate before being separated through centrifugation. In order to remove the structure-directing agent the particles were washed three times under ultra sonication at 60 °C in an ethanolic ammonium nitrate solution (6 g/L) for 1 h, followed by washing with ethanol. After each washing step the particles were separated by centrifugation and the supernatant was replaced. Finally, the particles were dried in a vacuum overnight at 70 °C.

### 4.2.2 Scanning electron microscopy (SEM)

The surface morphology and shape of MSNs were obtained using a Quanta 600 F emission scanning electron microscope (FEI Company). 1 mg MSNs were mounted on the holder and analysed using 5 kV beam at a high magnification (60k and 150K). The size was measured with Image J using SEM images and the average size was reported.

### 4.2.3 Transmission electron microscopy (TEM)

The size distribution was verified using Tecnai G2 Sphera transmission electron microscope (FEI Company) [24]. MSNs were dispersed in chloroform at 0.003wt% using an ultrasonic bath. The dispersed solution was applied on Cu200C grid and imaged under TEM. The average of 20 MSNs was analysed and the average size was reported.



#### **4.2.4 Preparation of electrospun scaffolds**

Supramolecular PCLBU polymer was synthesized by SyMO-Chem (Eindhoven University of Technology, The Netherlands) as reported previously [25-27]. The electrospinning solution was prepared by dissolving 15% (w/w) PCLBU ( $M_n$  2 kg/mol) polymer in a 15:85 w/w ratio of methanol and chloroform (amylene stabilized) from Sigma Aldrich. The solution was sealed and stirred at room temperature overnight. An electrospinning set up developed by IME Technologies was used for the scaffold fabrication. The polymeric solution was fed through a nozzle at a flow rate of 25  $\mu\text{L}/\text{min}$  and a voltage of 18 kV was maintained. The temperature and humidity were maintained at 23 °C and 30%, respectively. The solution formed micrometer range fibers which were collected on a grounded target. The collected fibrous mesh was placed under vacuum overnight to remove the remaining solvent. The average fiber diameter was determined with SEM.

#### **4.2.5 Adsorption of MSNs on electrospun scaffolds**

Electrospun PCLBU scaffolds of 1 cm diameter were cut from a fibrous mesh. The cut scaffolds were assumed to have the same structure, porosity and weight. The cut scaffolds were UV sterilized for 5 minutes. Subsequently these scaffolds were covered with 50 $\mu\text{L}$  of ethanolic dispersion containing 1 mg of MSNs. To ensure the scaffolds were homogeneously covered with MSNs, the well plate was placed on a shaker and left to dry at room temperature. The resulting MSN scaffolds were characterized using SEM imaging. MSN loaded with Alexa 488 were also dispersed on electrospun scaffold and visualized under confocal microscope

#### **4.2.6 Drug loading**

Recombinant MCP1 from Peprotech was used for loading the MSNs. Loose MSNs (without scaffold) were loaded with MCP1 to test if loaded MCP1 was released over time. Next, MSNs physio-adsorbed on electrospun were loaded with MCP1 to test if MSNs enhance the loading efficiency of scaffolds.

Loose MSNs (without scaffold): 1 mg of loose MSNs was carefully weighed in an eppendorf tube. MCP1 in PBS at a concentration of 100ng/ml and 300ng/ml (n = 9 per group) were added to the tubes. To ensure homogenous loading the MSN with MCP1, tubes were placed in ultrasonicator at 37°C for 1 hour.

**Table 4.1 Experimental conditions for the study.** Electrospun PCLBU scaffolds were loaded with MCP1 directly or MSNs were physio-adsorbed on scaffolds and then loaded with MCP1.

Scaffolds conditions	Description of scaffolds w.r.t. MCP1 and MSN
+ MCP1 scaffolds	PCLBU scaffolds loaded with MCP1
- MCP1 scaffolds	PCLBU scaffolds without MCP1
MSN + MCP1 scaffolds	PCLBU scaffolds with MSNs with MCP1
MSN - MCP1 scaffolds	PCLBU scaffolds with MSNs without MCP1

MSNs on scaffold: Table 4.1 gives a description of the experimental conditions used while loading scaffolds with MCP1. Scaffolds with MSNs were loaded with MCP1 by dispersing 3 mg MCP1 in 1mL PBS. 100  $\mu$ l of MCP1 stock solution was added to all scaffolds and incubated for 1 hour. The supernatant was collected and scaffolds were rinsed in PBS and immersed in medium (n = 9). Electrospun scaffolds (without MSN) were loaded directly with MCP1 and unloaded electrospun scaffold were used as control (-MCP1 scaffold). The next paragraph outlines the analysis to measure MCP1 concentration in collected supernatant and rinsed with PBS. The amount of MCP1 loaded on the scaffolds was determined indirectly as the difference in the total amount of MCP1 loaded and the amount of MCP1 in the supernatant (i.e. supernatant collected and rinsed PBS).

Loading efficiency % = (Amount of MCP1 loaded / total MCP1 amount) \* 100

#### 4.2.7 Release of MCP1

To measure the release of MCP1, scaffolds (n = 9) were incubated statically in Roswell Park Memorial Institute (RPMI) medium (1mL) for 7 days. Medium was collected (n = 9 per time point) at Day 1, Day 3, Day 5 and Day 7. Medium

was removed completely at each time point and replenished with same volume of fresh medium each time. The collected medium was stored at -80°C. The amount of MCP1 in the medium was measured using an ELISA kit (Human MCP1 Elisa kit, Ray Biotech) following the manufacturer's protocol. The obtained release was determined per scaffold with the following formula:

Protein (MCP1) release % = (Amount of MCP1 released/amount of MCP1 loaded) \* 100

#### **4.2.8 Human peripheral blood mononuclear cells (hPBMCs) isolation**

Human peripheral blood buffy coats were obtained from healthy donors after informed consent from Sanquin, The Netherlands. Lymphoprep density gradient was used for isolation of Human peripheral blood mononuclear cells (hPBMCs). After dilution of the buffy coats in 0.6% sodium citrate, lymphoprep solution (density 1.077 g/mL) was added and centrifuged for 15 minutes. A layer of mononucleated cells formed above lymphoprep. The layer was collected and centrifuged again followed by few washing steps. The resulting hPBMCs were counted using a nuclear counter, resuspended in freezing medium (RPMI with 20% fetal bovine serum and 10% dimethyl sulfoxide (Merck Millipore) and stored in liquid nitrogen.

#### **4.2.9 Migration assay**

The biological function of the released MCP1 was evaluated using a migration assay. Experiments were performed with 3 different donors with 3 repetitions per group. A Boyden chamber fitted in 24 well plate consisting of a 3µm porous PET membrane was used to access the migration of cells. All scaffolds (1 cm in diameter and 2.5 mg weight) with and without MSNs (1mg MSN / 50ul ethanolic dispersion / scaffold) and loaded with and without MCP1 (300ng MCP1) were placed below the Boyden chamber (in the bottom compartment). Additionally, free MCP1 was dissolved in medium. The concentration of free MCP1 corresponds to the release at the specific time point, in order to verify the biological effect of the released MCP1 (from MSNs). The concentration

---

added to medium as controls include 2.2 ng/ml (release at 4h) and 0.3 ng/ml (release at day 3) and 0.1 ng/ml (release at day 7). hPBMCs at a concentration of one million cells per mL were added in the upper compartment. After 4 h of incubation, the presence of cells on scaffolds (after 4 h) was assessed by staining for Phalloidin and DAPI. The cells attached to scaffolds were analysed by measuring DNA content using the Hoechst dye method [28]. The migrated cells were counted by haemocytometer for both compartments. The functionality (i.e. migration of cells towards released MCP1) of MCP1 was analysed at day 3 and day 7 using the same experimental set up, with two control media (free MCP1) at concentrations of 2.2ng/ml and 0.3 ng/ml respectively.

#### **4.2.10 Immunohistochemistry**

The scaffolds from the migration assay (n = 9, with 3 different donors) were fixed in 10% formalin and washed twice with PBS. The fixed samples were permeabilized using 0.5% Triton X-100 (Merck Serono, The Netherlands) in PBS for 20 minutes. Subsequently samples were incubated in 2% BSA for an hour to block nonspecific binding, followed by primary antibodies against CD3 and CD14 (Serotec, The Netherlands) incubation for 1 hour at room temperature. Secondary antibodies (goat anti rabbit A555 and goat anti mouse A647) were incubated for 1 hour at room temperature in the dark. Nuclei were stained with DAPI for 10 minutes in the dark. After washing with PBS three times, samples were mounted on glass slides with Mowiol (Calbiochem, San Diego).

#### **4.2.11 Cell viability (WST-8) assay**

In order to investigate the viability of cells on MSN scaffolds, a WST- 8 assay was performed. CCVK-I solution from Promo Kine was used. Cells were seeded on scaffolds with and without MSN for Day 1, Day 3, Day 5 and Day 7 (n = 9 per condition). After removing the medium the scaffolds were incubated with WST- 8 (1:100) medium for 4 h. Yellow dye formation was

observed and the absorbance was measured at 450nm on a multiwell reader (Tecan infinite). The results were reported as mean and standard deviation.

#### **4.2.12 Statistical analysis**

Data are presented as mean and standard deviation. Quantitative assay were performed in triplicate (n = 9). One way ANOVA followed by Tukey's test was performed and p value of 0.05 was considered statistically significant.

---

## 4.3 Results and Discussion

### 4.3.1 MSNs synthesis, characterization and adsorption to PCLBU electrospun scaffolds

The morphology and dimensions of MSNs were studied with scanning electron microscopy (SEM) images and transmission electron microscopy (TEM) images (Figure 4.1). SEM images (Figure 4.1A) verify the homogenous morphology of MSNs and an average size distribution of  $350 \pm 0.40$  nm. TEM was used to further confirm the diameter of  $395 \pm 19.5$  nm for the synthesized MSN (Figure 4.1B) and pore size was determined to 3 nm by nitrogen sorption experiment (data not shown).

### 4.3.2 Loading MSNs with MCP1

Amino functionalized MSNs (loose MSNs) were loaded with two different concentration of MCP1 and the amount of released MCP1 was monitored for 1 week (i.e. half-life of MCP1, Figure 4.S1A, pg 157). Table 4.2 indicates that an increase in the total loading concentration of MCP1 enhances the amount of MCP1 released from MSNs, while maintaining all other experimental conditions. Although the exact amount of MCP1 adsorbed on the MSNs was not measured, MSNs (1mg) loaded with 100 ng/ml of MCP1 demonstrates cumulative MCP1 release of  $8,3 \pm 0,4$  ng after 7 days and MSNs (1mg) loaded with 300 ng/ml MCP1 shows cumulative MCP1 release  $16,1 \text{ ng} \pm 0,2 \text{ ng}$  after 7 days (Table 4.2). This release data suggests that the loading concentration of MCP1 influences the release profile of MCP1 from MSNs (Table 4.2). Furthermore, these results suggest that loose MSNs (when loaded with 300ng/ml MCP1) display a fast release within few hours followed by a slow extended release of MCP1 up to 1 week. Thus MSNs can be employed as depots and the delivery of loaded drugs can be tune.

**Table 4.2 Release of MCP1 from amino functionalized MSNs loaded using concentration of 100ng or 300ng.** Loose MSNs (1mg) were loaded at concentration of 100ng/ml and 300ng/ml in eppendorf tubes. The loaded MSNs were incubated in medium and the amount of MCP1 released in time (at 1 h, 4 h, Day 1, Day 3, Day 5 and Day 7) was measured with enzyme-linked immunosorbent assay (ELISA).

MCP1 (ng/ml) released in time from MSNs	Loading conc. 100ng	Loading conc. 300ng
1h	3,27 ± 1,05	8,69 ± 0,49
4h	2,7 ± 0,45	1,94 ± 0,74
Day 1	1,92 ± 0,25	1,91 ± 0,25
Day 3	0,27 ± 0,03	0,88 ± 0,03
Day 5	0,13 ± 0,04	1,36 ± 0,00
Day 7	0,02 ± 0,00	1,36 ± 0,01
Cumulative release	8,32 ± 0,4	16,16 ± 0,2

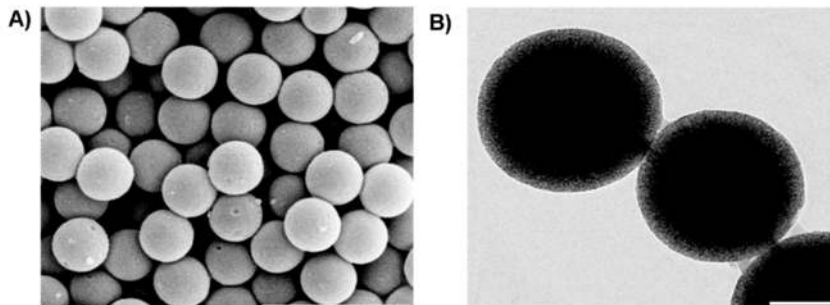


**Figure 4.1: Characterization of Mesoporous silica nanoparticles (MSNs) with SEM and TEM.** A) SEM images gives an overview of the homogenous morphology of the synthesized MSNs (Scale bar 1  $\mu$ m). B) An average size distribution of  $355 \pm 19,5$  nm was measured using TEM (scale bar 100nm).

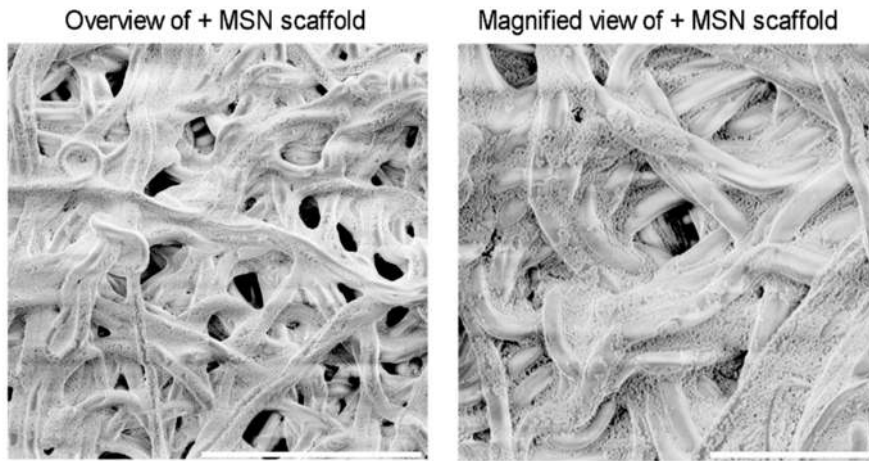


**Figure 4.2A: The distribution of MSNs on electrospun bisurea-modified polycaprolactone (PCLBU):** Electrospun PCLBU scaffolds (1cm diameter) drop casted with (1mg) MSNs ( $n = 9$ ) were observed under a scanning electron microscope (SEM). The left SEM image gives the overview of dispersed MSNs on electrospun PCLBU fibers with fiber diameter of  $5.1 \pm 0.40 \mu\text{m}$  (scale bar  $50\mu\text{m}$ ), while right image displays the magnified view of the scaffold with MSNs (scale bar  $20\mu\text{m}$ )



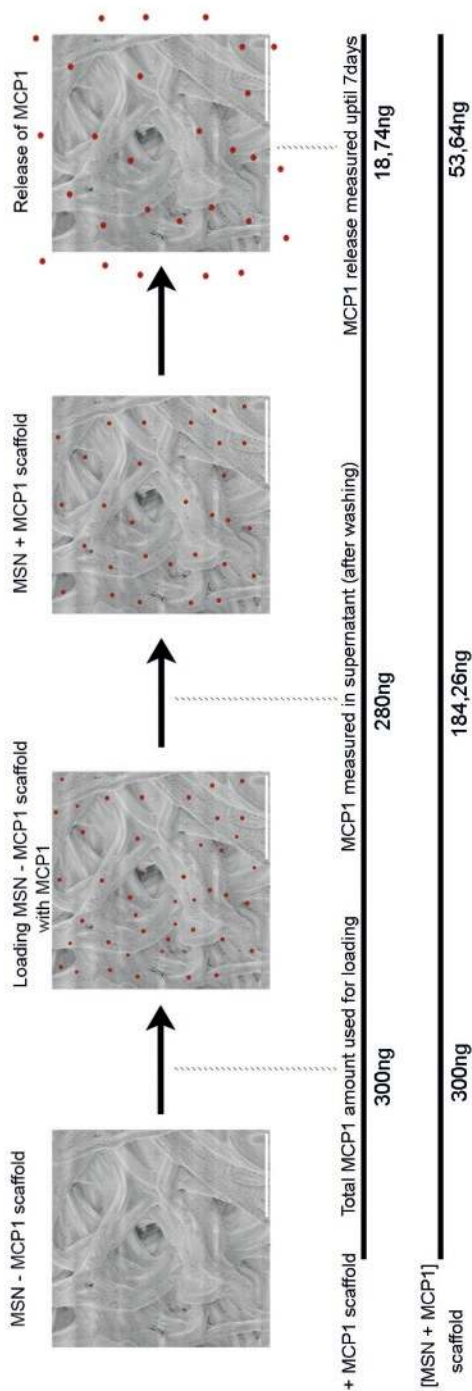


**Figure 4.2B: Procedure to load MSN physio-adsorbed scaffolds with MCP1:** The schematic representation gives an overview of the procedure followed to load scaffolds without/with MSNs (scale bar 20µm). The amount of MCP1 at each stage (MCP1 in the initial loading reaction, MCP1 left in the supernatant after adsorption and MCP1 released to the supernatant at time points 1h, 4h, day 1, day 3, day 5 and day 7) was measured.

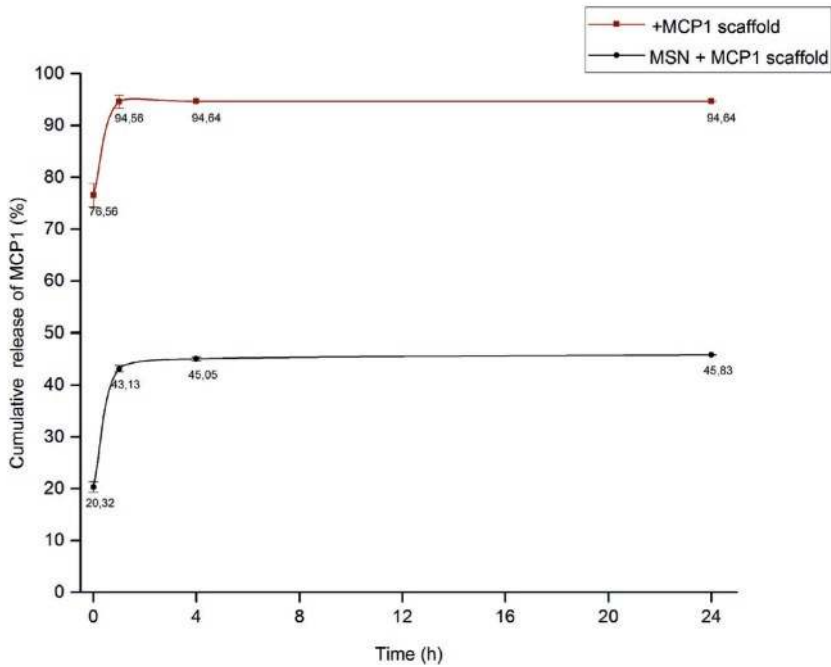


**Figure 4.3: Percentage of MCP1 released from scaffolds with / without MSN:** The percentage of MCP1 released was determined corresponding to the amount of MCP1 released ( $n=9$ ) at each time interval. + MCP1 scaffold demonstrated a burst release of 76.56 % (of adsorbed amount of MCP1) followed by 94.56 % release within the first hour and negligible release thereafter. [MSN + MCP1] scaffolds measured 20.32% burst release of adsorbed MCP1 loaded and slow extended release of 46 % till Day1.

**Table 4.3: Loading efficiency and cumulative release of MCP1 from scaffolds:** The loading efficiency % of MCP1 from + MCP1 scaffolds and [MSN + MCP1] scaffolds was determined as the percentage of protein loaded of the total MCP1 amount used for loading. The cumulative release of MCP1 from + MCP1 scaffolds and [MSN + MCP1] scaffolds was monitored up to 7 days. The total MCP1, the amount washed in supernatant and the cumulative release of MCP1 (from + MCP1 scaffolds and [MSN + MCP1] scaffolds) were all measured by enzyme-linked immunosorbent assay (ELISA). All scaffolds (n = 3, for 3 repetitions) were incubated in medium and the medium was analyzed for concentration of MCP1 released.

MCP1 measured	+ MCP1 scaffold	[MSN + MCP1] scaffold
Total MCP1 loaded (ng)	300	300
MCP1 in Supernatant ng/ml (after washing)	280,0 ± 1,05	184,2 ± 0,21
Cumulative release of MCP1 ng/ml (up to 1 week)	19,0 ± 1,18	52,6 ± 1,10
Efficacy of Loading %	6,6 % ± 0,9	38,5 % ± 1,1

#### 4.3.3 Loading and release of MCP1 from scaffolds with MSNs

The developed mesoporous silica nanoparticles (MSNs) were adsorbed on PCLBU scaffolds i.e. [MSN - MCP1] scaffold. The SEM images shown in Figure 4.2A are representative of different spots on the scaffold, demonstrating the dispersed MSNs on electrospun fibers. The higher magnification image confirms the distribution of the MSNs on the electrospun fibers. Fluorescent images (Figure 4.S3, pg 159) verify the presence of MSN (in green) on PCLBU scaffold (in red). Figure 4.2B gives the ELISA results of MCP1 concentration in the solution/supernatant, the release kinetics together with schematic representation of the procedure followed for loading [MSN - MCP1] scaffolds with MCP1. As shown, a total of 300ng of MCP1 was used for loading the scaffolds with and without MSNs. [MSN - MCP1] scaffolds were loaded with MCP1, (hereafter referred to as [MSN + MCP1] scaffolds) followed by rinsing in PBS. MCP1 in the solution/supernatant was measured as follows: the initial loading concentration, the amount in the supernatant after washing

---

and release after/over a period of one week for + MCP1 scaffolds (i.e. scaffolds with MCP1 & without MSNs) and [MSN + MCP1] scaffolds (i.e. scaffolds with MSNs & with MCP1) (Figure 4.2B).

Table 4.3 gives the loading efficiency of a bare scaffold without MSNs (i.e. + MCP1 scaffolds) as  $6.6 \pm 0.9$  % (i.e. approximately ~19 ng of MCP1 for 2,2 mg weight of scaffold when loaded with 300ng of protein, Table 4.S1, pg156). When the scaffolds were loaded with 300ng of MCP1,  $280,0 \pm 1,0$  ng MCP1 was detected in the supernatant, after washing, from + MCP1 scaffolds while  $184,2 \pm 0.2$  ng was measured in the supernatant, after washing, from [MSN + MCP1] scaffolds (Table 4.3). The amount of MCP1 adsorbed on the scaffolds was determined indirectly as the difference in the total amount of MCP1 loaded and the amount of MCP1 in the supernatant after washing. The loading efficiencies for + MCP1 scaffolds and [MSN + MCP1] scaffolds were found to be  $6,6 \pm 0,9$  % and  $38,5 \pm 1,1$ % of the total adsorbed amount of MCP1 added, respectively (Table 4.3). Of the total amount of MCP1 adsorbed on the scaffolds, a release of approximately  $19,0 \pm 1,1$  ng MCP1 and  $52,6 \pm 1,1$  ng MCP1 was measured for + MCP1 scaffolds and [MSN + MCP1] scaffolds respectively (Table 4.3). Although the experiments were performed with a specific concentration of 300ng MCP1 (for loading all the scaffolds), the obtained data suggest that the employed MSNs improves MCP1 loading efficiency of electrospun scaffolds.

Figure 4.3 demonstrated the percentage release of MCP1 from scaffolds. A burst release of 76% of the total concentration of adsorbed MCP1 corresponding to  $15,2 \pm 2,2$  ng was measured for + MCP1 scaffolds (Table 4. S2, pg 156). Furthermore, these scaffolds demonstrated approximately 94 % release of the loaded MCP within 1 h and the subsequent release was negligible. In case of [MSN + MCP1] scaffold, a burst release of approximately 20 % ( $23,5 \pm 0,9$  ng) of total amount of adsorbed MCP1 was measured. [MSN + MCP1] scaffolds release  $2,2 \pm 0,3$  ng of adsorbed MCP1 concentration at 4 h followed by  $0,9 \pm 0,0$  ng after 1 day subsequently reaching a plateau.

In the initial loading experiment, loose MSNs were loaded with MCP1 to test the release of loaded MCP1 from MSNs. We observed a cumulative release

of  $16,1 \text{ ng} \pm 0,2 \text{ ng}$  MCP1 after 7 days when 1mg MSNs were loaded with 300ng/ml MCP (Table 4.2). Even though the precise amount of MCP1 adsorbed on the MSNs was not analysed, the loose MSNs demonstrate a fast release within first few hours followed by a slow release up to 1 week. However, when MSNs were physio adsorbed to the scaffold (i.e. [MSN + MCP1] scaffold), the MSNs fail to demonstrate the slow extended release profile (Table 4.S2, pg 156). We speculate that the adsorption of MSNs on the scaffold limits the exposed surface area due to the contact with electrospun fibers. This could result in reduction of the diffusion area of MSNs thereby limiting the release of MCP1. Over a period of 7 days 46% (corresponding to  $52,6 \pm 1,1 \text{ ng}$  MCP1) of the total adsorbed MCP1 was released, while 54% of the loaded MCP1 remained entrapped within [MSN + MCP1] scaffolds. Studies have shown internalization of drug loaded MSN by cultured cells after 48 h and thereafter intracellular release of the drug [28]. Long term *in vitro* experiments should be performed using the developed [MSN + MCP1] scaffolds to understand the interaction of cells with MSNs, internalization of MSN by cells and release of MCP1 from internalized MSNs. Furthermore, shear flow has shown to affect monocyte recruitment into MCP1 loaded scaffolds and pulsatile flow could have an influence on the release of MCP1 from [MSN + MCP1] scaffolds [9]. To study the effect of pulsatile flow on the developed [MSN + MCP1] scaffolds, future experiments using *in vitro* mesofluidics models should be performed. The developed [MSN + MCP1] scaffolds exhibit fast release of the drug and these fast releasing scaffolds could be a treatment option for drugs where quick release is desired. The above findings emphasize the potential of MSNs as depots to enhance the drug loading efficiency of the electrospun scaffolds.

#### **4.3.4 Cytocompatibility of [MSN + MCP1] scaffolds**

Figure 4.4A demonstrates the cell viability of hPBMCs cultured on scaffolds up to one week, (n = 9 per experimental group, 3 different donors) measured using WST assay. At Day 1 and Day 3, viability was maintained above 80% (of cells seeded on the scaffold) on + MCP1 scaffold and [MSN + MCP1]

scaffold. A significant decrease in cell viability was observed on Day 5 for + MCP scaffold and – MCP scaffolds. A general trend of decrease in viability was observed at Day 5 and 7 compared to Day 3. At Day 7, scaffolds with MSNs (i.e. [MSN - MCP1] scaffolds and [MSN + MCP1] scaffolds) showed higher cell viability compared to scaffolds without MSNs (i.e. - MCP1 scaffolds and + MCP1 scaffolds). These cell viability data are in line with other studies where higher viabilities were observed with MSNs [29]. High cell viability was also demonstrated after incubation of cells with MSNs compared to other nanoparticles [30]. The cell viability on Day 7 for the [MSN + MCP1] scaffolds was 43.5% as compared to 13.7% and 8.43% on + MCP1 and – MCP1 scaffolds respectively. No influence of MCP1 was observed on cytocompatibility of + MCP1 scaffolds possibly due to negligible MCP1 release observed from the scaffolds at this time. Furthermore, we observed cell internalization of MSNs as shown in Figure 4.5B. The uptake of MSN does not influence the cell viability [31]. The cell viability data demonstrate that the amino functionalized MSNs are cytocompatible and do not negatively affect viability of hPBMCs.

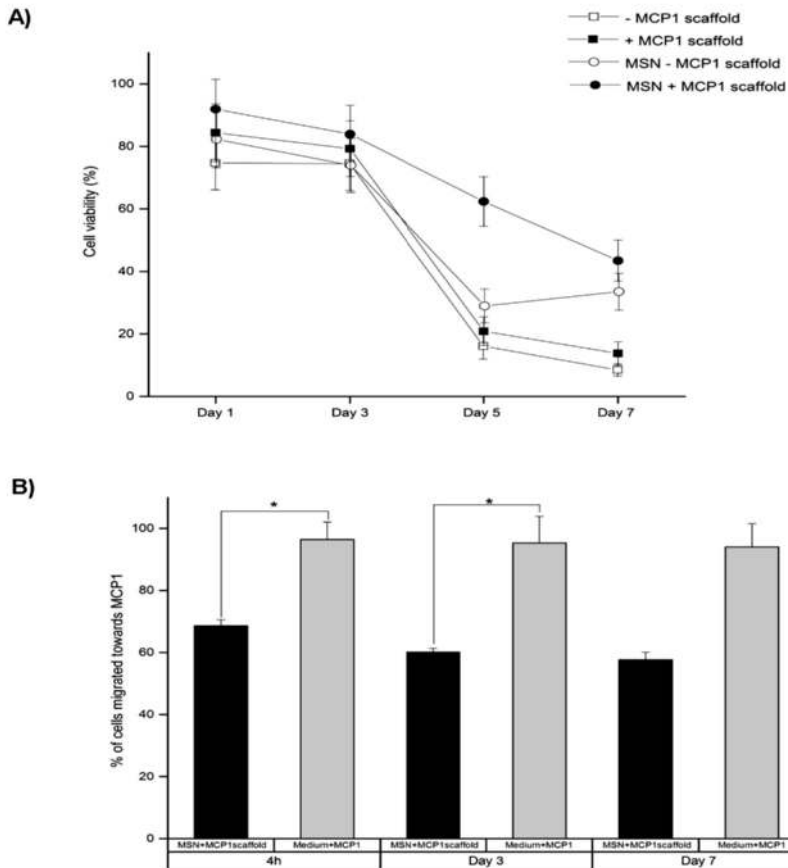


**Figure: 4.4: A) Cell viability on scaffolds with / without MSN:** hPBMCs were cultured on scaffolds (n = 9 using 3 donors for each time point) with/ without MSN and with/ without MCP1 (i.e. + MCP1 scaffolds, - MCP1 scaffolds, [MSN - MCP1] scaffolds and [MSN + MCP1] scaffolds,) for duration of one week. The percentage of cell viability at Day 1, Day 3, Day 5 and Day 7 were calculated using free MCP1 medium as a positive control. The cell viability was measured using WST 8 assay, normalized by setting the viability of cells in free MCP1 medium to 100%. Higher cell viability was observed towards [MSN + MCP1] scaffolds compared to all other groups. **B) Biological effect of MCP1:** The biological functionality of the release MCP1 was analysed using cell migration assay (n = 9 for all experimental conditions) at 4 h, Day 3 and Day 7. Direct addition of monocyte chemoattractant protein (free MCP1 medium) in medium (the concentration equal to release of MCP1 released from [MSN + MCP1] scaffold at specific time) was included as a positive control. Significantly higher number of cells migrated towards medium with MCP1 compared to [MSN + MCP1] scaffold after 4 h (\*indicates significant difference for  $p < 0.05$ ).

---

#### 4.3.5 The effect of released MCP1 on migration of cells towards the scaffold

The chemotactic effect of released MCP1 was analysed by the selective migration of human peripheral blood mononuclear cells (hPBMCs) towards the scaffold (Figure 4.4B). Chemotaxis assay was performed with MCP1 loaded scaffolds with/without MSNs (placed at the bottom of the Boyden chamber), by analysing the migration of suspended hPBMCs (in the upper Boyden chamber) towards the scaffold. The number of cells that migrated towards the scaffolds were counted after 4 h and the scaffolds (placed at bottom of Boyden chamber) were analysed for cell infiltration. Free MCP1 (directly added to medium) at concentration of 2,2ng/ml (release at 4 h) and 0,3 ng/ml (release at Day 3) in the absence of a scaffold were used as controls. A significant difference in cell migration towards [MSN + MCP1] scaffolds was observed after 4 h and Day 3, compared to the controls (i.e. free MCP1 in medium). [MSN + MCP1] scaffolds demonstrated a significant increase in migration of cells (Figure 4.S1B, pg 157) compared to + MCP1 scaffolds and MSN – MCP1 scaffolds after 4 h, Day 3 and Day 7. The migration of cells towards the MCP1 released from MSNs suggests the MSNs maintain the biological function of loaded MCP1.

Besides the migration towards the scaffolds, all the scaffolds were analysed for cell infiltration (after 4 h) by staining for monocyte marker CD14 and lymphocyte marker CD3 using immunofluorescence analyses. An increased cell attachment was observed on the surface of scaffolds loaded with MCP1 compared to scaffolds without MCP1 (Figure 4.5A). The cells attached on the scaffolds with MCP1 demonstrated CD14+ expression suggesting a selective migration and recruitment of monocyte towards MCP1 loaded scaffolds.



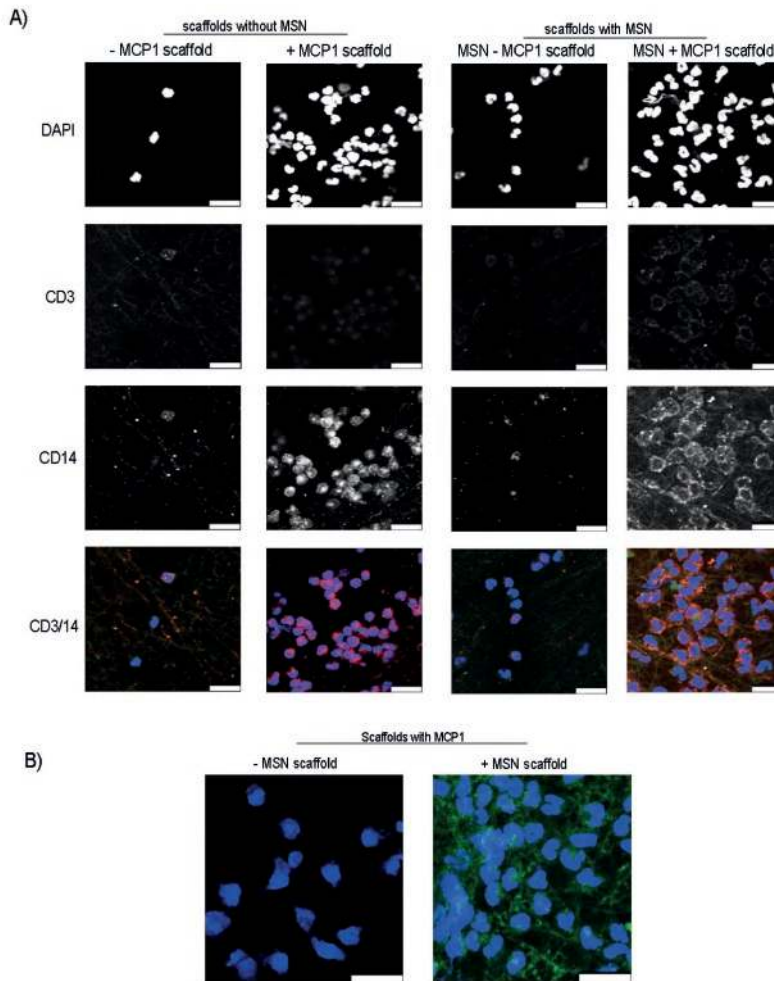


**Figure 4.5: Cell infiltration and attachment on scaffolds with and without MSN.** A) Cell infiltration on scaffolds with / without MSN: The type of cell infiltrated into the scaffolds (after 4h) was analysed after 4 h using immunofluorescent staining (n=9 using 3 donors). Following the migration assay, the scaffold were stained for CD3 (white), CD 14 (red), and nuclei with DAPI (blue), to detect the cell types attached on the scaffold. Higher number of cell nuclei (in blue) were visualized on scaffolds with MCP1 compared to scaffolds without MCP1. The images depict the attachment of cells on the surface of the scaffold (Scale bar 50  $\mu$ m). B) Monocytes attached on scaffolds with / without MSN: After completing 4 h of migration assay, the same scaffolds with/without MSN (n = 3 for each experimental condition, 3 repeated experiments) were stained to visualize cell nuclei (blue) and MSNs (green) (scale bar 10  $\mu$ m). The cells attached on the surface of -MSN scaffolds (i.e. scaffold with MCP1 & without MSN) maintained rounded cell nuclei while cell internalization of MSN (in green) was observed on [MSN+ MCP1] scaffolds (i.e. scaffold with MSN with MCP1)

Although quantitative cell count of infiltrated cells was not analysed, a homogenous infiltration of CD14<sup>+</sup> monocytes was observed for [MSN + MCP1] scaffolds compared to + MCP1 scaffolds (Figure 4.S2, pg 158). Thus, the released MCP1 supports selective migration and homogenous recruitment of monocytes within the scaffold under static conditions. This platform can be further be validated under hemodynamic conditions to evaluate the beneficial effect of MSNs in a physiological environment.

## 4.4 Conclusion

In this study, we developed a modular system for loading MCP1 by combining electrospun scaffolds and animofunctionalized MSNs. MSNs physio-adsorbed on the scaffold enhanced MCP1 loading efficiency and maintains the biological effect of MCP1 by inducing selective migration of monocyte towards the scaffolds. Scaffolds with MSNs were cytocompatible supporting cell viability up to 7 days. This study suggests that MSNs can serve as depots to enhance drug loading efficiencies of electrospun scaffolds.

## Acknowledgements

This work was supported by a grant from the Dutch government to the Netherlands Institute for Regenerative Medicine (NIRM). We would like to thanks Carlotta Mondadori and Libera Sacco their support in imaging particles with SEM and TEM.

---

## References

1. Goldbergova, M.P., et al., *RANTES, MCP-1 chemokines and factors describing rheumatoid arthritis*. Molecular Immunology, 2012. **52**(3-4): p. 273-278.
2. Frangogiannis, N.G., C.W. Smith, and M.L. Entman, *The inflammatory response in myocardial infarction*. Cardiovascular Research, 2002. **53**(1): p. 31-47.
3. Tucci, M., et al., *Deregulated expression of monocyte chemoattractant protein-1 (MCP-1) in arterial hypertension: role in endothelial inflammation and atheromasia*. Journal of Hypertension, 2006. **24**(7): p. 1307-1318.
4. O'Hayre, M., et al., *Chemokines and cancer: migration, intracellular signalling and intercellular communication in the microenvironment*. Biochemical Journal, 2008. **409**: p. 635-649.
5. Niu, J., et al., *Monocyte chemotactic protein (MCP)-1 promotes angiogenesis via a novel transcription factor, MCP-1-induced protein (MCPIP)*. Journal of Biological Chemistry, 2008. **283**(21): p. 14542-14551.
6. Melgarejo, E., et al., *Monocyte chemoattractant protein-1: A key mediator in inflammatory processes*. International Journal of Biochemistry & Cell Biology, 2009. **41**(5): p. 998-1001.
7. Deshmane, S.L., et al., *Monocyte Chemoattractant Protein-1 (MCP-1): An Overview*. Journal of Interferon and Cytokine Research, 2009. **29**(6): p. 313-326.
8. Roh, J.D., et al., *Tissue-engineered vascular grafts transform into mature blood vessels via an inflammation-mediated process of vascular remodeling*. Proceedings of the National Academy of Sciences of the United States of America, 2010. **107**(10): p. 4669-4674.
9. Smits, A.I.P.M., et al., *Shear flow affects selective monocyte recruitment into MCP-1-loaded scaffolds*. Journal of Cellular and Molecular Medicine, 2014. **18**(11): p. 2176-2188.
10. Talacua, H., et al., *In Situ Tissue Engineering of Functional Small-Diameter Blood Vessels by Host Circulating Cells Only*. Tissue Engineering Part A, 2015. **21**(19-20): p. 2583-2594.
11. Rosenholm, J.M., et al., *Mesoporous silica nanoparticles in tissue engineering - a perspective*. Nanomedicine, 2016. **11**(4): p. 391-402.
12. Mamaeva, V., et al., *Mesoporous Silica Nanoparticles as Drug Delivery Systems for Targeted Inhibition of Notch Signaling in Cancer*. Molecular Therapy, 2011. **19**(8): p. 1538-1546.
13. Heidegger, S., et al., *Immune response to functionalized mesoporous silica nanoparticles for targeted drug delivery*. Nanoscale, 2016. **8**(2): p. 938-948.
14. Rosenholm, J.M., et al., *Prolonged Dye Release from Mesoporous Silica-Based Imaging Probes Facilitates Long-Term Optical Tracking of Cell Populations In Vivo*. Small, 2016. **12**(12): p. 1578-1592.
15. Lee, J.E., et al., *Multifunctional Mesoporous Silica Nanocomposite Nanoparticles for Theranostic Applications*. Accounts of Chemical Research, 2011. **44**(10): p. 893-902.
16. Rosenholm, J.M., C. Sahlgren, and M. Linden, *Multifunctional Mesoporous Silica Nanoparticles for Combined Therapeutic, Diagnostic and Targeted Action in Cancer Treatment*. Current Drug Targets, 2011. **12**(8): p. 1166-1186.
17. Wiltschka, O., et al., *Preparation, characterization, and preliminary biocompatibility evaluation of particulate spin-coated mesoporous silica films*. Microporous and Mesoporous Materials, 2014. **188**: p. 203-209.
18. Slowing, I.L., et al., *Mesoporous silica nanoparticles as controlled release drug delivery and gene transfection carriers*. Advanced Drug Delivery Reviews, 2008. **60**(11): p. 1278-1288.
19. Vivero-Escoto, J.L., et al., *Mesoporous Silica Nanoparticles for Intracellular Controlled Drug Delivery*. Small, 2010. **6**(18): p. 1952-1967.
20. Zhu, M.T., et al., *Physicochemical Properties Determine Nanomaterial Cellular Uptake, Transport, and Fate*. Accounts of Chemical Research, 2013. **46**(3): p. 622-631.
21. Manzano, M., et al., *Studies on MCM-41 mesoporous silica for drug delivery: Effect of particle morphology and amine functionalization*. Chemical Engineering Journal, 2008. **137**(1): p. 30-37.

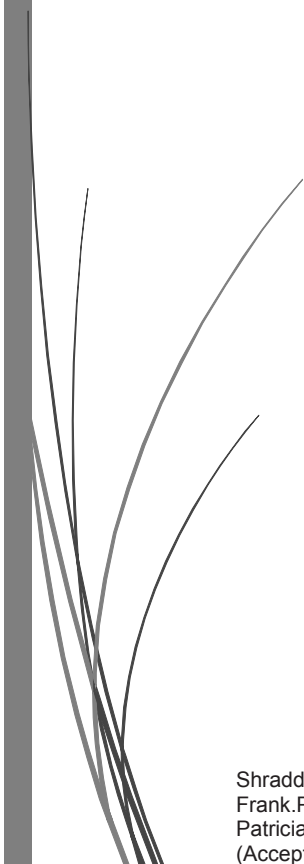
- 
22. Morishige, T., et al., *The effect of surface modification of amorphous silica particles on NLRP3 inflammasome mediated IL-1 beta production, ROS production and endosomal rupture*. Biomaterials, 2010. **31**(26): p. 6833-6842.
  23. Rosenholm, J.M., et al., *Targeted Intracellular Delivery of Hydrophobic Agents using Mesoporous Hybrid Silica Nanoparticles as Carrier Systems*. Nano Letters, 2009. **9**(9): p. 3308-3311.
  24. Pyrz, W.D. and D.J. Buttrey, *Particle Size Determination Using TEM: A Discussion of Image Acquisition and Analysis for the Novice Microscopist*. Langmuir, 2008. **24**(20): p. 11350-11360.
  25. Bastings, M.M.C., et al., *A Fast pH-Switchable and Self-Healing Supramolecular Hydrogel Carrier for Guided, Local Catheter Injection in the Infarcted Myocardium*. Advanced Healthcare Materials, 2014. **3**(1): p. 70-78.
  26. Wisse, E., et al., *Molecular recognition in poly(epsilon-caprolactone)-based thermoplastic elastomers*. Biomacromolecules, 2006. **7**(12): p. 3385-3395.
  27. Wisse, E., et al., *Unusual tuning of mechanical properties of thermoplastic elastomers using supramolecular fillers*. Macromolecules, 2006. **39**(21): p. 7425-7432.
  28. Shokry, H., et al., *Mesoporous silica particle-PLA-PANI hybrid scaffolds for cell-directed intracellular drug delivery and tissue vascularization*. Nanoscale, 2015. **7**(34): p. 14434-43.
  29. Bocking, D., et al., *Mesoporous silica nanoparticle-based substrates for cell directed delivery of Notch signalling modulators to control myoblast differentiation*. Nanoscale, 2014. **6**(3): p. 1490-1498.
  30. Xia, B., et al., *Highly efficient uptake of ultrafine mesoporous silica nanoparticles with excellent biocompatibility by Liriodendron hybrid suspension cells*. Science China Life Sciences, 2013. **56**(1): p. 82-89.
  31. Witasp, E., et al., *Efficient internalization of mesoporous silica particles of different sizes by primary human macrophages without impairment of macrophage clearance of apoptotic or antibody-opsonized target cells*. Toxicology and Applied Pharmacology, 2009. **239**(3): p. 306-319.





Chapter 5

Dual electrospun  
supramolecular polymer  
systems for selective cell  
migration



Shraddha Thakkar, Andrea Di Luca, Sabrina Zaccaria,  
Frank.P.T. Baaijens, Carlijn.V.C. Bouten and  
Patricia.Y.W. Dankers  
(Accepted for publication in *Macromolecular Bioscience*, April 2018)

## Abstract

Dual electrospinning can be used to make multifunctional scaffolds for regenerative medicine applications. Here, two supramolecular polymers with different material properties were electrospun simultaneously to create a multi-fibrous mesh. Bisurea (BU) based polycaprolactone, an elastomer providing strength to the mesh, and ureido-pyrimidinone (UPy) modified poly(ethylene glycol) (PEG), a hydrogelator, introducing the capacity to deliver compounds upon swelling. The dual spun scaffolds were modularly tuned by mixing UPyPEG hydrogelators with different polymer lengths, to control swelling of the hydrogel fiber, while maintaining the mechanical properties of the scaffold. Stromal cell derived factor 1 alpha (SDF1 $\alpha$ ) peptides were embedded in the UPyPEG fibers. The swelling and erosion of UPyPEG increased void spaces and released the SDF1 $\alpha$  peptide. The functionalized scaffolds demonstrated preferential lymphocyte recruitment proposed to be created by a gradient formed by the released SDF1 $\alpha$  peptide. This delivery approach offers the potential to develop multi-fibrous scaffolds with various functions.

---

## 5.1. Introduction

Dual electrospinning offers the possibility to combine two polymers in separate fibers, ultimately to make multi-functional hybrid scaffolds with customised properties for *in situ* tissue engineering. Importantly, this technique gives the freedom to independently tune the separate fibers via polymer concentration [1-3], the voltage applied, the distance between nozzles [4-5], and the placement of nozzles i.e. opposite [6-7] or angular [8-10]. Next to this, the technique helps to fabricate combinations of nanometer to micrometer range fibers, which is proposed to mimic the fibrous structure of the natural extracellular matrix (ECM). While nanofibrous architectures encompass a large surface to volume ratio that promotes cell in growth [11-12], several studies have reported restricted cell infiltration [13-16], due to closely packed nanometer fibers [13, 17]. Besides that, dual electrospinning offers the advantage of increasing the porosity of the scaffold by eroding one of the polymers from the scaffold [18-19]. Baker et al dual spun polycaprolactone (PCL) and poly (ethylene glycol) (PEG) to produce composite scaffolds. The porosity of the scaffold was controlled by increasing the PEG concentration and thereby improving cell infiltration [20]. Additionally, studies have demonstrated that varying the concentration of eroding polymer improves the pore size [21-22] and also influences the mechanical properties [23-24].

Biological cues, such as chemokines, are intimately involved in tissue repair and are important regulators for modulating the inflammatory and regenerative microenvironment of the cells [25-26]. The chemokines released from damaged tissue creates a gradient and the cells respond by mobilizing towards the gradient [27]. Thus, functionalization of dual electrospun scaffold with a bioactive helps to modulate the cell response [28-29]. Stromal cell derived factor 1 alpha (SDF1 $\alpha$ ) is a chemoattractant of lymphocytes, monocytes and progenitor cells [26, 30-32], and has been incorporated in various electrospun scaffolds and hydrogel systems. We hypothesize that electrospun scaffolds functionalized with SDF1 $\alpha$  peptide may guide preferential recruitment of cells, aid the inflammatory response and, therewith,



eventually improve tissue regeneration. Yu et al fabricated SDF1 $\alpha$ -heparin scaffolds by electrospinning blends of poly (L-lactic acid) and PCL [33]. The study demonstrated that the immobilized SDF1 $\alpha$  increased the recruitment of progenitor cells compared to adsorbed SDF1 $\alpha$  [33]. The use of synthetic peptides as bioactive moieties is another approach to introduce tuneable bioactivity and better stability compared to full length proteins. A short SDF1 $\alpha$  peptide was designed with a receptor activated domain similar to the full length protein. This peptide was tethered to form nanofibers at physiological pH [34]. The nanofiber mediated delivery of SDF1 $\alpha$  peptide improved the cardiac function compared to native SDF1 $\alpha$  and promoted tissue repair [34]. Another example by our group showed supramolecular incorporation of SDF1 $\alpha$  peptide in a supramolecular material. We showed that SDF1 $\alpha$  peptide grafts increased attachment of lymphocytes with monocytes and reduced inflammatory signal compared to controls *in vitro* and increase in cellularity after one week of implantation [35].

Here, we present a delivery approach based on two different fibers using supramolecular polymers with dual function in order to ultimately be able to control the release and immobilization of bioactives (fiber type 1) while optimizing the structure and mechanical properties (fiber type 2) of the scaffold. In the past, our group has developed hydrogen bonded supramolecular polymers based on ureido-pyrimidinone (UPy) moieties [36-38] or bisurea units (BU) [39-40]. Here, we use both systems in one scaffold. UPy-modified poly (ethylene glycol) is used to achieve fibers that are able to swell, form a hydrogel and concomitantly release a bioactive compound (fiber type 1) [36-38], and bisurea-modified poly (caprolactone) (PCLBU) is used to obtain fibers that are mechanically stable (fiber type 2) [39-40]. The UPyPEG fibers were tuned in a modular approach by mixing two different UPyPEG polymers with Mn of 10k and 20k, abbreviated as UPyPEG 1 and UPyPEG 2, respectively. We studied the influence of UPyPEG<sub>1:2</sub> layer erosion on porosity of the scaffolds and SDF1 $\alpha$  peptide release (Figure 5.1). First, the optimal ratios of UPyPEG were investigated followed by introduction of SDF1 $\alpha$  peptide into the UPyPEG<sub>1:2</sub>. The erosion of UPyPEG<sub>1:2</sub> enhance the void spaces within

the scaffold thereby modifying the anisotropic architecture and the released SDF1 $\alpha$  peptide creates a gradient and supports selective migration of human peripheral blood mononuclear cells (hPBMCs).

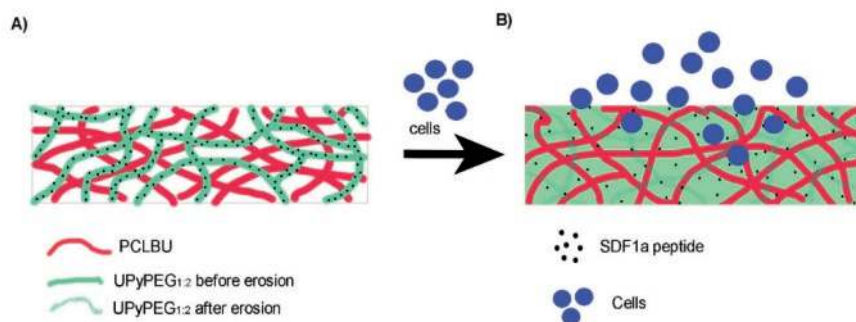
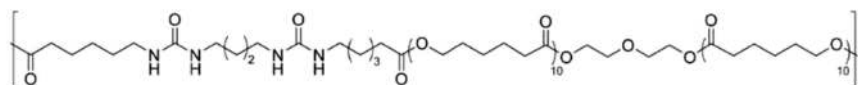


**Figure 5.1. Schematic representation of the side view of dual spun PCLBU and UPyPEG1:2 with SDF1 $\alpha$  peptide.** A) The structure of PCLBU/ UPyPEG<sub>1:2</sub> before immersion in medium. PCLBU fibers are depicted in red, UPyPEG<sub>1:2</sub> in green and SDF1 $\alpha$  peptide (as dots) in black. B) After immersion in medium, PCLBU fibers (red) maintain mechanical stability, UPyPEG<sub>1:2</sub> fibers hydrogelate (green) and act as delivery vehicle for the release of an SDF1 $\alpha$  peptide (black), while cells (blue) infiltrate the scaffold.

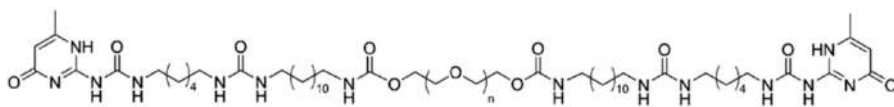
## 5.2. Experimental section

### 5.2.1 Supramolecular polymers and SDF1 $\alpha$ peptide

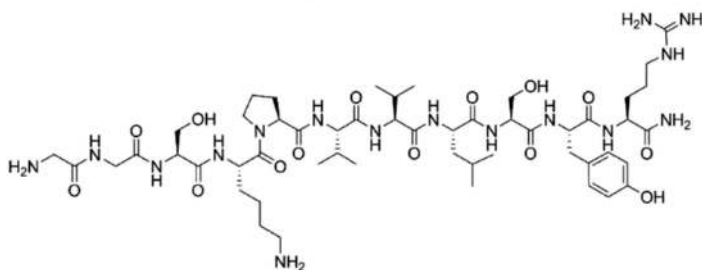
The supramolecular polymers PCLBU and UPyPEG were synthesized by SyMO-Chem (Scheme 1) (Eindhoven University of Technology, The Netherlands) as previously reported [37, 39-40]. For electrospinning, 15% (w/w) PCLBU (Mn 2 kg mol<sup>-1</sup>) polymer was dissolved in solution consisting of 15:85 w/w ratio of hexafluoroisopropanol from Acros Organics and chloroform (amylene stabilized) from Sigma Aldrich.



PCLBU



UPyPEGx



SDF1α peptide

**Scheme 1: Chemical Structure of components used:** Polycaprolactone bisurea – PCLBU, Poly (ethylene glycol) hydrogelator – UPyPEG<sub>10k:20k</sub> Where **x** represents UPyPEG1 ( $M_{n, PEG} = 10\text{kDa}$ ) and UPyPEG2 ( $M_{n, PEG} = 20\text{kDa}$ ) Mixed UPyPEG1: UPyPEG2 = UPyPEG<sub>1:2</sub> which represents different ratios. For example UPyPEG1: UPyPEG2 mixed in 50:50 is represented as UPyPEG<sub>50:50</sub>

UPyPEG was synthesized using PEG with  $M_n$  of 10 kg mol<sup>-1</sup> or 20 kg mol<sup>-1</sup> for UPyPEG 1 and UPyPEG 2, respectively, as previously reported [41-44]. The blends of UPyPEG 1 and UPyPEG 2 were defined as UPyPEG<sub>1:2</sub> (where 1:2 represents the w/w ratio of UPyPEG 1 and UPyPEG 2 respectively) i.e. 50:50 (UPyPEG<sub>50:50</sub>), 70:30 (UPyPEG<sub>70:30</sub>), 90:10 (UPyPEG<sub>90:10</sub>) and 100:0 (UPyPEG<sub>100:0</sub>). Blends of UPyPEG 1 and UPyPEG 2 were dissolved in 10% w/w concentration in a solution consisting of a 1:99 w/w ratio of methanol (Sigma Aldrich) and chloroform (amylene stabilized). Before electrospinning the UPyPEG solution was sealed and stirred at room temperature overnight. The SDF1α peptide was synthesized via standard Fmoc-based manual solid phase peptide synthesis (SPPS). The synthesis was performed on a 200 μmol

scale using Rink Amide 4-Methylbenzhydrylamine resin (MBHA) as solid support, O-(6-Chlorobenzotriazol-1-yl)-N, N, N', N'-tetramethyluronium hexafluorophosphate (HCTU) as the coupling agent and N-methyl-2-pyrrolidinone (NMP) as solvent. MBHA resin, Fmoc-protected amino acids, and HCTU were purchased from Nova Biochem. Each amino acid was coupled for 6 minutes. After synthesis the resin was washed with NMP and dichloromethane and dried in vacuum. The peptide was cleaved from resin and de-protected using a solution of TFA/TIS/H<sub>2</sub>O (95 / 2.5 / 2.5 v/v %), concentrated and precipitated in 50 ml of Diethylether/hexane (8/2). The pellet was then redissolved in H<sub>2</sub>O/acetonitrile (4/1), freeze dried and used without further purification. The synthesized SDF1 $\alpha$  peptide (sequence GGSKPVLSYR) was analysed with RP-LCMS using a gradient of acetonitrile in water with 0.1% formic acid.

### 5.2.2 Preparation of electrospun scaffolds

Scaffolds were fabricated using dual nozzle electrospinning set up developed by IME Technologies. In this study UPyPEG 1 and UPyPEG 2 were mixed in different ratios. The blends are defined as UPyPEG<sub>1:2</sub> where 1:2 represents the w/w ratio of UPyPEG 1 and UPyPEG 2, respectively: i.e. 50:50 (UPyPEG<sub>50:50</sub>), 70:30 (UPyPEG<sub>70:30</sub>), 90:10 (UPyPEG<sub>90:10</sub>) and 100:0 (UPyPEG<sub>100:0</sub>). Scaffolds were fabricated by simultaneously electrospinning UPyPEG blends with PCLBU for the same duration. The hollow target (diameter 21 mm) was set to rotation speed of 1200 rpm. UPyPEG<sub>1:2</sub> (spinneret 1) was electrospun in front of the target and PCLBU (spinneret 2) from the top of the target. The flow rate of PCLBU was set to 25  $\mu$ L / min and a voltage of 18 kV was maintained. The temperature and humidity were maintained at 23 °C and 30%, respectively. As a next step a bioactive scaffold was developed using the most optimum UPyPEG<sub>1:2</sub> solution for delivery. Truncated SDF1 $\alpha$  derived peptide (concentration 2.5 mol %) was added to the optimum UPyPEG<sub>1:2</sub> solution. The solution was stirred at room temperature for 3 hours to ensure homogenous dissolution of SDF1 $\alpha$  peptide. The resulting solution was dual spun with PCLBU.

### **5.2.3 Scanning electron microscopy**

Scanning electron microscopy (SEM) images were taken using Quanta 600F field emission scanning electron microscope (FEI Company, USA). SEM was used to study the morphological structure (fibers diameter, pore size) of electrospun fibers. Samples were imaged after contact with medium at 1 h, 4 h and 24 h and compared to dry samples (0 h). The sample was mounted on a holder and analysed using a 2 kV beam. 20 fibers per condition were analysed for fiber diameter using Image J software (Image J 1.48v, National Institutes of Health, and USA), and the average results were reported. Pore size was measured using live wire (plug in) with Image J.

### **5.2.4 Mechanical characterisation of electrospun meshes**

Mechanical properties of electrospun scaffolds were measured using biaxial tensile testing (Bio tester, 1.5 N load cell, CellScale, Canada) at room temperature. The obtained data was collected with LabJoy software (V8.01, CellScale, Canada). Scaffold stripes (1 cm x 1cm) were cut and thickness of the scaffolds was measured using digital electron Microscope (Keyance, Belgium). Samples were clamped and preconditioned with five loading cycles before the final measurements. The samples were stretched equibiaxially in both directions from 10, 20, 30 and 50% strain, at a strain rate of 100% per minute. After each stretch, the samples were allowed to recover to 0% strain and a rest cycle of 54 s. The stresses and strains were calculated from the last cycle of each measurement, averaged over three samples, and plotted with standard deviations.

### **5.2.5 Scaffold incubation / erosion of UPyPEG**

Samples grouped for erosion of UPyPEG<sub>1:2</sub> were weighed in dry condition, and subsequently submerged in cell culture media for three different time points i.e. 1 h, 4 h and 24 h. Scaffold samples were dehydrated overnight in vacuum and weighed to measure weight loss. The obtained weight loss was represented as a percentage with respect to PCLBU scaffolds. Percentage weight loss was taken as an indication for erosion of UPyPEG<sub>1:2</sub>.

### **5.2.6 UV irradiation and fluorescent microscopy**

Electrospun PCLBU, UPyPEG<sub>90:10</sub> and PCLBU/UPyPEG<sub>90:10</sub> were spun using dual electrospinning setup. Scaffolds of 1 cm x 1cm were cut and dipped in medium for 24 h. These scaffolds were dried in vacuum and UV irradiated for 16 h under UV lamp (Osram, HNS 30W G13, 13.4 W radiated power UVC 200–280 nm, with 90% of relative spectral radial power at 254 nm) at a distance of 10–20 cm, inside a lamellar airflow cabinet. The UV irradiated samples were visualised under Leica confocal fluorescent microscope. Control scaffolds were imaged directly. Scaffolds were sequential scanned for Alexa 488 (PCLBU) and Alexa 647 (UPyPEG). The final merged images were exported to JPEG format format.

### **5.2.7 hPBMCs isolation**

Human peripheral blood buffy coats were obtained from 3 healthy donors after informed consent from patients (Sanquin, The Netherlands). Human peripheral blood mononuclear cells (hPBMCs) were isolated using density gradient centrifugation using Lymphoprep (axis-shield). Briefly, the buffy coats were diluted in 0.6% sodium citrate followed by addition of lymphoprep solution (density 1.077 g/mL). Upon centrifugation, mononucleated cells form a layer above lymphoprep, due to density lighter than 1.077 g/mL. Subsequent to washing steps, the viability and yield of hPBMCs were measured using nuclear counter. hPBMCs were resuspended in freezing medium (RPMI with 20% fetal bovine serum and 10% dimethyl sulfoxide (Merck Millipore) and stored in liquid nitrogen until further use.

### **5.2.8 Migration Assay**

The bioactivity of SDF1 $\alpha$  peptide was evaluated using a migration assay. Cell migration was assessed using a Boyden chamber in a 24 well plate fitted with a transparent PET membrane with 3  $\mu$ m pores (ThinCerts, Griner Bio-One, Germany). As a control bare PCLBU scaffold was used. All electrospun scaffolds (with and without SDF1 $\alpha$  peptide) were placed at the bottom of the Boyden chamber and covered with serum free medium. The chemotactic

effects of SDF1 $\alpha$  peptide in electrospun scaffolds were compared with SDF1 $\alpha$  peptide and full length SDF1 $\alpha$  directly dissolved in medium at similar concentrations. For all conditions, hPBMCs were added to the upper compartment at a concentration of one million cells per mL. After 4 h of incubation at 37 °C, the migrated cells towards the scaffolds were counted using a haemocytometer.

### **5.2.9 Cell attachment by electrospun SDF1 $\alpha$ peptide scaffolds**

To study the effect of the SDF1 $\alpha$  peptide on cell recruitment, hPBMCs were cultured *in vitro* for one day. Electrospun scaffolds with and without SDF1 $\alpha$  peptide were considered. As a control bare PCLBU scaffold was used. Circular scaffolds of diameter 10 mm were cut for each condition from the respective electrospun meshes. The circular scaffolds were UV sterilized for 30 minutes (each side 15 minutes), washed with PBS and transferred to 48 wells plate. The sterilized scaffolds were soaked in medium overnight. Consequently, hPBMCs from a single donor were seeded at a density of  $2.5 \times 10^5$  cells / mm and incubated for 2 h at 37 °C and 5% CO<sub>2</sub> to allow cell attachment on the scaffold. Next, 0.75 mL medium was added to each well. Scaffolds were analysed using scanning electron microscope (SEM) and the amount of cell infiltration was quantified with a DNA assay.

### **5.2.10 DNA assay**

The number of cell attachment on the scaffold was analysed using DNA assay. After 1 day, samples were lyophilized and digested in digestion papain buffer (100 mM phosphate buffer, 5 mM l-cysteine, 5mM ethylene diamine tetra-acetic acid and 140  $\mu$ g / mL papain) for 16 h at 60 °C. From the digested samples DNA content was measured with Hoechst dye method and calf thymus DNA (Sigma) was used as a reference [45].

### **5.2.11 Cell morphology**

Cell morphology and distribution of seeded cells on the scaffold was evaluated after 1 day of culture. Scaffolds were fixed in glutaraldehyde overnight and washed twice in phosphate saline buffer (PBS) for 10 minutes. Subsequently,

samples were dipped in dehydration series starting from 50% to 100% ethanol (v/v). Ethanol concentration was increased 10% each time and samples were immersed for 10 minutes in each concentration. After overnight drying at room temperature, samples were visualized in high vacuum with an electron beam of 2 kV (Quanta 600F, FEI).

### **5.2.12 Immunohistochemistry**

Scaffolds were fixed in 10% formalin and washed twice with PBS. The fixated samples were permeabilized using 0.5% Triton X-100 (Merck Serono, The Netherlands) in PBS for 20 minutes. Subsequently samples were incubated in 2% BSA for an hour to block non-specific binding, followed by primary antibodies against CD3 and CD14 (Serotec, The Netherlands) incubation for 1 hour at room temperature. Secondary antibodies (goat anti rabbit A555 and goat anti mouse A647) were incubated for 1 hour at room temperature shielded from the light. Nuclei were stained with DAPI for 10 minutes in the dark. After washing with PBS three times, samples were mounted on glass slides with Mowiol (Calbiochem, San Diego, CA) and imaged with confocal microscopy ((TCS SP5X, Leica Microsystems, Wetzlar, Germany).

### **5.2.13 Statistical analysis**

All data from fiber diameter, migration assay, DNA assay, are expressed as mean and standard deviation. Quantitative assays were performed with 4 samples (n=4). One way ANOVA followed by post-hoc Tukey test was performed and p value < 0.05 was considered statistically significant.



## 5.3. Results and Discussion

### 5.3.1 Production and characterization of dual spun supramolecular polymer meshes

Various fibrous scaffolds were fabricated by simultaneous electrospinning of PCLBU with UPyPEG<sub>50:50</sub>, UPyPEG<sub>70:30</sub>, UPyPEG<sub>90:10</sub> and UPyPEG<sub>100:0</sub>. The mean fiber diameter of the PCLBU fiber was  $3.0 \pm 0.6 \mu\text{m}$  while the UPyPEG<sub>1:2</sub> fiber diameter ranged from  $0.9 \pm 0.6 \mu\text{m}$  to  $1.9 \pm 0.4 \mu\text{m}$  (Table 5.1). In general the fiber diameter increased with an increase in the fraction of UPyPEG **1** in the blend. However when fibers were spun with pure UPyPEG **1** (UPyPEG<sub>100:0</sub>) a smaller fiber diameter of  $0.9 \pm 0.2 \mu\text{m}$  was observed; which was the smallest diameter compared to all the scaffolds fabricated with other blends of UPyPEG<sub>1:2</sub> in this study

**Table 5.1: Fiber diameter.** The mean averaged fiber diameter of electrospun scaffolds measured using Image J.

Conditions	Fiber diameter ( $\mu\text{m}$ )
PCLBU	$3.0 \pm 0.6$
UPyPEG <sub>50:50</sub>	$1.6 \pm 0.6$
UPyPEG <sub>70:30</sub>	$1.8 \pm 0.4$
UPyPEG <sub>90:10</sub>	$1.9 \pm 0.4$
UPyPEG <sub>100:0</sub>	$0.9 \pm 0.2$

**Table 5.2: Pore size and weight loss.** The UPyPEG<sub>1:2</sub> were mixed in ratios of 50:50, 70:30, 90:10 and 100:0 and dual spun with PCLBU. The pore size was measured using live wire (plug in) with Image J. The percentage weight loss after erosion was analysed after 1 h, 4 h and 24 h.

Conditions	Pore size ( $\mu\text{m}^2$ )				Weight loss (%)		
	0 h	1 h	4 h	24 h	1 h	4 h	24 h
PCLBU	58.7 $\pm$ 33.0	77.3 $\pm$ 36.0	50.8 $\pm$ 32.0	63.7 $\pm$ 38.0	0.5 $\pm$ 0.6	1.2 $\pm$ 0.3	1.5 $\pm$ 0.2
PCLBU/UPyPEG <sub>50:50</sub>	105.0 $\pm$ 11.5	48.5 $\pm$ 5.2	93.3 $\pm$ 4.7	112.0 $\pm$ 8.8	14.6 $\pm$ 1.4	14.2 $\pm$ 1.2	17.3 $\pm$ 1.0
PCLBU/UPyPEG <sub>70:30</sub>	73.9 $\pm$ 17.8	49.3 $\pm$ 25.1	69.0 $\pm$ 17.8	80.3 $\pm$ 12.3	6.9 $\pm$ 0.5	9.8 $\pm$ 0.5	7.8 $\pm$ 0.5
PCLBU/UPyPEG <sub>90:10</sub>	88.9 $\pm$ 11.0	11.9 $\pm$ 7.9	27.1 $\pm$ 14.1	33.9 $\pm$ 7.3	3.9 $\pm$ 0.5	12.9 $\pm$ 0.3	13.5 $\pm$ 1.0
PCLBU/UPyPEG <sub>100:0</sub>	27.0 $\pm$ 24.8	0	10.1 $\pm$ 11.4	5.5 $\pm$ 8.3	0.6 $\pm$ 1.7	8.1 $\pm$ 1.4	5.1 $\pm$ 0.4

After immersion of scaffolds in medium for 1 h, 4 h and 24 h, instant swelling of the UPyPEG<sub>1:2</sub> was observed. Scaffold incubation led to erosion of UPyPEG<sub>1:2</sub>, was confirmed by measuring percentage weight loss of the scaffold (Table 5.2). The highest weight loss percent was observed for PCLBU/UPyPEG<sub>50:50</sub> scaffolds after 24 h. A general trend of increasing weight loss after increased immersion time was observed for most scaffolds. Furthermore, pure UPyPEG **2** (UPyPEG<sub>0:100</sub>) dissolves almost instantaneously when put into an aqueous environment (data not included). Erosion of UPyPEG<sub>1:2</sub> has an influence on pore formation of the scaffolds. The blends of UPyPEG<sub>1:2</sub> show desired pore formation and dissolve slowly over 24 hours or longer. The pore size of PCLBU/UPyPEG<sub>50:50</sub> was  $112 \pm 8.8 \mu\text{m}^2$  after 24 h which was higher compared to  $105 \pm 11.5 \mu\text{m}^2$  at 0 h. In all scaffolds the pore sizes initially reduce followed by a gradual increase with increasing submersion time. However after 24 h pore sizes of PCLBU/UPyPEG<sub>50:50</sub> and PCLBU/UPyPEG<sub>70:30</sub> were similar to those of the scaffolds at 0 h (Figure 5.S2, pg 161). Thus complete erosion of UPyPEG<sub>1:2</sub> occur from these scaffolds within 24 h, thereby limiting use of these particular blends as a delivery layer. Insignificant erosion of UPyPEG<sub>100:0</sub> was observed even after 24 h, thereby forming a continuous dense layer over the scaffold [36]. Consequently inhibiting pore formation, slower release of drug and concealed electrospun

fibers under the UPyPEG<sub>1:2</sub> layer may hinder cell attachment and infiltration on the scaffold. On the other hand, the blend PCLBU/UPyPEG<sub>90:10</sub> show electrospun fibers partially embedded in a thin layer of UPyPEG<sub>90:10</sub>, the pore size measured was  $33.9 \pm 7.3 \mu\text{m}^2$  verifying the presence of UPyPEG<sub>90:10</sub> after 24 h (Figure 5.2).

We propose that PCLBU fibers induce cell adhesion while the UPyPEG<sub>90:10</sub> acts as a delivery layer of the SDF1 $\alpha$  peptide. Accordingly PCLBU/UPyPEG<sub>90:10</sub> was considered as the most feasible scaffold, with an optimal balance between pore size, delivery layer, and detectable fibers. The UPyPEG<sub>90:10</sub> fiber was further supplemented with truncated SDF1 $\alpha$  derived peptide to facilitate cell infiltration upon release of the peptide (Figure 5.1). The morphology of scaffold with/without SDF1 $\alpha$  peptide is shown in Figure 5.S1 (pg 160).

**Table 5.3: Mechanical properties of PCLBU/UPyPEG<sub>1:2</sub>.** The mechanical properties of PCLBU/UPyPEG<sub>1:2</sub> were analysed using biaxial tensile tester. The table shows the stress (kPa) measured in both directions at 50% strain. Scaffolds were analysed before and after 1 h, 4 h and 24 h immersion in medium.

Stress (kPa) Conditions	0 h		1 h		4 h		24 h	
	x	y	x	y	x	y	x	y
PCLBU	576 $\pm 69$	574 $\pm$ 62	675 $\pm$ 63	731 $\pm$ 71	1097 $\pm 12$	887 $\pm 98$	1008 $\pm 11$	1499 $\pm 17$
PCLBU/UPyPEG <sub>50:50</sub>	856 $\pm 10$	1108 $\pm$ 13	812 $\pm$ 94	1044 $\pm 94$	1025 $\pm 13$	1154 $\pm 14$	593 $\pm 73$	769 $\pm 86$
PCLBU/UPyPEG <sub>70:30</sub>	946 $\pm 10$	1062 $\pm$ 11	1179 $\pm$ 134	1316 $\pm 14$	986 $\pm 11$	954 $\pm 10$	737 $\pm 85$	997 $\pm 11$
PCLBU/UPyPEG <sub>90:10</sub>	876 $\pm 69$	847 $\pm$ 62	2196 $\pm$ 30	2385 $\pm 34$	1239 $\pm 15$	1510 $\pm 18$	1008 $\pm 11$	1499 $\pm 17$
PCLBU/UPyPEG <sub>100:0</sub>	918 $\pm 12$	1006 $\pm$ 12	2125 $\pm$ 28	2264 $\pm 31$	1507 $\pm 19$	1667 $\pm 19$	1425 $\pm 15$	1228 $\pm 13$

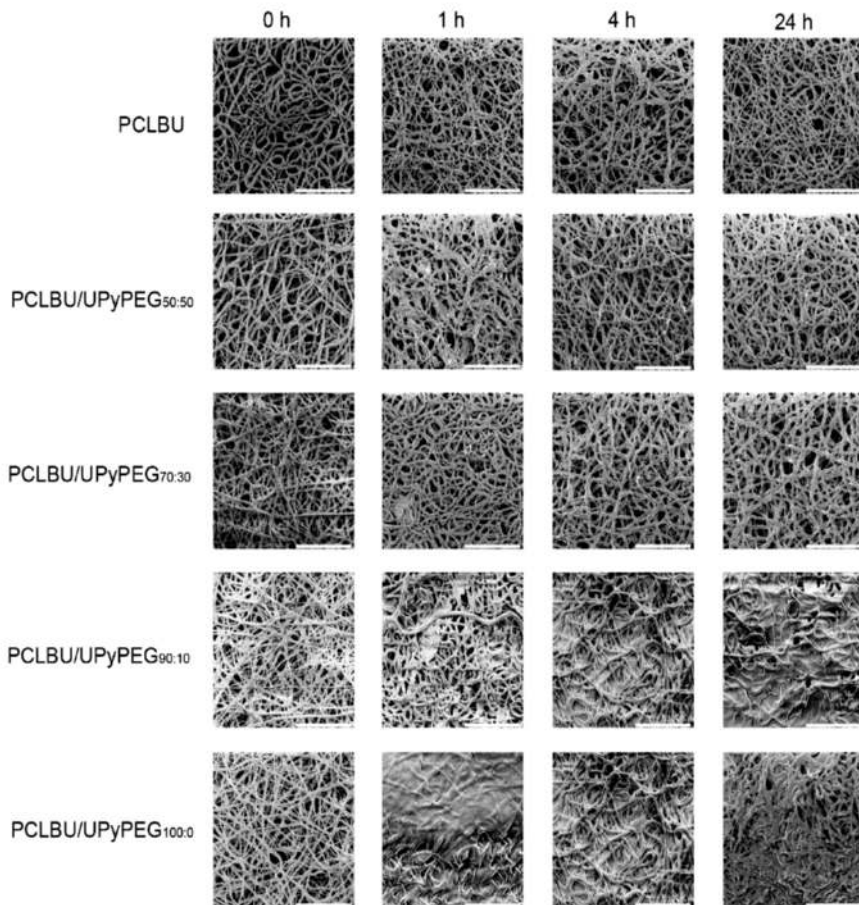


**Figure 5.2: SEM images of dual spun PCLBU and UPyPEG<sub>1,2</sub> before and after immersion in medium** A) 100% PCLBU B) PCLBU/UPyPEG<sub>50:50</sub> C) PCLBU/UPyPEG<sub>70:30</sub> D) PCLBU/UPyPEG<sub>90:10</sub> E) PCLBU: UPyPEG<sub>100:0</sub>. Scale bar represents 100  $\mu\text{m}$ .

### 5.3.2 Mechanical properties of dual spun meshes

Good mechanical stability is one of the most important parameter for the success of the scaffold [46-47]. Therefore, biaxial tensile tests were performed before and after 1 h, 4 h and 24 h of hydration (Figure 5.3). PCLBU/UPyPEG<sub>50:50</sub> and PCLBU/UPyPEG<sub>70:30</sub> scaffolds (0 h) measured stress of  $856 \pm 10$  kPa and  $946 \pm 10$  kPa in x direction (horizontal direction) at 50% strain while y direction (vertical direction) the measured stresses were  $1108 \pm 13$  kPa and  $1062 \pm 11$  kPa (Table 5.3). After 24 h no significant change in mechanical stability was observed. PCLBU/UPyPEG<sub>90:10</sub> shows an significant increase from  $876 \pm 69$  kPa to  $2196 \pm 30$  kPa in x direction and  $847 \pm 62$  to  $2385 \pm 34$  kPa in y direction between 0 h and 1 h (Table 5.3). A similar trend was also observed for PCLBU/UPyPEG<sub>100:0</sub>. Addition of higher ratio of UPyPEG<sub>1:2</sub> results in further formation of a hydrogel layer, thereby demonstrating an increase in mechanical stability. However, this difference was not significant after 4 h and 24 h. A possible explanation could be that the swelling of UPyPEG<sub>1:2</sub> within the first hour results in significant increase in stress, however after stabilization of UPyPEG<sub>1:2</sub> layer, the hydrogel would start eroding (at 4 h and 24 h) thereby regaining its mechanical stability. Thus mechanical properties of these scaffolds was maintained after swelling of UPyPEG<sub>1:2</sub>.

Electrospun PCLBU/UPyPEG<sub>90:10</sub>, 100% PCLBU and 100% UPyPEG<sub>90:10</sub> scaffolds were UV irradiated and imaged to distinguish PCLBU fibers and UPyPEG<sub>90:10</sub> fibers. The fluorescence microscopy images represent PCLBU fibers in red and UPyPEG<sub>90:10</sub> in green colour (Figure 5.4A). Before hydration, PCLBU fibers (red) as well as UPyPEG fibers (green) were identified for PCLBU/UPyPEG<sub>90:10</sub> scaffolds. Incubation in medium for 24 h results in erosion of UPyPEG<sub>90:10</sub> forming a gel layer on the scaffold. We visualize the formed layer in green confirming the erosion of UPyPEG<sub>90:10</sub> fibers and embedded PCLBU fibers in red (Figure 5.4A). A corresponding art graph of electrospun PCLBU/UPyPEG<sub>90:10</sub> with supplemented SDF1a peptide (in black) is shown in Figure 5.4B. These findings are comparable with our SEM images.

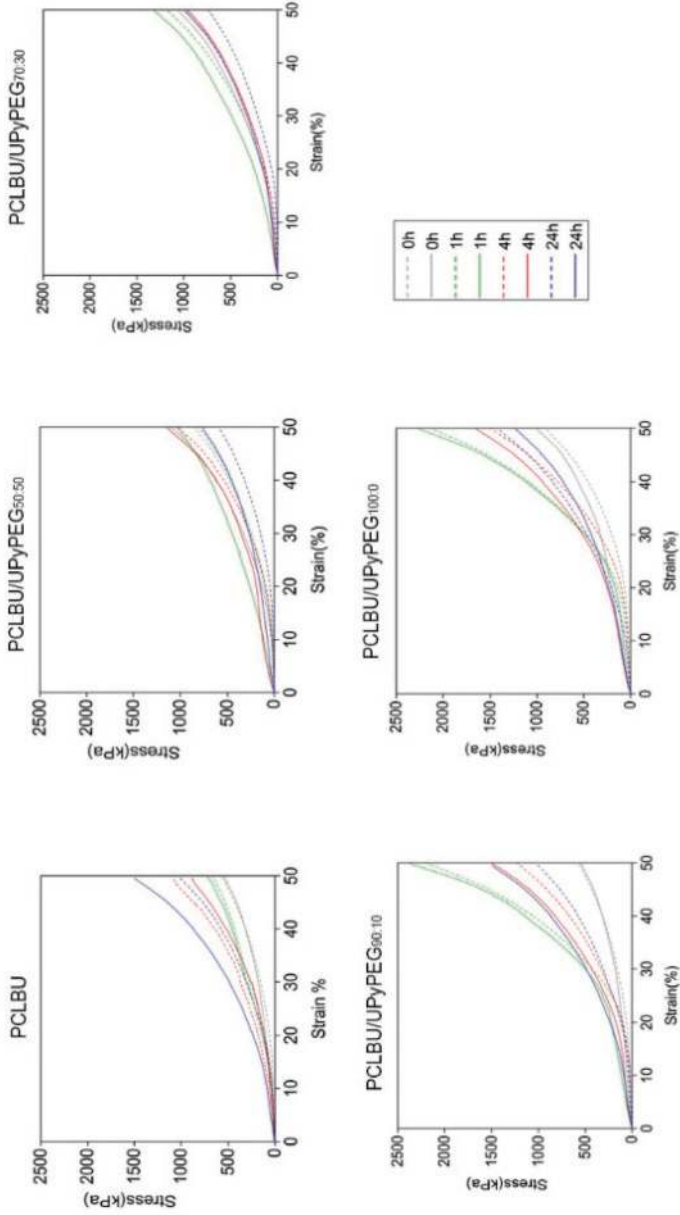


**Figure 5.3: UPyPEG<sub>1,2</sub> were mixed in different ratios and dual spun with PCLBU.** The scaffolds were subjected to biaxial testing to analyse the change in mechanical properties before and after removal of UPyPEG<sub>1,2</sub>.

### 5.3.3 Bioactivity of SDF1 $\alpha$ peptide

The gelation of UPyPEG<sub>90:10</sub> followed by erosion was proposed to stimulate the release of the SDF1 $\alpha$  peptide incorporated. The chemotactic effect of the SDF1 $\alpha$  peptide was investigated using a migration assay with human peripheral blood mononuclear cells (hPBMCs), using a Boyden chamber in which the scaffolds, or soluble SDF1 $\alpha$  peptide or soluble full length SDF1 $\alpha$  as Figure 5.5B references, were positioned in bottom compartment (B) (Figure 5.5A). It was demonstrated that the migration profiles towards SDF1 $\alpha$  peptide scaffolds were similar as to soluble SDF1 $\alpha$  peptide and full length SDF1 $\alpha$  in medium. A significant difference was observed in migration profile with soluble SDF1 $\alpha$  peptide. A significant migration of hPBMCs towards SDF1 $\alpha$  peptide scaffolds was detected, confirming the bioactivity of electrospun SDF1 $\alpha$  peptide (Figure 5.5B). Our results show that few cells were entrapped in the membrane and remaining cells were attached to the scaffolds (data not shown). This confirms that the bioactivity of SDF1 $\alpha$  peptide was not influenced by electrospinning in UPyPEG<sub>90:10</sub> or by its incorporation in the hydrogelator UPyPEG fibers.

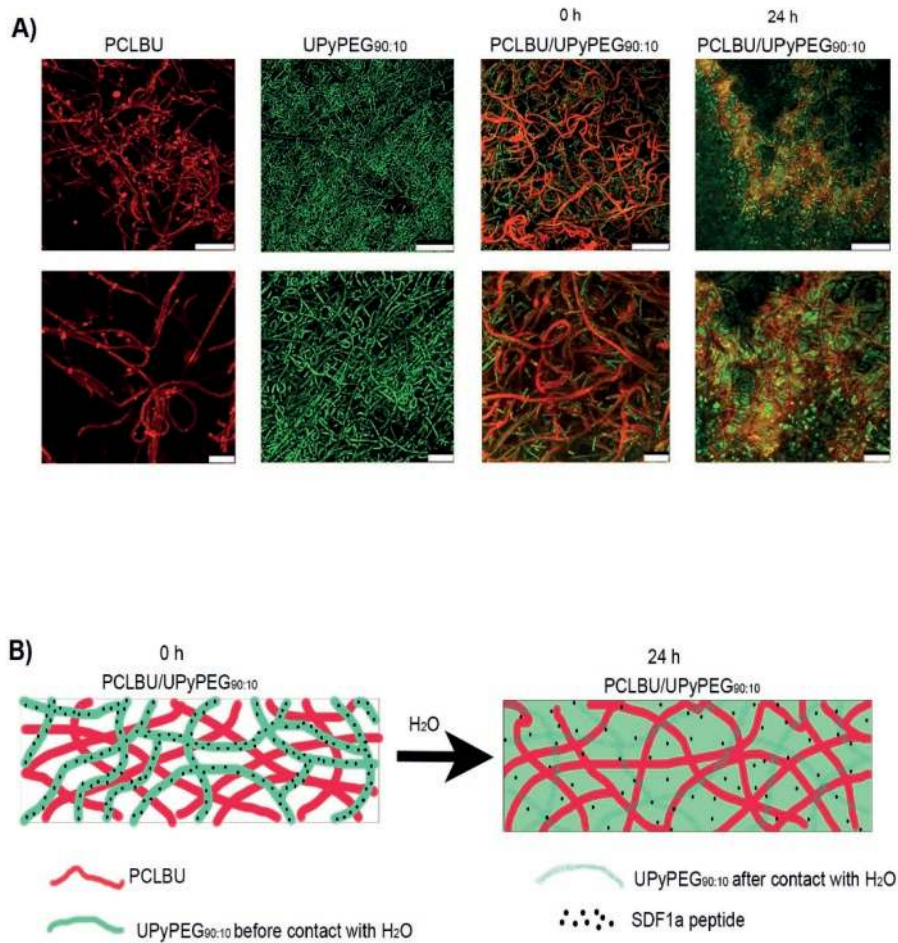


**Figure 5.4: Images of electrospun 100% PCLBU and 100% UPyPEG<sub>90:10</sub> and PCLBU/UPyPEG<sub>90:10</sub> scaffolds & corresponding art graph.** A) Electrospun 100% PCLBU and 100% UPyPEG<sub>90:10</sub> and PCLBU/UPyPEG<sub>90:10</sub> scaffolds were imaged before (0 h) and after (24 h) formation of hydrogel. The scaffolds were UV irradiated for 16 hours. PCLBU fibers represented in red and UPyPEG<sub>90:10</sub> fibers in green. Scale bar 50  $\mu\text{m}$  (first row) for overview images and 25  $\mu\text{m}$  (second row) for magnified images. B) Corresponding art graph of PCLBU/UPyPEG<sub>90:10</sub> scaffolds before (0 h) and after (24 h) formation of hydrogel. PCLBU fibers depicted in red, UPyPEG<sub>90:10</sub> fibers in green with SDF1a peptide in black before immersion in water. UPyPEG<sub>90:10</sub> fibers swell to form hydrogel shown in green and release SDF1a peptide (black).



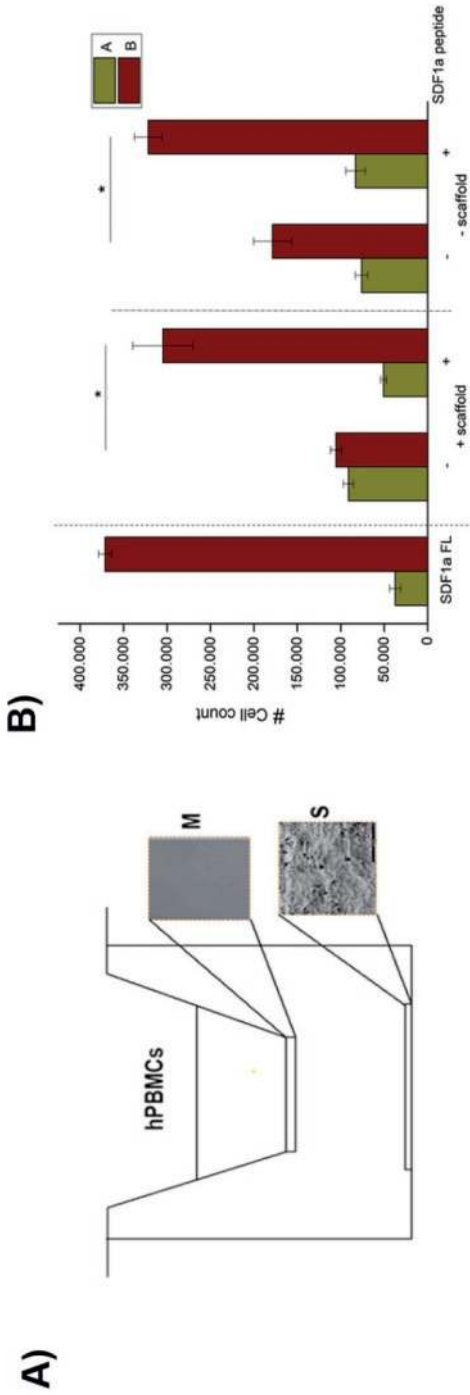


**Figure 5.5: Electrospun scaffolds of PCLBU/UP-yPEG<sub>90:10</sub> functionalised without and with SDF1a peptide were fabricated. A)** The schematic drawing of transwell system is shown and the scaffold was placed at the bottom of the well and hPBMCs were suspended in the upper chamber of transwell. **B)** The graph shows the results of migration assay performed in which the migration of cells towards the scaffold guided by SDF1a peptide was analysed.

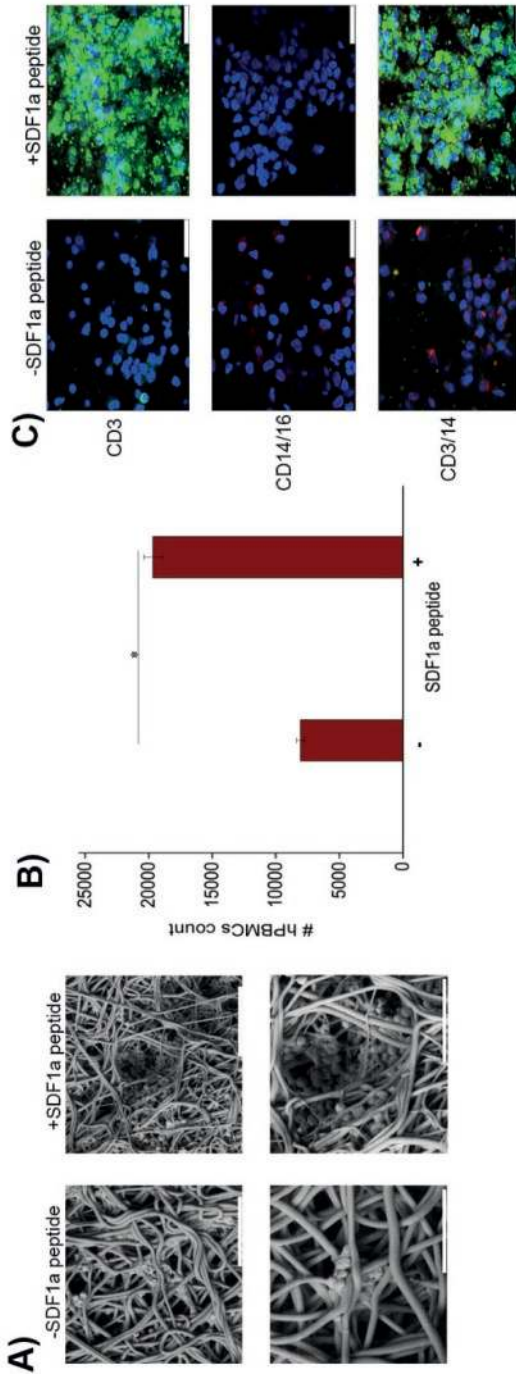


**Figure 5.6: hPBMCs were cultured on electrospun scaffolds without and with SDF1a peptide for one day.** A) The SEM images show the number of cells attached on scaffolds without and with the peptide. First row gives an overview of scaffold with cells (scale bar 50  $\mu\text{m}$ ) and magnified images in the second row show the round morphology of cells attached to scaffolds with sdf1a peptide and the entrapped cells in scaffolds without SDF1a peptide (scale bar 30  $\mu\text{m}$ ). B) The graph demonstrated the DNA assay performed after day 1 on scaffolds without and with the SDF1a peptide (i.e. the number of hPBMCs attached to the scaffolds). C) Electrospun scaffolds of PCLBU/UPyPEG<sub>90:10</sub> functionalised without and with SDF1a peptide were stained for CD14 (red) and CD3 (green) and nuclei (in blue) after 1 day. The confocal images were scanned at the cell scaffold interface, scale bar 25  $\mu\text{m}$ . (Reduction in sharpness is due to embedding of cells within the hydrogel.)

### 5.3.4 Cell recruitment on electrospun scaffolds with SDF1 $\alpha$ peptide

hPBMCs seeded scaffolds show circular morphology and higher attachment at the center of the scaffolds after day 1 (Figure 5.6A). A higher number of hPBMCs attached on scaffolds with SDF1 $\alpha$  peptide compared to the controls (Figure 5.S3A, pg 162), indicating the influence of the peptide. We observed (from magnified images in lower row of Figure 5.6A) that the cells did not attach to the electrospun fibers in scaffolds without SDF1 $\alpha$  peptide, but were trapped in the hydrogel. The DNA assay (Figure 5.6B) shows significantly higher cell count on SDF1 $\alpha$  peptide scaffolds compared to the controls (Figure 5.S3B, pg 162). These results are in line with SEM images, which show that SDF1 $\alpha$  peptide facilitates cell recruitment. Thus it was proposed that the cells react to the presence of SDF1 $\alpha$  peptide in the scaffold.

### 5.3.5 Immunohistochemistry

Erosion of UPyPEG<sub>90:10</sub> fibers stimulate the release of SDF1 $\alpha$  peptide from PCLBU/UPyPEG<sub>90:10</sub> scaffolds. Our *in vitro* analyses after 1 day culture showed less cell attachment on scaffolds without peptide while the presence of SDF1 $\alpha$  peptide enhances the attachment (Figure 5.6C, Figure 5.S3C on pg 162). Furthermore, selective retention of lymphocytes (CD3+) on SDF1 $\alpha$  peptide scaffolds (Figure 5.6C) indicates on delivery of peptide upon erosion of UPyPEG<sub>90:10</sub>. These outcomes confirm the earlier results from our group demonstrating significantly higher degree of lymphocytes in electrospun scaffolds with a short SDF1 $\alpha$  derived peptide after 14 h under pulsatile flow conditions [48]. In addition, significantly less monocytes (CD14 or CD16) were detected in scaffolds with peptides, comparable to the earlier study in our group (Figure 5.6C). After gaining control on fabrication of scaffold and functionalizing with SDF1 $\alpha$  peptide subsequent step would be *in vivo* application of our scaffold.

## 5.4. Conclusion

In this study, we demonstrated a modular approach to develop scaffolds with two different fiber functionalities, in which one type of fiber provides mechanical stability, and the other type of fiber acts as delivery vehicle for the release of an SDF1a peptide. The mechanically stable fibers were composed of a PCL-based polymer (PCLBU), and the delivery fibers consisted of a PEG-based hydrogelator material (UPyPEG). The composition of the PEG-based fiber was tuned to obtain optimal swelling and release properties via different PEG lengths, resulting in the use of a 90:10 ratio of UPyPEG10k:UPyPEG20k. It was shown that the SDF1a peptide released, facilitates selective lymphocyte recruitment *in vitro*. This modular system offers the possibility to design functionalized scaffolds with different fiber composition and bioactive molecules of interest based on the specific application envisioned.

## Acknowledgements

The author would like to thank SyMO-Chem for providing the supramolecular materials. The authors would like to thank C. Mondadori and L. Sacco for their technical assistance and M. Putti for useful discussions. This research was supported by a grant from the Dutch government to the Netherlands Institute for Regenerative Medicine (NIRM) and their contribution is gratefully acknowledged. Additionally, this work was supported by the Ministry of Education, Culture and Science (Gravity program 024.001.035) and the European Research Council (FP7/2007-2013) ERC Grant Agreement 308045.

## References

1. Duan, B., et al., Hybrid nanofibrous membranes of PLGA/chitosan fabricated via an electrospinning array. *Journal of Biomedical Materials Research Part A*, 2007. 83A(3): p. 868-878.
2. Kang, J.C., M. Wang, and X.Y. Yuan, An investigation into dual-source and dual-power electrospinning of nanofibrous membranes for medical applications. *Multi-Functional Materials and Structures, Pts 1 and 2*, 2008. 47-50: p. 1454-1457.
3. Min, B.M., et al., Formation of nanostructured poly(lactic-co-glycolic acid)/chitin matrix and its cellular response to normal human keratinocytes and fibroblasts. *Carbohydrate Polymers*, 2004. 57(3): p. 285-292.
4. Ryu, G.S., J.T. Oh, and H. Kim, Observation of Spline Behavior of Dual Nozzle Electrospinning and Its Fiberweb Morphology. *Fibers and Polymers*, 2010. 11(1): p. 36-41.
5. Gu, M.B., et al., Preparation and Characterization of PVA/PU Blend Nanofiber Mats by Dual-jet Electrospinning. *Fibers and Polymers*, 2011. 12(1): p. 65-72.
6. Pan, H., et al., Continuous aligned polymer fibers produced by a modified electrospinning method. *Polymer*, 2006. 47(14): p. 4901-4904.
7. Xu, F., L. Li, and X. Cui, Fabrication of Aligned Side-by-Side TiO<sub>2</sub>/SnO<sub>2</sub> Nanofibers via Dual-Opposite-Spinneret Electrospinning. *Journal of Nanomaterials*, 2012: p. 5.
8. Tijging, L.D., et al., One-step fabrication of antibacterial (silver nanoparticles/poly(ethylene oxide)) - Polyurethane bicomponent hybrid nanofibrous mat by dual-spinneret electrospinning. *Materials Chemistry and Physics*, 2012. 134(2-3): p. 557-561.
9. Park, C.H., et al., An angled robotic dual-nozzle electrospinning set-up for preparing PU/PA6 composite fibers. *Textile Research Journal*, 2013. 83(3): p. 311-320.
10. Tijging, L.D., et al., Two-nozzle electrospinning of (MWNT/PU)/PU nanofibrous composite mat with improved mechanical and thermal properties. *Current Applied Physics*, 2013. 13(7): p. 1247-1255.
11. Agarwal, S., J.H. Wendorff, and A. Greiner, Use of electrospinning technique for biomedical applications. *Polymer*, 2008. 49(26): p. 5603-5621.
12. Li, W.J., et al., Electrospun nanofibrous structure: A novel scaffold for tissue engineering. *Journal of Biomedical Materials Research*, 2002. 60(4): p. 613-621.
13. Blakeney, B.A., et al., Cell infiltration and growth in a low density, uncompressed three-dimensional electrospun nanofibrous scaffold. *Biomaterials*, 2011. 32(6): p. 1583-1590.
14. Shabani, I., et al., Cellular infiltration on nanofibrous scaffolds using a modified electrospinning technique. *Biochemical and Biophysical Research Communications*, 2012. 423(1): p. 50-54.
15. Sundararaghavan, H.G. and J.A. Burdick, Gradients with Depth in Electrospun Fibrous Scaffolds for Directed Cell Behavior. *Biomacromolecules*, 2011. 12(6): p. 2344-2350.
16. Zhong, S.P., Y.Z. Zhang, and C.T. Lim, Fabrication of Large Pores in Electrospun Nanofibrous Scaffolds for Cellular Infiltration: A Review. *Tissue Engineering Part B-Reviews*, 2012. 18(2): p. 77-87.
17. Pham, Q.P., U. Sharma, and A.G. Mikos, Electrospun poly(epsilon-caprolactone) microfiber and multilayer nanofiber/microfiber scaffolds: Characterization of scaffolds and measurement of cellular infiltration. *Biomacromolecules*, 2006. 7(10): p. 2796-2805.
18. Ji, Y., et al., Dual-syringe reactive electrospinning of cross-linked hyaluronic acid hydrogel nanofibers for tissue engineering applications. *Macromolecular Bioscience*, 2006. 6(10): p. 811-817.
19. Shin, J.W., et al., Manufacturing of Multi-Layered Nanofibrous Structures Composed of Polyurethane and Poly(ethylene oxide) as Potential Blood Vessel Scaffolds. *Journal of Biomaterials Science-Polymer Edition*, 2009. 20(5-6): p. 757-771.
20. Baker, B.M., et al., The potential to improve cell infiltration in composite fiber-aligned electrospun scaffolds by the selective removal of sacrificial fibers. *Biomaterials*, 2008. 29(15): p. 2348-2358.

21. Shin, J.W., et al., Hybrid nanofiber scaffolds of polyurethane and poly(ethylene oxide) using dual-electrospinning for vascular tissue engineering. 3rd Kuala Lumpur International Conference on Biomedical Engineering, 2006. 15: p. 692-695.
22. You, Y., et al., Preparation of porous ultrafine PGA fibers via selective dissolution of electrospun PGA/PLA blend fibers. *Materials Letters*, 2006. 60(6): p. 757-760.
23. Zhang, Y.Z., et al., Electrospinning of gelatin fibers and gelatin/PCL composite fibrous scaffolds. *Journal of Biomedical Materials Research Part B-Applied Biomaterials*, 2005. 72B(1): p. 156-165.
24. Milleret, V., et al., Tuning Electrospinning Parameters for Production of 3d-Fiber-Fleeces with Increased Porosity for Soft Tissue Engineering Applications. *European Cells & Materials*, 2011. 21: p. 286-303.
25. Balaji, S., et al., Chemokine Involvement in Fetal and Adult Wound Healing. *Advances in Wound Care*, 2015. 4(11): p. 660-672.
26. Lau, T.T. and D.A. Wang, Stromal cell-derived factor-1 (SDF-1): homing factor for engineered regenerative medicine. *Expert Opinion on Biological Therapy*, 2011. 11(2): p. 189-197.
27. Kucia, M., et al., Tissue-specific muscle, neural and liver stem/progenitor cells reside in the bone marrow, respond to an SDF-1 gradient and are mobilized into peripheral blood during stress and tissue injury. *Blood Cells Molecules and Diseases*, 2004. 32(1): p. 52-57.
28. Kim, G., H. Yoon, and Y. Park, Drug release from various thicknesses of layered mats consisting of electrospun polycaprolactone and polyethylene oxide micro/nanofibers. *Applied Physics a-Materials Science & Processing*, 2010. 100(4): p. 1197-1204.
29. Kim, T.G., D.S. Lee, and T.G. Park, Controlled protein release from electrospun biodegradable fiber mesh composed of poly(epsilon-caprolactone) and poly(ethylene oxide). *International Journal of Pharmaceutics*, 2007. 338(1-2): p. 276-283.
30. Cherla, R.P. and R.K. Ganju, Stromal cell-derived factor 1 alpha-induced chemotaxis in T cells is mediated by nitric oxide signaling pathways. *Journal of Immunology*, 2001. 166(5): p. 3067-3074.
31. Durr, C., et al., CXCL12 Mediates Immunosuppression in the Lymphoma Microenvironment after Allogeneic Transplantation of Hematopoietic Cells. *Cancer Research*, 2010. 70(24): p. 10170-10181.
32. Bleul, C.C., et al., A highly efficacious lymphocyte chemoattractant, stromal cell-derived factor 1 (SDF-1). *Journal of Experimental Medicine*, 1996. 184(3): p. 1101-1109.
33. Yu, J., et al., The effect of stromal cell-derived factor-1 $\alpha$ /heparin coating of biodegradable vascular grafts on the recruitment of both endothelial and smooth muscle progenitor cells for accelerated regeneration. *Biomaterials*, 2012. 33(32): p. 8062-8074.
34. Segers, V.F.M., et al., Local delivery of protease-resistant stromal cell derived factor-1 for stem cell recruitment after myocardial infarction. *Circulation*, 2007. 116(15): p. 1683-1692.
35. Muylaert, D.E.P., et al., Early in-situ cellularization of a supramolecular vascular graft is modified by synthetic stromal cell-derived factor-1 alpha derived peptides. *Biomaterials*, 2016. 76: p. 187-195.
36. Dankers, P.Y.W., et al., Hierarchical Formation of Supramolecular Transient Networks in Water: A Modular Injectable Delivery System. *Advanced Materials*, 2012. 24(20): p. 2703-2709.
37. Bastings, M.M.C., et al., A Fast pH-Switchable and Self-Healing Supramolecular Hydrogel Carrier for Guided, Local Catheter Injection in the Infarcted Myocardium. *Advanced Healthcare Materials*, 2014. 3(1): p. 70-78.
38. Pape, A.C.H., et al., Mesoscale Characterization of Supramolecular Transient Networks Using SAXS and Rheology. *International Journal of Molecular Sciences*, 2014. 15(1): p. 1096-1111.
39. Wisse, E., et al., Molecular recognition in poly(epsilon-caprolactone)-based thermoplastic elastomers. *Biomacromolecules*, 2006. 7(12): p. 3385-3395.
40. Wisse, E., et al., Unusual tuning of mechanical properties of thermoplastic elastomers using supramolecular fillers. *Macromolecules*, 2006. 39(21): p. 7425-7432.
41. Sijbesma, R.P., et al., Reversible polymers formed from self-complementary monomers using quadruple hydrogen bonding. *Science*, 1997. 278(5343): p. 1601-1604.

42. Dankers, P.Y.W., et al., Chemical and biological properties of supramolecular polymer systems based on oligocaprolactones. *Biomaterials*, 2006. 27(32): p. 5490-5501.
43. Koudstaal, S., et al., Sustained Delivery of Insulin-Like Growth Factor-1/Hepatocyte Growth Factor Stimulates Endogenous Cardiac Repair in the Chronic Infarcted Pig Heart. *Journal of Cardiovascular Translational Research*, 2014. 7(2): p. 232-241.
44. Kloxin, A.M., et al., Mechanical Properties of Cellularly Responsive Hydrogels and Their Experimental Determination. *Advanced Materials*, 2010. 22(31): p. 3484-3494.
45. Bouten, C.V.C., et al., Substrates for cardiovascular tissue engineering. *Advanced Drug Delivery Reviews*, 2011. 63(4-5): p. 221-241.
46. O'Brien, F.J., Biomaterials & scaffolds for tissue engineering. *Materials Today*, 2011. 14(3): p. 88-95.
47. Hollister, S.J., Porous scaffold design for tissue engineering. *Nature Materials*, 2006. 5(7): p. 590-590.
48. Muylaert, D.E.P., et al., Early in-situ cellularization of a supramolecular vascular graft is modified by synthetic stromal cell-derived factor-1 $\alpha$  derived peptides. *Biomaterials*, 2016. 76 (Supplement C): p. 187-195.



Chapter 6

General Discussion



## 6.1. Introduction

In recent years, advanced development in the field of cardiovascular tissue engineering (CVTE) has enabled direct implantation of the scaffold within the body, eliminating the *in vitro* cell harvesting step [1]. This approach, defined as *in-situ* CVTE, relies on the body's reparative capacity and biologic resources to create a living functional tissue at the site of injury. The implanted scaffold should provide an appropriate environment that supports cell infiltration, eventually triggering tissue regeneration [2]. Consequently, scaffold design and structural architecture are the most important parameters in this approach [3]. These features help to modulate and guide the regenerative process in collaboration with the physiological milieu. Previous research has shown that synthetic materials used for fabrication of such scaffolds fail to generate the required native microenvironment, especially due to the lack of bioactive molecules [4].

## 6.2. Key Findings

As described in previous chapters, functionalized scaffolds were fabricated using different techniques to introduce bioactive molecules in constructs that aimed to modulate an early immune response and facilitate tissue regeneration. Electrospinning was employed to fabricate scaffolds with similar morphology to the native ECM structures. This technique offers an inherent advantage of being able to generate nanometer to micrometer range fibres, based on the specific application [5]. In this thesis, biological components were introduced either before or after electrospinning the scaffold (Figure 1.2 in Chapter 1 on pg 11) using three different approaches. For each approach, we investigated the interaction of the functionalized scaffold with human peripheral blood mononuclear cells (hPBMCs) with respect to migration, infiltration and attachment of cells. In the first (A) approach the biological component was mixed with synthetic polymer prior to electrospinning. The fabricated functionalized scaffold promoted monocyte recruitment and skewed macrophage polarization towards the M2 phenotype. The second (B)

---

approach involved the use of mesoporous nanoparticles (MSN) as depots for loading MCP1 bioactive agents. The employed MSNs enhanced the loading efficiency, preserved the biological function and released MCP1 from the scaffold. In the third (C) approach, SDF1 $\alpha$  peptide was incorporated (prior to electrospinning) in hydrogelator fibers of the electrospun scaffold. The peptide released upon erosion of the hydrogelator supported preferential lymphocyte migration in the direction of the scaffold.

### **6.2.1. Decellularized extracellular matrix incorporated in both 2D and 3D influences macrophage polarization**

Although electrospun scaffolds mimic the structure of the native extracellular matrix (ECM), they lack the existence of a biological element. Consequently, in [Chapter 3](#), (Figure 1.2, pg 11, approach A) decellularized extracellular matrix (dECM) was blended with a synthetic polymer prior to electrospinning in order to incorporate bioactivity to the electrospun scaffold. Human mesenchymal stem cells (hMSC) were selected as a cell source due to their known immunosuppressive properties [6]. We hypothesized that ECM derived from hMSC would promote monocyte recruitment and macrophage polarization, both in 2D and on an electrospun scaffold (3D). Our results demonstrate a significant change in biochemical composition of dECM compared to ECM prior decellularization. These findings are in line with previous studies that review the effects of decellularization on the ECM composition [7-9]. We demonstrate that dECM maintains a beneficial bioactive function after decellularization, lyophilisation treatment, and after electrospinning. The bioactive function was verified using a cell migration assay, which demonstrates the movement of hPBMCs towards ECM before and after processing. The observed chemoattractant property suggests the presence of bioactive moieties such as chemokines or proteins within the ECM derived from *in vitro* hMSCs [10]. For the dECM group, the observed increase in expression of surface proteins (CD163 and CD206), along with a decrease in gene expression M1 markers (CD64 and CCR7), indicates polarization towards M2 phenotype. These findings suggest that dECM

enhances monocyte recruitment and polarizes macrophage towards M2 phenotype, thereby suggesting maintenance of immunomodulatory properties after decellularization. Further experiments using mass spectrometry and bioinformatic analysis to characterize dECM should be performed to obtain a detailed inventory of proteins and molecular composition of dECM, which may regulate macrophage polarization towards the M2 phenotype.

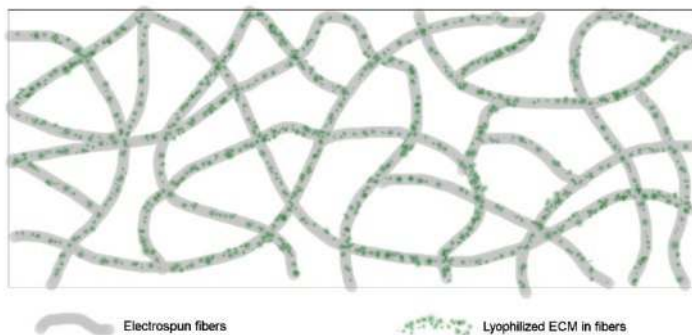


**Figure 6.1: Schematic representation of electrospun Lyophilized ECM:** hMSC deposited ECM was decellularized (dECM) and further lyophilized (LECM) to remove water. LECM (in green) was electrospun with synthetic polymer (in grey) to fabricate LECM scaffold.

The above 2D results were further evaluated in a 3D ECM scaffold environment. We processed scaffolds with lyophilized ECM (derived from hMSC) and PCL (Figure 6.1). We speculated that surface migration of proteins was due to field driven surface enrichment during electrospinning [11]. A limiting factor were the low LECM concentrations used, as higher concentrations failed to dissolve completely. However, the LECM integrated into the scaffold fibers was adequate to influence cell morphology. Elongated morphology acquired by cells on LECM scaffolds along with increased expression of M2 markers and decrease in M1 markers suggests that LECM scaffold modulates the morphology of the cells. However, isolation of RNA was a technical limitation due to limited cell attachment, and the gene expression profile could not be analysed. Besides the biological cues in LECM, the microstructure of the 3D LECM electrospun scaffold provides cues

that alter the macrophage phenotypic profile [12]. These results suggest that LECM scaffold provides an engineered cytokine environment that could support polarization towards a regenerative M2 phenotype. Although the results do not define the exact mechanisms through which the ECM facilitates the specific cellular response, it gives a positive indication of the influence of hMSC derived ECM on modulating early immune response.

### 6.2.2. Extended release of bioactive factors through incorporation of mesoporous silica nanoparticles

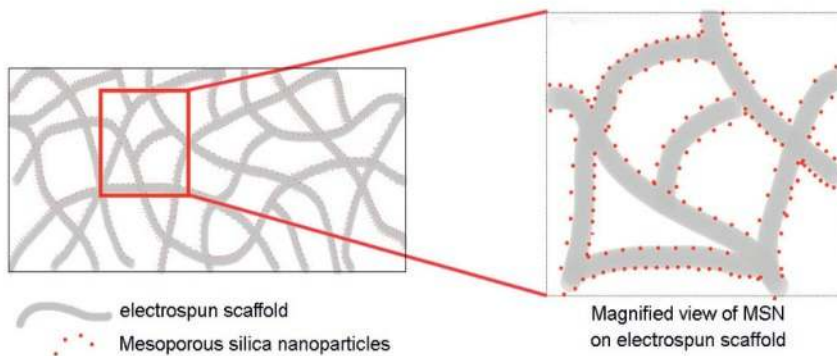


**Figure 6.2: Electrospun scaffold with MSNs:** MSN were physio adsorbed on electrospun scaffold and the scaffolds with MSNs were loaded with 300ng of MCP1. The release of MCP1 was measured at different time points up to one week.

Besides using ECM as a biological component ([Chapter 3](#)) to modulate the inflammatory response, the native microenvironment consists of cytokines that regulate the immune and inflammatory response, thereby influencing tissue formation. Cytokines have been classified based on their presumed functions, and their effect on target cells [13]. Specific cytokines can be incorporated within the scaffold to selectively recruit specific immune cells or to create a microenvironment that influences the phenotype of the infiltrating cells. One important cytokine that guides the inflammatory process towards positive tissue formation is Monocyte Chemoattractant Protein (MCP1) [14]. As explained in [Chapter 4](#), Approach B (Figure 1.2, pg 11) was employed to locally load MCP1 using animofunctionalized mesoporous silica nanoparticles (MSN). MSN physio adsorbed on polycaprolactone bisurea electrospun

scaffolds were loaded with MCP1, hereafter referred to as [MSN + MCP1] scaffolds (Figure 6.2). The loading efficiency was enhanced to  $38 \pm 1.1\%$  with [MSN + MCP1] scaffolds compared to  $6.6 \pm 0.9\%$  with + MCP1 scaffolds. Furthermore, a burst release of  $23 \pm 0.99$  ng of loaded MCP1 (i.e. 20%) and  $15 \pm 2.25$  ng corresponding to approximately 76% of loaded MCP1 was measured for [MSN + MCP1] and + MCP1 scaffolds respectively was observed. [MSN + MCP1] scaffolds reach a plateau after day 1 after releasing  $52 \pm 0.37$  ng MCP1, exhibiting a fast release profile in contrast to the hypothesized prolonged released over a period of 1 week. Selective migration of monocytes towards [MSN + MCP1] scaffolds was observed, confirming the beneficial effect of released MCP1. Furthermore, scaffolds with MSNs supported hPBMCs viability until 7 days, suggesting compatibility of MSNs with hPBMCs.

It was observed that approximately 46% of adsorbed MCP1 was released, while 54% of the adsorbed MCP1 remained entrapped within [MSN + MCP1] scaffolds. The experiment was performed in static condition, thus future studies can be performed to understand the effect of pulsatile flow on the release of MCP1 from scaffold with MSNs. The developed scaffolds with MSN improved the loading efficacy of MCP1 on the scaffolds and displayed a fast drug releasing profile. These findings suggest that MSNs can serve as a depot to enhance drug loading efficiency of scaffolds.

### 6.2.3. Release of bioactives factors via selective removal of a supramolecular hydrogelator

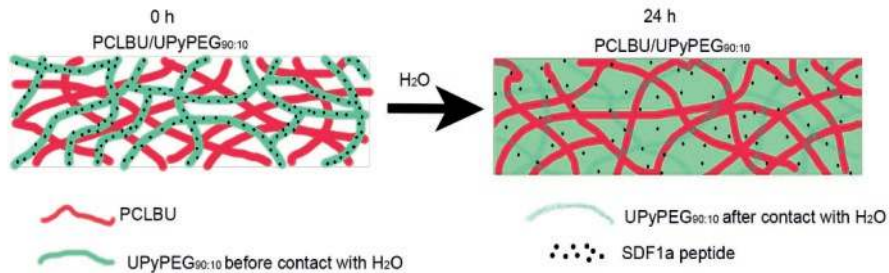


**Figure 6.3: Electrospun supramolecular polymers with SDF1 $\alpha$  peptide:** PCLBU (in red) and UPyPEG hydrogelator (in green) were dual spun to fabricate an electrospun scaffold. SDF1 $\alpha$  peptide (black dots) embedded in UPyPEG fibers was released upon erosion of the hydrogelator fibers.

In [Chapter 5](#), electrospun scaffolds were fabricated using stromal cell derived factor 1 $\alpha$  (SDF1 $\alpha$ ), which is another important chemokine (like MCP1) known to attract lymphocytes, monocytes and progenitor cells [15]. A scaffold was dual spun using two supramolecular polymers UPyPEG 1 and UPyPEG 2, and SDF1 $\alpha$  peptide was incorporated into the electrospun scaffold (Approach C, Figure 1.2 on pg 11). The gelation property of the scaffold was successfully tuned by mixing two UPyPEG hydrogelators with different polymer lengths, while maintaining the construct's mechanical properties. Due to technical spinning limitations, the polymers 90:10 (UPyPEG<sub>90:10</sub>) and 100:0 (UPyPEG<sub>100:0</sub>) were spun at a higher flow rate compared to the remaining blends of UPyPEG<sub>1:2</sub>. The use of a different solvent could circumvent this limitation, but the variation in solvents may have an influence on polymer concentration. Hence, all blends of UPyPEG<sub>1:2</sub> were dual spun with PCLBU for same duration of time. Future studies could focus on an array of design of experiments, and evaluate the effect of solvents, for tuning to an optimal polymer solvent combination.

Of all the different combinations used, UPyPEG<sub>90:10</sub> represented an optimal balance with detectable PCLBU fibers and hydrogel UPyPEG fibers. Eventual swelling and erosion of UPyPEG fibres (after 24 h) resulted in an increase in

void spaces within the formed scaffold (Figure 6.3). SDF1 $\alpha$  peptide released from hydrogel fibers supported preferential lymphocyte migration and recruitment, probably due to the gradient created by the released peptide. These results are in line with the previous study that demonstrates the influence of SDF1 $\alpha$  peptide on lymphocyte migration *in vivo* [16]. The amount of SDF1 $\alpha$  peptide released could not be measured since the commercially available ELISA kits fail to measure the released SDF1 $\alpha$  peptide. This study suggests that application of the above developed functionalised SDF1 $\alpha$  scaffold could be further extended to an *in vivo* environment.

#### **6.2.4. Techniques for developing functionalized scaffolds**

Different techniques of introducing bioactives factors within the scaffold have been employed in [Chapter 3](#), [Chapter 4](#) and [Chapter 5](#). The bioactive molecules can be incorporated in an electrospun scaffold post processing or can be integrated into the scaffold during fiber generation [17]. For fabricating such functionalized electrospun scaffolds, a physical adsorption technique has been employed in [Chapter 4](#) and blend electrospinning in [Chapter 3](#) and [Chapter 5](#). Physical adsorption is the easiest way to load bioactives factors, in which the bioactive molecules can be delivered directly through the electrospun scaffold or additional release system (micro particles or nanoparticles) could be combined with electrospun scaffold to load the bioactive molecules [18-20]. This technique does not interfere with the loaded bioactive factors, and the release rate is faster compared to blend electrospinning technique. It has been shown that bone morphogenic protein-2 (BMP2) loaded on PLGA scaffolds was released up to 75 % within 5 days and was completely released within 20 days. This release was faster compared to BMP2 loaded on PLGA scaffolds using blend electrospinning [21].

In blend electrospinning, the bioactive molecules are mixed into the polymeric solution; this mixed solution is used to fabricate a scaffold using electrospinning. With this technique, the bioactive molecules localize within the fibers rather than adsorbed on the surface. This technique is cost effective

and offers the possibility of combining specific bioactive factors based on the application. A typical release profile from blend electrospinning is an initial burst release followed by sustained release close to linear mode [22-23]. The release profile can be modulated by improving the hydrophilicity of electrospun scaffolds, i.e. enhancing the water uptake of the scaffold which accelerates the release of bioactive agents [24]. In [Chapter 3](#) and [Chapter 5](#), the release of bioactive was analysed indirectly using cell migration assay. Lastly, a known limitation of this technique is loss of bioactivity of proteins upon contact with the organic solution environment. Alternatives for maintaining protein stability have been studied [25-26]. The incorporated ECM in [Chapter 3](#) demonstrated immunomodulatory properties suggesting the perseverance of ECM in the scaffold. Blend electrospinning technique was combined with supramolecular hydrogelator, to tune pore size in [Chapter 5](#). The gelation of UPyPEG released the incorporated SDF1 $\alpha$  peptide which supported migration of lymphocytes. These findings suggest stability of the incorporated bioactive using blend electrospinning. Furthermore, different techniques can be combined to sequentially release the incorporated bioactives (for instance MCP1 release followed by SDF1 $\alpha$ ) to modulate the regenerative response, thus fabricating an optimal bioactive scaffolds for *in situ* CVTE.

### **6.3. Towards the design of an immunomodulatory scaffold**

This thesis highlights the introduction of bioactive factors as a powerful tool to fabricate immune modulatory scaffolds. Results obtained from this thesis provide critical inputs for designing scaffold properties, which helps in developing improved functionalized electrospun scaffolds for *in situ* CVTE.



## Engineering an optimal bioactive scaffold

This thesis proposes some of the main parameters that should be considered in order to mediate an early immune response when designing a scaffold for cardiovascular application:

1. Selection of an appropriate scaffold material
2. The microstructure of the scaffold
3. Bioactive molecules
4. Techniques of introducing bioactive within the scaffold microstructure
5. Scaffold degradation

**Selection of an appropriate scaffold material** is a crucial prerequisite towards designing an optimum scaffold. Polycaprolactone (PCL) is a polymer with slow degradation properties and has demonstrated enhanced tissue formation (*in vitro*) as a cardiovascular scaffold [27]. However, the hydrophobicity of PCL affects the cell response. Thus, PCL scaffolds used in [Chapter 3](#) were conditioned in cell culture medium to augment the hydrophilicity of PCL. Brugmans *et al.* compared the degradation pathways for PCL and a supramolecular polymer, called polycaprolactone based bisurea (PCLBU). It was demonstrated that the degradation response depends on the morphological and chemical modification of the material [28]. PCLBU was prone to oxidative degradation and its degradation properties can be tailored by combining PCL backbones with supramolecular moieties. Lastly, PCLBU exhibits better fatigue resistant properties compared to PCL [29]. Thus, PCLBU was selected as a scaffold material for later studies ([Chapter 4](#) & [Chapter 5](#)). [Chapter 5](#) illustrates the enhanced gelation properties of another supramolecular polymer, UPyPEG hydrogelators, for fabrication of an electrospun scaffold with an optimum pore size. These inherent advantages of such materials can be further explored with other supramolecular polymers in future studies.

---

**The microstructure of the scaffold** is a prerequisite for successful tissue regeneration. The microstructure or the architecture of the scaffold modulates interaction of the immune cells and influences cell infiltration and cell behaviour [12, 30]. For instance, fiber diameter and distance between fibers regulates cell attachment, spreading and proliferation [31]. Furthermore, pore size has shown to affect cell phenotype. Porous scaffolds with pore size of 30-40µm demonstrated minimal fibrosis along with higher M2/M1 macrophage ratio [32]. Scaffold microstructure in terms of fiber diameter and porosity has been demonstrated to regulate macrophage polarization [12]. Macrophages cultured on electrospun meshes with thin fiber diameters (less than 1µm) polarize towards the pro inflammatory phenotype while those cultured on thick fiber diameters (more than 5µm) polarize towards the M2 phenotype [45]. In [Chapter 3](#), LECM scaffolds with fiber diameter of  $2.8 \pm 0.6 \mu\text{m}$  modulate the morphology of seeded cells mostly towards elongated shape, implying polarization towards M2 phenotype. Although the precise fiber diameter that directly correlates to positive M2 polarization is ambiguous, it is clear that the microstructure of the 3D scaffold provides the local cues for immunomodulation. Bioactive molecules could be incorporated into the microstructure of the scaffold to create an engineered bioactive microenvironment, to which the cells are in direct contact [33].

Besides using microstructure for immune modulation, **bioactive molecules** (incorporated into the biomaterial) can modulate the scaffold microenvironment locally. In the native wound healing environment, the signalling factors regulate the actions of the immune cells and enhance the healing process [34]. Several studies have employed bioactive molecules to orchestrate the response of cells. VEGF has shown to induced neovascularization by highlighting the essential paracrine role of myeloid cells [35]. Jay et al. combined delivery of multiple proteins with independent release kinetics and doses that facilitate distinct biological functions [36]. Dual delivery of VEGF and MCP1 supported functional vessel formation from transplanted endothelial cells [36]. In another study, burst release of MCP1 has shown to improve the formation of functional neoarteries in rats [37]. Besides using

specific signalling molecules, single extracellular molecules can also impact cell behaviour and modulate cell response. For instance, glucocorticoids has shown to regulate the phenotype of macrophage and lymphocytes [38]. After selection of the preferred bioactive molecule, strategies to introduce the bioactive molecules into the electrospun scaffolds are discussed in the next paragraph.

Preserving the bioactivity of proteins / chemokines is an essential prerequisite for the success of any incorporation technique. Different **techniques of introducing bioactive molecules** within the scaffold microstructure such as physical adsorption ([Chapter 4](#)) and blend electrospinning ([Chapter 3](#) and [Chapter 5](#)) have been employed in this thesis. Besides these techniques, coaxial electrospinning and covalent immobilization can also be employed to incorporate bioactives molecules [39].

In coaxial electrospinning, two solutions (i.e. polymeric solution and biological solution) spun coaxially to generate composite fibers with core shell structures [40]. The release profile demonstrates a burst release followed by sustained released, similar to blend electrospinning. The protein diffusion rate through the core shell fiber can be controlled, thereby regulating the burst release rate and maintaining a sustained release of protein [41]. Besides incorporating bioactives during the fabrication process, covalent immobilization is another technique that immobilizes molecules on the surface of the scaffold via chemical bond [42]. With this technique, not only the surface properties of scaffold improve but also a controlled release of bioactive molecules can obtained [43]. However, this technique is not frequently used for delivery of bioactive factors due to lot of technical complexity. Choosing specific protein binding sites in protein molecules is a major challenge.

In *in situ* approach, **scaffold degradation** is a crucial component, since the scaffold should degrade in coordination with development of the neotissue. The degradation of the scaffold not only affects the mechanical properties but also influences the release profile of the bioactive [44-45]. Furthermore, the degradation products may interfere with the host response and effect tissue formation [46]. Studies have focussed on development of different pathways

---

to control and tune degradation of the scaffold [47-48], in order to regulate the release of bioactive factors and maintain mechanical properties of the scaffold.

## 6.4. Study limitations

This thesis focuses primarily on introducing bioactivity in electrospun scaffolds using different techniques, starting with hybrid scaffolds and moving to purely synthetic scaffolds. In this section we report the engineering and biological limitations of this thesis.

Throughout the thesis, peripheral mononuclear blood cells (hPBMCs) were used to study the interaction with functionalized scaffolds. Isolated peripheral mononuclear blood cells (hPBMCs) reduced the complexity found in the *in vivo* situation, and help to understand the initial cell material interaction. However, the interplay of other cell types (found in the blood) and their interaction with the functionalized scaffold was not been investigated.

This thesis is further limited to studies / experiments conducted in static conditions, with main focus on development of functionalized scaffold by introducing bioactivity and studying its initial interaction with cells. The findings of this research provide the initial understanding of the effect of incorporated bioactive molecule on cells. Future studies should be conducted in a hemodynamic environment using *in vitro* mesofluidics platforms towards more realistic models to interpret the effect of flow on the release of the bioactive factors. For instance the erosion of dual spun PCLBU and UPyPEG<sub>1:2</sub> scaffolds in [Chapter 5](#) was examined up to 24 h under static conditions. To mimic the *in vivo* scenario, the developed functionalised scaffolds could be exposed to physiological conditions to understand polymer erosion over prolonged periods. A pilot experiment performed using an *in vitro* mesofluidic system demonstrated complete erosion of UPyPEG<sub>90:10</sub> after 4 h (n=1) with increase in pore size of the scaffold (Figure 6.4). Additional experiments need to be conducted to understand the influence of flow on erosion of polymer and release of peptide.

Poor cell attachment was another limitation of all *in vitro* studies, thereby restricting RNA isolation and gene expression analysis specifically for 3D scaffolds. This limitation would be most likely circumvented under physiological conditions, where circulating cells are continuously replenished and offer opportunity for the relevant cells to attach to the scaffold. Limited amount of surface markers and genes were selected for characterization of different cell types (monocytes, lymphocytes, macrophages). Future work could look into a more exhaustive range of gene analysis by qPCR and quantification of cytokine release at protein level. Lastly, in order to mimic the native cardiovascular environment scaffolds should be subjected to mechanical forces. Mechanical strain has shown to have a positive effect on macrophage polarization and early matrix deposition [49]. Thus, 3D scaffolds should be subjected to mechanical stimuli.

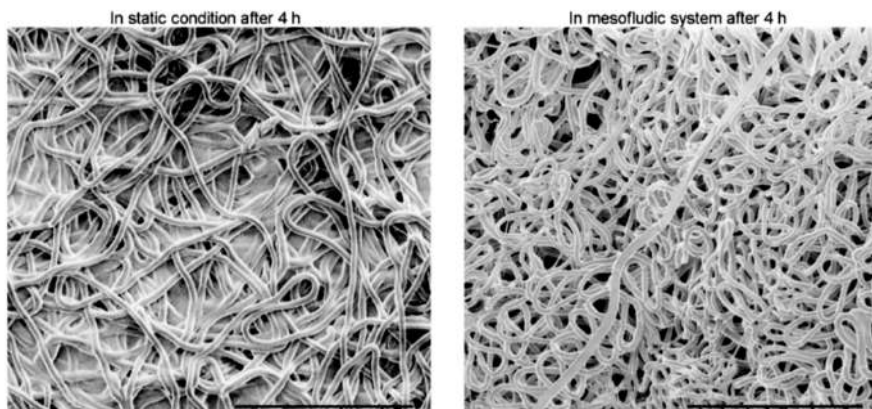


**Figure 6.4:** SEM image of dual spun PCLBU/UPyPEG<sub>90:10</sub> after 4 h in static conditions (A) and in a mesofluidic system (B). This demonstrates reduction in pore size in static condition and increase in pore size after 4 h in mesofluidic flow set up. Scale bar 100µm

---

## 6.5. Future perspectives

Our findings concerning ECM can be used as a preliminary step in order to gain insights and gather information for designing functionalized electrospun scaffolds to modulate an early immune response. Future studies could employ proteomic analysis of dECM and LECM. Such studies could provide data on the key components present in the ECM, which play a crucial role in influencing macrophage polarization. Furthermore, taking advantage of supramolecular material chemistry, an ECM mimicking peptide could be designed consisting of short amino acid sequences of essential proteins influencing macrophage polarization. Thus the molecular design of the ECM peptide should mimic the functional features of native ECM. The ECM peptide could be introduced in PCLBU, or any other supramolecular polymer, using different approaches [50]. To tune the pore size of the scaffold, supramolecular hydrogelator polymers could be employed. These supramolecular materials can be simultaneously electrospun with ECM peptides to fabricate a hybrid scaffold. Lastly, an *in vitro* mesofluidic platform should be applied in corporation with mechanical strain to evaluate the effect of ECM peptide under haemodynamic conditions. Regarding the interaction of cells with the ECM peptide, hPBMCs from healthy and diseased donors could be exposed to the hybrid scaffold in static and flow conditions. Lastly, to understand the dynamic process of macrophage polarization, real time imaging could be performed. ECM peptide thus, is a potential candidate for an immune modulatory scaffold for *in situ* CVTE applications.

Currently, individual peptide sequences have been fabricated using supramolecular materials ([Chapter 5](#)). The fabricated supramolecular peptide can be modified to maintain its functionality in an aggressive solvent environment. Supramolecular bioactive component UPy-modified Arg-Gly-Asp peptide (UPy-RGD) was incorporated into the electrospinning solution. The bilayered scaffold formed was able to stimulate cell adhesion [51]. Future developments could involve combining several individual peptides to the electrospun scaffold to introduce an engineered bioactive environment, which

could mimic the native ECM. However, realisation of such peptide combinations could lead to a complex set of variables, which would need to be appropriately modulated. Besides incorporation of supramolecular peptides, tuning scaffold properties with respect to degradation and mechanical properties remains a challenge. In an ideal *in vivo* scenario, scaffold degradation and tissue formation should be complementary. Thus, the scaffold should maintain a balance between structural integrity and degradation rate, and induce immunomodulation to promote tissue regeneration.

## 6.6. Conclusion

This thesis focuses on various techniques to introduce and test bioactive factors into electrospun scaffolds. The developed functionalized scaffolds were evaluated to guide and modulate initial immune response. The first part of the thesis was focused on fabrication of scaffolds using native decellularized extracellular matrix while the later part was focused on making purely synthetic scaffolds using supramolecular polymers and peptide.

Our findings suggest that introducing bioactivity into electrospun scaffolds with bioactive molecules can create a beneficial and positive immunomodulatory response. Future studies should concentrate on the effect of this bioactivity on the scaffolds, used for long term tissue regeneration in appropriate *in vivo* models while comparing the techniques with pristine scaffolds or with regularly used natural derived scaffolds to test their potential superiority for *in situ* CVTE applications.

---

## References

1. Li, S., D. Sengupta, and S. Chien, Vascular tissue engineering: from in vitro to in situ. *Wiley Interdisciplinary Reviews-Systems Biology and Medicine*, 2014. 6(1): p. 61-76.
2. Bouten, C.V., A. Driessen-Mol, and F.P. Baaijens, In situ heart valve tissue engineering: simple devices, smart materials, complex knowledge. *Expert Review of Medical Devices*, 2012. 9(5): p. 453-455.
3. Loon, S.L.M.v., et al., *The Immune Response in In Situ Tissue Engineering of Aortic Heart Valves*. 2013.
4. Murdock, M.H. and S.F. Badylak, Biomaterials-based in situ tissue engineering. *Current Opinion in Biomedical Engineering*, 2017. 1(Supplement C): p. 4-7.
5. Shamnugasundaram, S., et al., Applications of electrospinning: Tissue engineering scaffolds and drug delivery system. *Proceedings of the IEEE 30th Annual Northeast Bioengineering Conference*, 2004: p. 140-141.
6. Yi, T. and S.U. Song, Immunomodulatory Properties of Mesenchymal Stem Cells and Their Therapeutic Applications. *Archives of Pharmacal Research*, 2012. 35(2): p. 213-221.
7. Crapo, P.M., T.W. Gilbert, and S.F. Badylak, An overview of tissue and whole organ decellularization processes. *Biomaterials*, 2011. 32(12): p. 3233-3243.
8. Gilbert, T.W., T.L. Sellaro, and S.F. Badylak, Decellularization of tissues and organs. *Biomaterials*, 2006. 27(19): p. 3675-3683.
9. Joddar, B., et al., Stem cell culture using cell-derived substrates. *Biomaterials Science*, 2014. 2(11): p. 1595-1603.
10. Harvey, A., et al., Proteomic Analysis of the Extracellular Matrix Produced by Mesenchymal Stromal Cells: Implications for Cell Therapy Mechanism. *Plos One*, 2013. 8(11): p. e79283.
11. Sun, X.Y., et al., Field-driven biofunctionalization of polymer fiber surfaces during electrospinning. *Advanced Materials*, 2007. 19(1): p. 87-+.
12. Wang, Z., et al., The effect of thick fibers and large pores of electrospun poly(epsilon-caprolactone) vascular grafts on macrophage polarization and arterial regeneration. *Biomaterials*, 2014. 35(22): p. 5700-10.
13. Bellanti, J.A., J.V. Kadlec, and A. Escobar-Gutierrez, Cytokines and the immune response. *Pediatr Clin North Am*, 1994. 41(4): p. 597-621.
14. Roh, J.D., et al., Tissue-engineered vascular grafts transform into mature blood vessels via an inflammation-mediated process of vascular remodeling. *Proceedings of the National Academy of Sciences of the United States of America*, 2010. 107(10): p. 4669-4674.
15. Muylaert, D.E.P., et al., Early in-situ cellularization of a supramolecular vascular graft is modified by synthetic stromal cell-derived factor-1 alpha derived peptides. *Biomaterials*, 2016. 76: p. 187-195.
16. Muylaert, D.E.P., et al., Early in-situ cellularization of a supramolecular vascular graft is modified by synthetic stromal cell-derived factor-1 $\alpha$  derived peptides. *Biomaterials*, 2016. 76(Supplement C): p. 187-195.
17. Ji, W., et al., Bioactive Electrospun Scaffolds Delivering Growth Factors and Genes for Tissue Engineering Applications. *Pharmaceutical Research*, 2011. 28(6): p. 1259-1272.
18. Li, J.K., N. Wang, and X.S. Wu, A novel biodegradable system based on gelatin nanoparticles and poly(lactic-co-glycolic acid) microspheres for protein and peptide drug delivery. *J Pharm Sci*, 1997. 86(8): p. 891-5.
19. Cleland, J.L., Protein delivery from biodegradable microspheres. *Pharm Biotechnol*, 1997. 10: p. 1-43.
20. Sinha, V.R. and A. Trehan, Biodegradable microspheres for protein delivery. *Journal of Controlled Release*, 2003. 90(3): p. 261-80.
21. Nie, H., et al., Three-dimensional fibrous PLGA/HAp composite scaffold for BMP-2 delivery. *Biotechnology and Bioengineering*, 2008. 99(1): p. 223-34.
22. Chew, S.Y., et al., Sustained release of proteins from electrospun biodegradable fibers. *Biomacromolecules*, 2005. 6(4): p. 2017-24.



23. Fu, Y.C., et al., Optimized bone regeneration based on sustained release from three-dimensional fibrous PLGA/HAp composite scaffolds loaded with BMP-2. *Biotechnology and Bioengineering*, 2008. 99(4): p. 996-1006.
24. Li, Y., H. Jiang, and K. Zhu, Encapsulation and controlled release of lysozyme from electrospun poly(epsilon-caprolactone)/poly(ethylene glycol) non-woven membranes by formation of lysozyme-oleate complexes. *J Mater Sci Mater Med*, 2008. 19(2): p. 827-32.
25. Lebreton, B., J. Huddleston, and A. Lyddiatt, Polymer-protein interactions in aqueous two phase systems: fluorescent studies of the partition behaviour of human serum albumin. *J Chromatogr B Biomed Sci Appl*, 1998. 711(1-2): p. 69-79.
26. Knoll, D. and J. Hermans, Polymer-protein interactions. Comparison of experiment and excluded volume theory. *Journal of Biological Chemistry*, 1983. 258(9): p. 5710-5.
27. Brugmans, M.M.C.P., et al., Poly-ε-caprolactone scaffold and reduced in vitro cell culture: beneficial effect on compaction and improved valvular tissue formation. *Journal of Tissue Engineering and Regenerative Medicine*, 2015. 9(12): p. E289-E301.
28. Brugmans, M.C.P., et al., Hydrolytic and oxidative degradation of electrospun supramolecular biomaterials: In vitro degradation pathways. *Acta Biomaterialia*, 2015. 27: p. 21-31.
29. LAVRIJSEN, T., A. NANDAKUMAR, and M.A.J. Cox, Implant. 2014, Google Patents.
30. Garg, K., et al., Macrophage functional polarization (M1/M2) in response to varying fiber and pore dimensions of electrospun scaffolds. *Biomaterials*, 2013. 34(18): p. 4439-4451.
31. Lowery, J.L., N. Datta, and G.C. Rutledge, Effect of fiber diameter, pore size and seeding method on growth of human dermal fibroblasts in electrospun poly(epsilon-caprolactone) fibrous mats. *Biomaterials*, 2010. 31(3): p. 491-504.
32. Brown, B.N., et al., Macrophage polarization: an opportunity for improved outcomes in biomaterials and regenerative medicine. *Biomaterials*, 2012. 33(15): p. 3792-802.
33. Losi, P., et al., Fibrin-based scaffold incorporating VEGF- and bFGF-loaded nanoparticles stimulates wound healing in diabetic mice. *Acta Biomaterialia*, 2013. 9(8): p. 7814-7821.
34. Franz, S., et al., Immune responses to implants - a review of the implications for the design of immunomodulatory biomaterials. *Biomaterials*, 2011. 32(28): p. 6692-709.
35. Grunewald, M., et al., VEGF-Induced Adult Neovascularization: Recruitment, Retention, and Role of Accessory Cells. *Cell*. 124(1): p. 175-189.
36. Jay, S.M., et al., Dual delivery of VEGF and MCP-1 to support endothelial cell transplantation for therapeutic vascularization. *Biomaterials*, 2010. 31(11): p. 3054-3062.
37. Talacua, H., et al., In Situ Tissue Engineering of Functional Small-Diameter Blood Vessels by Host Circulating Cells Only. *Tissue Engineering Part A*, 2015. 21(19-20): p. 2583-2594.
38. Barbara Rolfe, J.M., Bing Zhang, Sani Jahnke, Sarah-Jane Le, Yu-Qian Chau, Qiping Huang, Hao Wang, Gordon Campbell and Julie Campbell (2011). *The Fibrotic Response to Implanted Biomaterials: Implications for Tissue Engineering, Regenerative Medicine and Tissue Engineering - Cells and Biomaterials*, Prof. Daniel Eberli (Ed.), InTech, , *The Fibrotic Response to Implanted Biomaterials: Implications for Tissue Engineering, Regenerative Medicine and Tissue Engineering - Cells and Biomaterials*, Prof. Daniel Eberli (Ed.), InTech, . 2011.
39. Szentivanyi, A., et al., Electrospun cellular microenvironments: Understanding controlled release and scaffold structure. *Adv Drug Deliv Rev*, 2011. 63(4-5): p. 209-20.
40. Chakraborty, S., et al., Electrohydrodynamics: A facile technique to fabricate drug delivery systems. *Adv Drug Deliv Rev*, 2009. 61(12): p. 1043-54.
41. Huang, Z.M., et al., Encapsulating drugs in biodegradable ultrafine fibers through coaxial electrospinning. *Journal of Biomedical Materials Research Part A*, 2006. 77A(1): p. 169-179.
42. Ji, W., et al., Bioactive electrospun scaffolds delivering growth factors and genes for tissue engineering applications. *Pharm Res*, 2011. 28(6): p. 1259-72.
43. Li, W.S., et al., Electrospun nanofibers immobilized with collagen for neural stem cells culture. *Journal of Materials Science-Materials in Medicine*, 2008. 19(2): p. 847-854.

44. Markenscoff, P. and K. Zygourakis. Pore structure and hydration rates modulate the release of bioactive agents from degradable scaffolds. in Proceedings of the First Joint BMES/EMBS Conference. 1999 IEEE Engineering in Medicine and Biology 21st Annual Conference and the 1999 Annual Fall Meeting of the Biomedical Engineering Society (Cat. N. 1999).
45. Zustiak, S.P. and J.B. Leach, Hydrolytically degradable poly(ethylene glycol) hydrogel scaffolds with tunable degradation and mechanical properties. *Biomacromolecules*, 2010. 11(5): p. 1348-1357.
46. Sung, H.J., et al., The effect of scaffold degradation rate on three-dimensional cell growth and angiogenesis. *Biomaterials*, 2004. 25(26): p. 5735-5742.
47. Dong, Y.X., et al., Degradation Behaviors of Electrospun Resorbable Polyester Nanofibers. *Tissue Engineering Part B-Reviews*, 2009. 15(3): p. 333-351.
48. Lam, C.X.F., et al., Dynamics of in vitro polymer degradation of polycaprolactone-based scaffolds: accelerated versus simulated physiological conditions. *Biomedical Materials*, 2008. 3(3).
49. Ballotta, V., et al., Strain-dependent modulation of macrophage polarization within scaffolds. *Biomaterials*, 2014. 35(18): p. 4919-4928.
50. Goor, O.J.G.M., *Supramolecular biomaterials in action : bioactivation through surface modifications*. 2017.
51. Mollet, B.B., et al., A modular approach to easily processable supramolecular bilayered scaffolds with tailorable properties. *Journal of Materials Chemistry B*, 2014. 2(17): p. 2483-2493.





Supporting data



## 3.1 Chapter 3

### 3.1.1 Phalloidin and DAPI Staining

Phalloidin & DAPI staining was used to analyse removal of cell debris from dECM. The decellularized ECMs (i.e.  $\text{NH}_4\text{OH}$  treated ECM and CHAPS treated ECM) were fixated in formalin for 3 minutes followed by 15 mins permeabilization using 0.5% Triton X-100. The permeabilized samples were washed in PBS (15 mins) and stained with Phalloidin (1:200) and DAPI (1:500) for an hour at room temperature. After washing with PBS, the samples were mounted on slides and observed under fluorescence microscope.

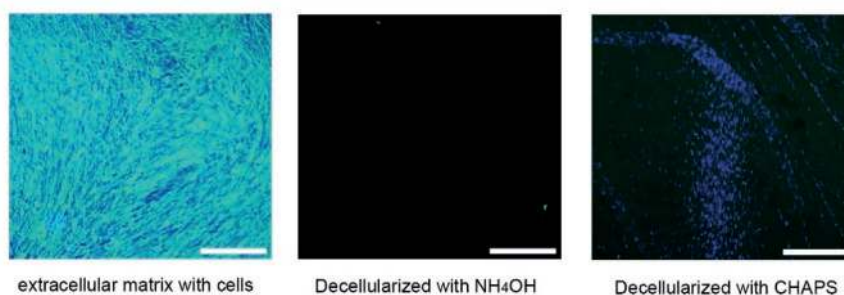


**Figure 3.S1: Phalloidin & DAPI staining.** The fluorescent images demonstrate the presence of cell nuclei and debris after decellularization treatment. Extracellular matrix with cells was used as a positive control, cell nuclei visible in blue and Phalloidin in green. No cellular remnants were observed after decellularization with  $\text{NH}_4\text{OH}$  treatment. Cell nuclei remnants were observed after decellularization using CHAPS treatment

### 3.1.2 DNA Assay

DNA assay was used to analyse the cell number attached to the scaffolds at Day 3 and Day 9. Hoechst dye method was used to measure the DNA content in the samples. Electrospun samples were lyophilized prior to digestion. All samples were digested in papain buffer (100 mM phosphate buffer, 5 mM L-cysteine, 5mM ethylene diamine tetra-acetic acid and 140  $\mu\text{g}$  / mL papain) for 16 h at 60 °C. Calf thymus DNA (Sigma) was used as a reference. Hoechst dye was added to the samples and the distinct fluorescence emission spectra were measured at 490 nm.

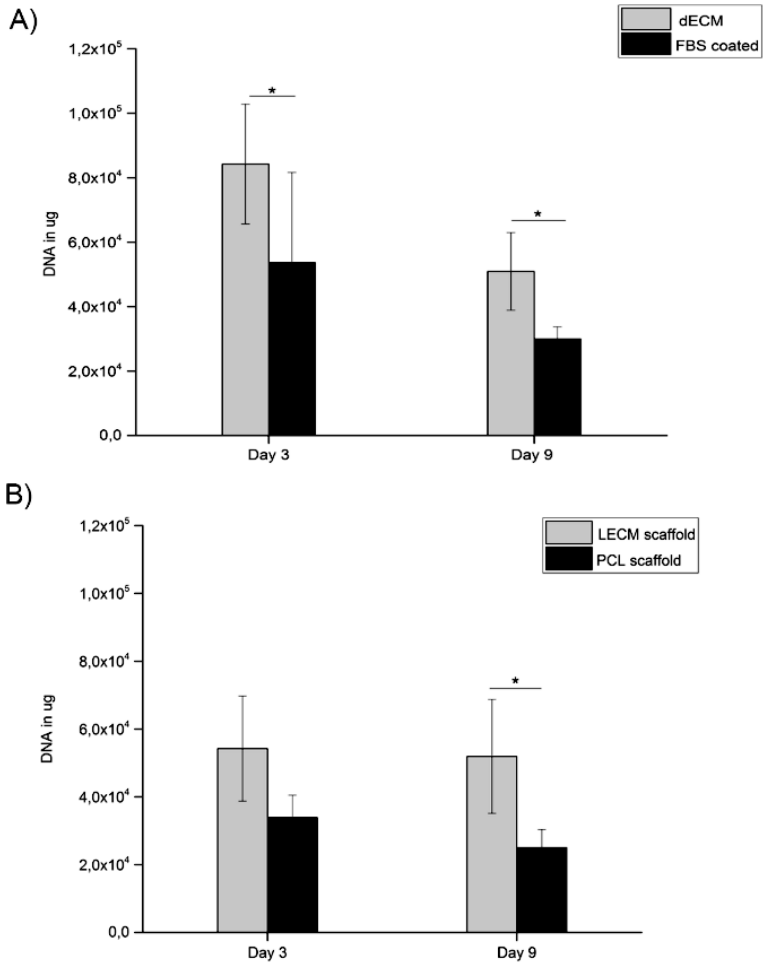


**Figure 3.S2: Cell attachment on A) dECM (2D) and B) LECM scaffolds (3D).** A) DNA assay performed at Day 3 and Day 9 showed significantly higher cell attachment on dECM than FBS group. B) LECM scaffolds had significant cell attachment at Day 9 compared to PCL scaffolds.

## 4.1 Chapter 4

Release of MCP1 (ng/ml) in time from bare PCLBU scaffolds	Loading conc. 100ng	Loading conc. 300ng
Burst release	15,71 ± 0,05	15,24 ± 2.25
1h	2,08 ± 0,05	3,58 ± 1,25
4h	0,02 ± 0,13	0,01 ± 0,02
Day 1	0,00 ± 0,15	0,00 ± 0,05
Day 3	0,01 ± 0,10	0,00 ± 0,06
Day 5	0,01 ± 0,07	0,02 ± 0,04
Day 7	0,00 ± 0,04	0,01 ± 0,30
Cumulative release	17,81 ± 0,99	19,01 ± 1,18
Amount of MCP1 loaded	17.9 ± 0,90	19,05 ± 0,50

**Table 4.S1: Bare PCLBU scaffolds were loaded with two different MCP1 at concentration (100ng & 300ng):** The loading efficiency % of PCLBU scaffolds was analyzed using loading concentration of 100ng or 300ng. Loading efficiency % was calculated as a percentage of the amount of MCP1 loaded on the scaffolds compared the total concentration of MCP1. The amount of MCP1 (n=9) released in time (at 1h, 4h, Day 1, Day 3, Day 5 and Day 7) was measured with enzyme-linked immunosorbent assay (ELISA).

Release of MCP1 (ng/ml) in time from scaffolds	+ MCP1 scaffold	[MSN + MCP1] scaffold
Burst release	15,24 ± 2.25	23,52 ± 0,99
1h	3,58 ± 1,25	26,40 ± 0,63
4h	0,01 ± 0,02	2,21 ± 0,37
Day 1	0,00 ± 0,05	0,90 ± 0,06
Day 3	0,00 ± 0,06	0,27 ± 0,05
Day 5	0,02 ± 0,04	0,22 ± 0,02
Day 7	0,01 ± 0,30	0,10 ± 0,03
Cumulative release	19,01 ± 1,18	52,65 ± 1,10
Total MCP1 release %	95,57 % ± 0,5	46,35 % ± 1,5

**Table 4.S2: Scaffolds with and without MSNs were loaded with MCP1 at concentration (300ng) and the release was observed till day 7:** The release of MCP1 i.e. burst release, after

1h, 4h, Day 1, Day 3, Day 5 and Day 7 was measured. All scaffolds (n=3 for each experimental condition, 3 repeated experiments) were incubated in medium and the concentration of MCP1 released in the medium was measured using ELISA. The cumulative release and total release % were calculated.

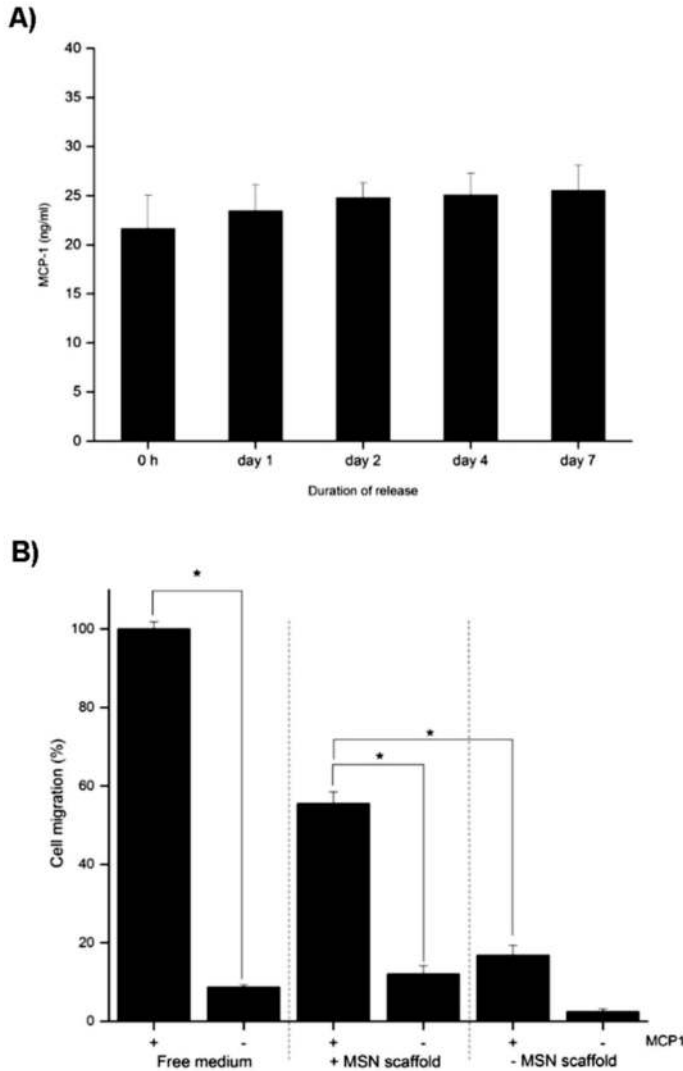


**Figure 4.S1: A) Half-life of MCP1:** MCP-1 at concentration 20ng/ml was measured in medium (n=9) at 37°C. MCP-1 maintains biological stability upto one week. **B) Cell migration towards MCP1 scaffolds:** The migration of monocyte towards the MCP1 (chemoattractant) was analyzed after 4 hours. Scaffolds with/ without MSNs (n = 9) were loaded with/without MCP1 to analyze the migration of cells towards the scaffolds. 100 % cell migration was considered in free MCP1



## Supporting data

medium (i.e. medium with soluble MCP1). Significantly higher cells migrated towards [MSN + MCP1] scaffolds compared to [MSN – MCP1] scaffolds and + MCP1 scaffolds. (\*indicates significant difference for  $p < 0.05$ ).

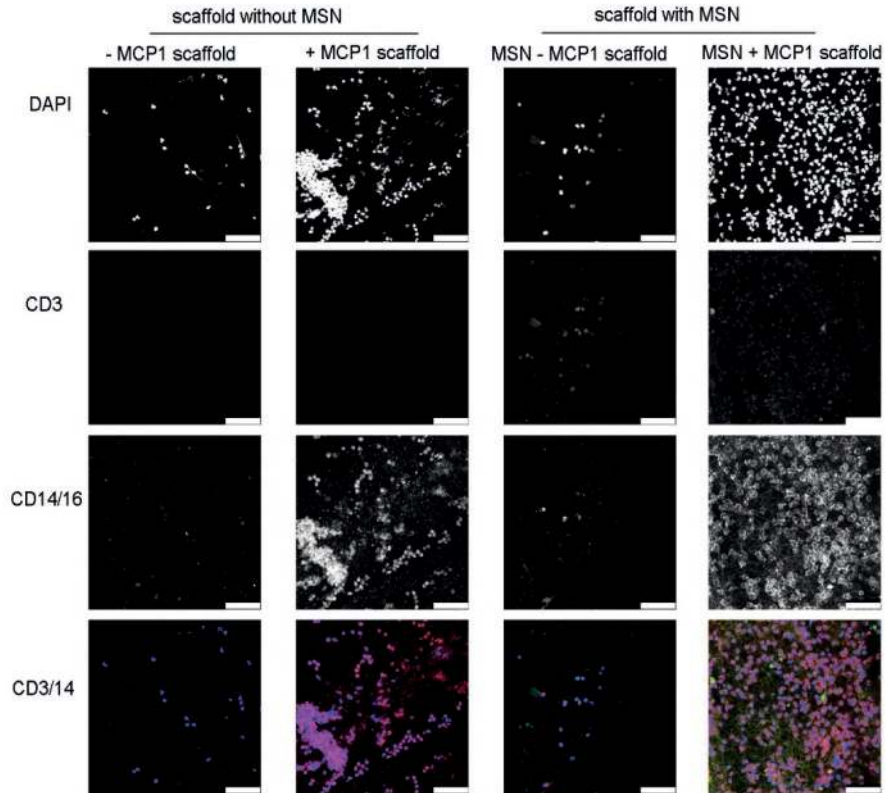


**Figure 4.S2: Cell infiltration on scaffolds with / without MSN:** An overview of cell distribution on the scaffolds ( $n = 9$  per experimental condition) was visualized by staining cell infiltrated scaffolds with CD3 marker, CD 14 and CD16 marker (red) and double stained with CD3/14 along with cell nuclei stained with DAPI (blue). A homogenous infiltration of monocytes was observed on [MSN + MCP1] scaffolds compared to + MCP1 scaffold (scale bar 50  $\mu\text{m}$ ).

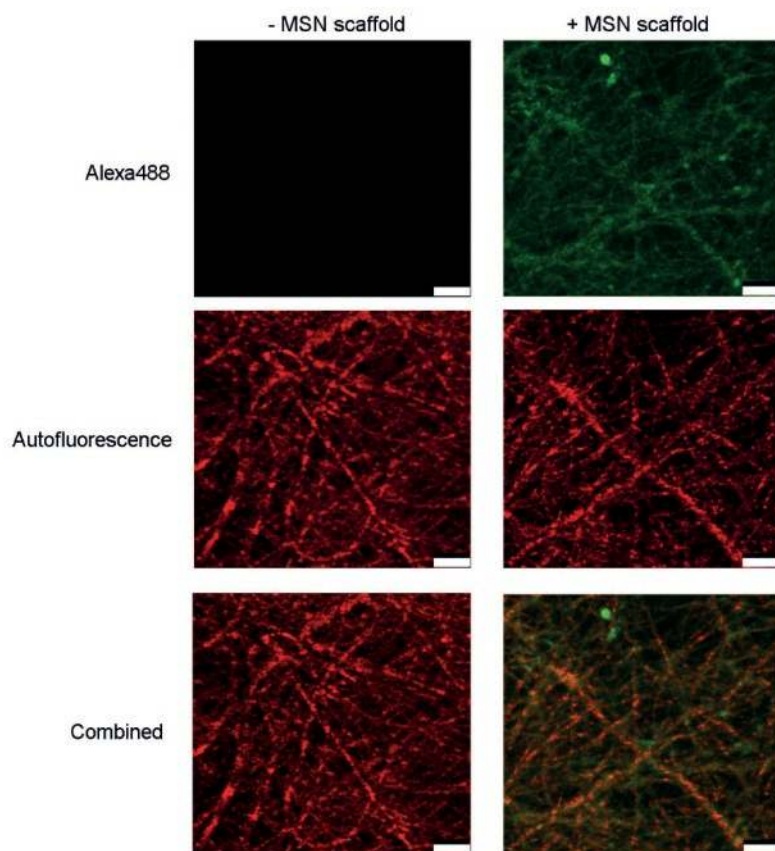


**Figure 4.S3: Presence of MSNs on electrospun scaffolds:** The distribution of MSNs on electrospun scaffolds ( $n = 9$ ) were analysed by loading MSNs with Alexa 488. Auto fluorescence was observed for both (+ MSN and – MSN) scaffolds without loading MCP1. + MSN scaffolds demonstrated MSNs in green while no green fluorescence was demonstrated by – MSN scaffolds (scale bar  $10\mu\text{m}$ ).

## 5.1. Supporting Data

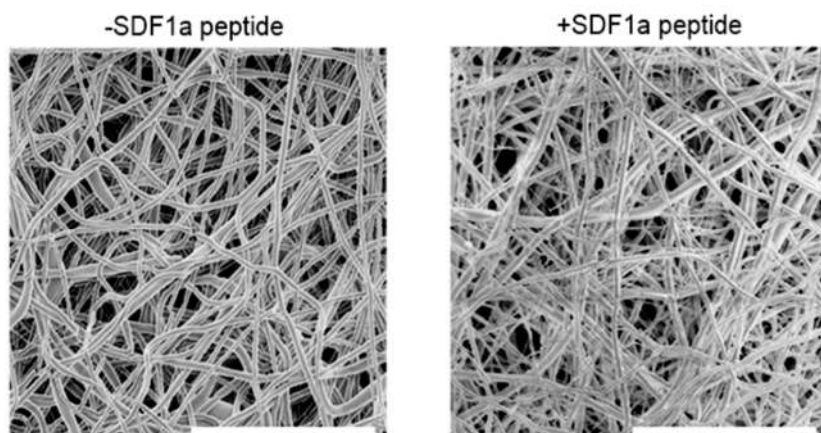


**Figure 5.S1: Images after dual electrospinning PCLBU/UPyPEG<sub>90:10</sub> without and with SDF1 $\alpha$  peptide:** SEM image of electrospun PCLBU/UPyPEG<sub>90:10</sub> scaffolds without and with SDF1 $\alpha$  peptide. Scale bar represents 50  $\mu$ m.

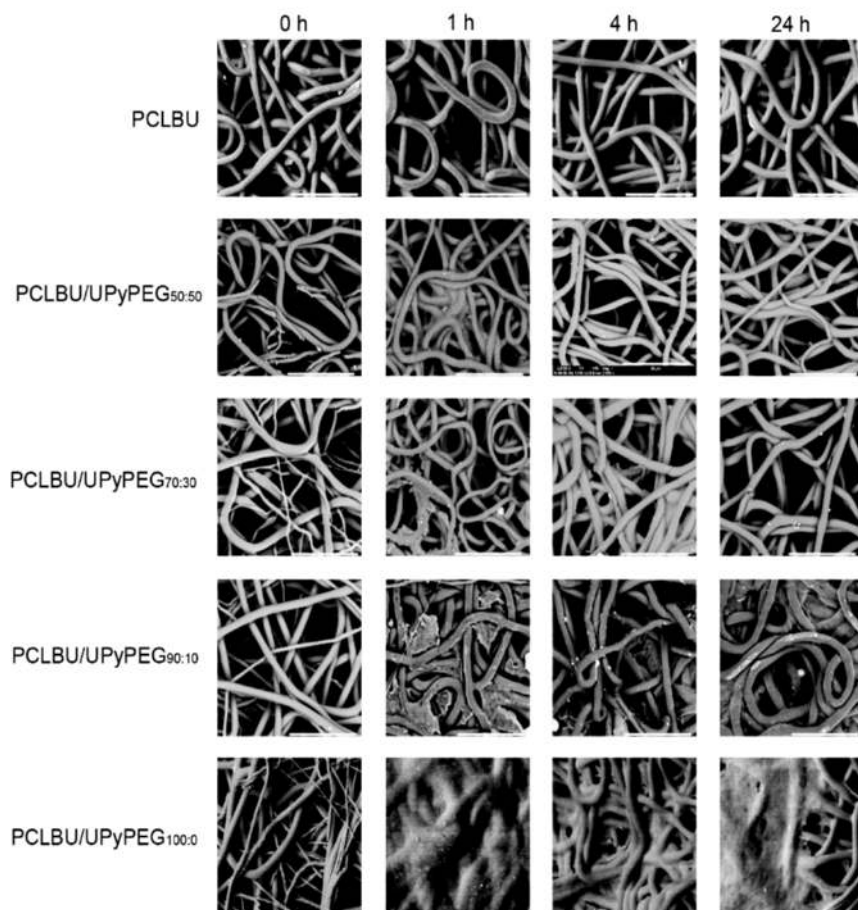


**Figure 5.S2: Magnified SEM images of dual spun PCLBU and UPyPEG 1:2 for measuring pore size before and after immersion in medium a) 100% PCLBU b) PCLBU/UPyPEG<sub>50:50</sub> c) PCLBU/UPyPEG<sub>70:30</sub> d) PCLBU/UPyPEG<sub>90:10</sub> e) PCLBU:UPyPEG<sub>100:0</sub> - Scale bar 30  $\mu$ m**

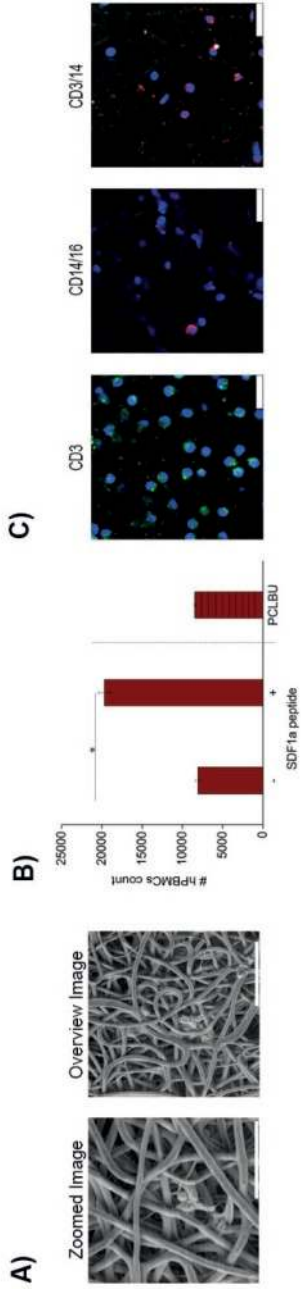
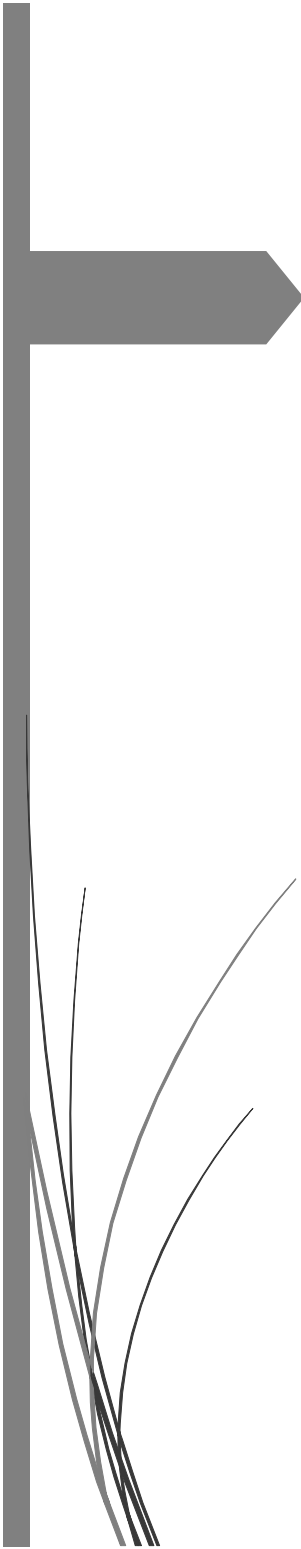


**Figure 5.S3: hPBMCs were cultured on electrospun scaffolds for one day:** A) The Left SEM image gives overview of cells attached to PCLBU scaffold (scale bar 50  $\mu\text{m}$ ) and magnified image on the right (scale bar 30  $\mu\text{m}$ ). B) The graph demonstrates the number of cells that migrated towards the scaffold with and without SDF peptide, and PCLBU was used as a control. C) PCLBU scaffolds were stained and observed under fluorescent microscope. Scaffold was stained for CD3 (green), CD14 and CD16 (red) and nuclei in blue. Scale bar 50  $\mu\text{m}$  (SEM image) and 25  $\mu\text{m}$  (microscopy images)



# Acknowledgements

This PhD journey has been a life-changing and unforgettable experience. Besides producing a Thesis, I became a mother, changed my nationality, got through the Dutch driving exams (wow they are tough), while trying to be a “good” house wife (my husband better agree!). This would not have been possible without the love and support of several people I came across, during this rollercoaster ride.

First of all, I would like to thank Frank for giving me the opportunity to join his group as a PhD student. I would like to specially acknowledge Carlijn for her support and guidance during the various stages of my PhD. I would like to thank my co-promotor Patricia for mentoring me and helping me throughout my PhD. I always appreciated your directness and down-to-earth attitude.

I thank the all the members of doctorate committee for taking time to read my thesis and giving valuable feedback. I thank Prof. Gerrit Peters and Prof. Lorenzo Moroni for being a part of my doctorate committee. Lorenzo, thank you for introducing me to electrospinning world during my Masters in Twente. I would also like to thank Cecilia for her support and guidance. Anthal, I deeply appreciate your mentoring during the last phase of my PhD. Thank you for your help and guidance. Thank you Leda for your help with my thesis.

I spent a lot of time in the lab and would like to thank all the lab members for making it an enjoyable experience. Moniek thanks for helping with everything related to cell lab, and letting me skip lab cleaning during my pregnancy. Marloes, I really appreciated your help during my pregnancy. Thank you Marina and Sylvia for your help and inputs for all my projects. Thanks to Vale, Tamar, Nicole, Matilde, Chenket, Samaneh, Andrea di luca, Francesca, Inge, Renee, Bart, Stefan, Carlotta, Libera, Nidhi and Nikita for the nice time during lunch and coffee breaks.

A special thanks to Johanna for all the help in the lab, giving me company working in the lab during weekends, awesome cakes, funny student stories and unusual news reports. I also enjoyed our “cultural” discussions ;). Tommaso, although you did not really work in the lab, you were in the lab

most weekends 😊. I admire your simplicity and honesty. I will always remember your response about my pregnancy. It still brings a smile on my face. Thank you for your company during the coffee breaks. Moving forward from here I will miss your Italian cookies ;). Thank you guys for all your support. I wish both of you success in your personal and professional life.

Thanks to Chiara-Duy, Giulia-Michele, Gor-Margarita, Anindita-Supriyo, Sandeep-Jalaja, Arianna-Francesco, Johanna-Tommaso, Hamad-Urooj, Erwin-Karen for the nice dinners / birthday parties you have organized. Falguni-Jigar and Pravin uncle and Seema aunty, you have been like my family here in Netherlands. Thank you for the nice dinners, outings and events.

Though I am continents away, my friends across the globe have constantly supported me. Remya and Jahanvi, thanks for the long conference calls/hangouts, listening to me and your support. Our calls were difficult to schedule in 3 different time zones but they were worth it. I look forward to our calls and relive our bachelor days. Although we meet once a decade, your friendship has always been precious to me (we should meet more often). I hope to see you both this year in NL. Monica and Mahima your whatsapp support has cheered me up on bad lab days ;). Thanks for all the tips-and-tricks on life ;). Trish, you have been a dear friend. Thanks for your all your help. Dilip, thanks for being a good friend. I look forward to meeting you, Sangeeta and Ethan again. Thank you Vaibhav for pushing me with your fitbit challenges. Thanks also to Nirav, AM, MK, DJ, HB and the entire E2E gang. Thank you Ashish and Naseef for the fun times.

My family has been very supportive at every stage of my PhD. My parents deserve special thanks for the love and support they provided me throughout my life. Thank you mummy & daddy for your continuous encouragement and moral support during my PhD. Mummy tari help vagar PhD puru no kari sakat. Gaya varse te NL ma 6 mahina rahi ne Krish nu dhayan rai khu tyare hu PhD par kaam kari saki. Mayur ne toh khava piwani maaja hati. Thank you for everything. Tamz, talking to you always relaxes me. Taru opinion



mari mate important che. Thanks for your support during challenging times and for making time for skype calls despite the time difference. I wish you and Rutvi happy married life. I would like to thank my parents-in-law, Sandeep bhaiya & Jyoti for their love and support.

Last but not the least, I thank the two most important boys in my life, my husband Mayur and our son Krish. Mayur, thank you for your valuable support, love, care and patience. Thanks for being by my side and supporting me through thick-and-thin. I am deeply indebted to you for all your help since I have come to Netherlands. From being my boyfriend to husband and now father to our son, life with you in last 2 decades has been wonderful. I love u baby ☺. Krish, Thank you for changing my life. The best day of my life was the first time you were placed in my arms. Since then, your smiles, your baby talks, and watching you grow up has given me immense happiness. Baa bu Kanha.

# Curriculum Vitae

Shraddha (Tina) Thakkar was born on 11<sup>th</sup> October 1981 in Bombay, India. She completed her Bachelors in Biomedical Engineering in 2003 from Mahatma Gandhi Mission college of Engineering and Technology, University of Mumbai, India. She completed her Master in Business Administration from Narsee Monjee Institute of Management studies, Mumbai, India. Tina then studied Master in Biomedical Engineering at University of Twente in Enschede, The Netherlands. In 2012 she graduated within the group of Tissue Regeneration, her thesis focused on evaluating the power of extracellular matrix. From August 2012 she started as a PhD candidate at TU/e, in the Soft Tissue Engineering and Mechnobiology group of research. Her PhD project was focused on introducing bioactivity into electrospun scaffolds in order to modulate the immune response. The results of this project are presented in this thesis.



# List of Publications

S.H.Thakkar, C Ghebes, M Ahmed, C Kelder, C.A.V. Blitterswijk, D Saris, H.A.M. Fernandes, and L Moroni. Mesenchymal stromal cell-derived extracellular matrix influences gene expression of chondrocytes, *Biofabrication*, August 2003, vol 5 (2).

S.H.Thakkar, H.A.M. Fernandes, and L Moroni. Decellularized Extracellular Matrix scaffolds for cartilage tissue engineering. *Methods Mol Biol.* August 2015;1340:133-51.

D.E. Muylaert, G.C van Almen, H.Talacua, J.O. Fledderus, J. Kluin, S.I.Hendrikse, J.L.van Dongen, E. Sijbesma, A.W.Bosman, T.Mes , S.H.Thakkar, A.I.Smits, C.V.Bouten, P.Y.Dankers, M.C.Verhaar. Early in situ cellularization of a supramolecular vascular grafts is modified by synthetic stromal cell-derived factor-1 $\alpha$  derived peptides. *Biomaterials.* 2016 Jan; 76:187-95

S.H.Thakkar, A. Drissen-Mol, F.P.T.Baaijens, C.V.C.Bouten. Porous Scaffolds Using Dual Electrospinning for in situ Cardiovascular Tissue Engineering. *Handbook of Intelligent Scaffolds for Tissue Engineering and Regenerative Medicine*, Second Edition, April 2017

S.H.Thakkar, M.W.J.T.Jassen-van den Broek, M.Van Doeselaar, A.I.P.M.Smits and C.V.C.Bouten. *Submitted*

S.H.Thakkar, A.Di Luca, S.Zaccaaria, F.P.T.Baaijens, C.V.C.Bouten and P.Y.W.Dankers. Accepted for publication in *Macromolecular Bioscience*, April 2018





